

# **Dopaminergic influence on cortical processing in rodents by optogenetic stimulation of the ventral tegmental area**

## **Dissertation**

**zur Erlangung des akademischen Grades**

**doctor rerum naturalium (Dr. rer. nat.)**

genehmigt durch die Fakultät für Naturwissenschaften der Otto-von-Guericke-  
Universität Magdeburg

Von M.Sc. Michael G.K. Brunk

Geb. am 23.08.1988 in Köln

Gutachter: PD. Dr. Max F. K. Happel

Prof. Dr. Manfred Kössl

eingereicht am 12.02.2020

verteidigt am 14.09.2020



*Experience is the name everyone gives to their mistakes.*

– Oscar Wilde, 1892 –



## **Declaration of criminal convictions**

I hereby declare that I have not been found guilty of scientific and/or academic misconduct.

Magdeburg, 12/2/2020

A handwritten signature in black ink, appearing to read "Brunk".

Michael Brunk



## **Declaration of honor**

„I hereby declare that I prepared this thesis without impermissible help of third parties and that none other than the indicated tools have been used; all sources of information are clearly marked, including my own publications. In particular I have not consciously:

- Fabricated data or rejected undesired results
- Misused statistical methods with the aim of drawing other conclusions than those war-ranted by the available data
- Plagiarized external data or publications
- Presented the results of other researchers in a distorted way

I am aware that violations of copyright may lead to injunction and damage claims of the author and also to prosecution by the law enforcement authorities. I hereby agree that the thesis may be reviewed for plagiarism by mean of electronic data processing.

This work has not yet been submitted as a doctoral thesis in the same or a similar form in Germany or in any other country. It has not yet been published as a whole.”

Magdeburg, 12/2/2020



Michael Brunk



## **Keywords**

Auditory Cortex (ACx), current source density (CSD), Mongolian Gerbil, ventral tegmental area (VTA), dopamine (DA), optogenetic stimulation

## **Zusammenfassung**

Lern- und Belohnungsassoziationen sind eng mit der kortikalen Plastizität verbunden. In früheren Studien konnte gezeigt werden, dass die Lernleistung während einer Ton assoziierten Vermeidungsaufgabe mit der relativen Zunahme von kortikalem Dopamin (DA) innerhalb des primären auditorischen Kortex (A1) korreliert. Eine Hauptquelle des kortikalen DA ist die Area tegmentalis ventralis (VTA). Die gleichzeitige Stimulation der VTA in Verbindung mit einer spezifischen Tonpräsentation verändert nachweislich die kortikale Verarbeitung zu Gunsten des stimulationsgebundenen Tons. Die unmittelbaren Auswirkungen dieser belohnungsassoziierten DA Ausschüttung auf die kortikale Verarbeitung sind jedoch noch nicht geklärt.

Im Rahmen meiner Promotionsthesis, habe ich eine optogenetische Stimulation der VTA bei Mongolischen Wüstenrennmäusen (*Meriones unguiculatus*) verwendet, um die unmittelbare DA-induzierten zeitliche Veränderung der kortikalen Verarbeitung zu untersuchen. Dies geschah in drei verschiedenen Tiergruppen: C1V1, YFP und einer naiven Kontrolle. Die Tiere der optogenetischen C1V1-Gruppe wurden vor den elektrophysiologischen Experimenten zunächst in einem optogenetischen intrakraniellen Selbststimulationsparadigma (O-ICSS) trainiert, um eine ausreichende Menge an belohnungsassozierter DA zu gewährleisten. Potenziell unterschiedliche Leistungen im O-ICSS wurden in drei verschiedene Leistungsgruppen (High-, Medium-, Low-Performer; HP, MP, LP) eingeteilt, um die potentielle Kausalität in Bezug auf potentielle Parameter wie die Eigenschaften der Fasern vor (T0) und nach den Experimenten (T1), den Abstand zwischen der Faserspitze des optogenetischen Implantats und dem transduzierten Bereich darunter sowie die anatomische Positionierung der Stimulationsseite zu untersuchen. Im elektrophysiologischem Experiment untersuchte ich die zeitlichen Veränderungen der kortikalen Verarbeitung auf der säulen- und schichtenspezifisch. Ich fand eine schichtspezifische kumulative Zunahme der kortikalen Verarbeitung und der kortikokortikalen Kommunikation, die die

Grundlage für das Remodelling der Säule und damit der Belohnung assoziierten Plastizität des Neokortexes sein könnten.

## **Abstract**

Learning and reward associations have been tightly linked towards cortical plasticity. In previous studies, it has been shown that the performance during an auditory engaged avoidance task correlates with relative increase of cortical dopamine (DA) within the primary auditory cortex (A1). One major source of cortical DA is the ventral tegmental area (VTA). Simultaneous stimulation of the VTA coupled with a specific tone presentation has been shown to change the cortical processing in favor of the presented tone. However, the immediate effects of this reward associated DA on cortical processing are still unsolved.

Within this thesis, I utilized an optogenetic stimulation of the VTA within the Mongolian gerbil (*Meriones unguiculatus*) to investigate the immediate DA-induced temporal changes on cortical processing. I was investigating the potential temporal effects of DA on the tone evoked cortical processing with three different animal groups: C1V1, YFP and naïve control. Animals of the optogenetic C1V1 group, were initially trained in an optogenetic intracranial self-stimulation (O-ICSS) paradigm prior to the electrophysiological experiments to ensure a sufficient amount of reward associated DA. Potentially different performances in the O-ICSS were denoted into three distinct performance groups (High-, Medium-, Low-Performer; HP, MP, LP, respectively) to investigate the potentially causality in respect of potential parameters such as like the properties of the fibers before (T0) and after the experiments (T1), the distance between the fiber tip of the optogenetic implant and the transduced area underneath as well as the anatomical positioning of the stimulation side. For the experimental setup I was investigating the temporal changes of cortical processing on the columnar and layer-wise level. Eventually, I found prominent accumulative effects in distinct layers and the corticocortical communication, which might be the foundation for the remodeling of the column and therefore the plasticity of the reward associated remapping within the neocortex.

# Index of Contents

<i>Declaration of criminal convictions.....</i>	<i>I</i>
<i>Declaration of honor.....</i>	<i>III</i>
<i>Keywords.....</i>	<i>V</i>
<i>Zusammenfassung.....</i>	<i>V</i>
<i>Abstract.....</i>	<i>VII</i>
<i>Index of Contents.....</i>	<i>VIII</i>
<b><i>I. Introduction .....</i></b>	<b><i>1</i></b>
<b>I.I The neocortex – The new trait to a conscious mind?.....</b>	<b>1</b>
<b>I.II Engram formation and memory recall.....</b>	<b>3</b>
<b>I.III Microarchitecture of the auditory cortex .....</b>	<b>5</b>
I.III.I Properties of cortical layers .....	5
I.III.II Properties of cortical columns .....	13
<b>I.IV The Mongolian gerbil and its auditory cortex as a model organism of choice for hearing research.....</b>	<b>14</b>
<b>I.V Local field potentials and current source density.....</b>	<b>16</b>
<b>I.VI The origins and influence of cortical dopamine in the primary auditory cortex.....</b>	<b>17</b>
I.VI.I Is there a thalamo-cortical pathway between the ventral tegmental area and the auditory cortex? 20	20
<b>I.VII Optogenetics and its application for brain stimulation.....</b>	<b>22</b>
<b>I.VIII Motivation and aims of this work .....</b>	<b>24</b>
<b><i>II. Material and Methods.....</i></b>	<b><i>26</i></b>
<b>II.I Optogenetic fiber implants .....</b>	<b>26</b>
II.I.I Optogenetic preparation and intracranial self-stimulation .....	27
II.I.II Anatomical and histological validation of fiber position.....	30
<b>II.II Acute setup for electrophysiological recordings .....</b>	<b>31</b>
II.II.I Acute measurements and experimental paradigm.....	32
<b>II.III Mesoscopic investigation of cortical circuit functions using current-source-density recordings .....</b>	<b>34</b>

<b>II.IV</b>	<b>Data processing and sorting.....</b>	<b>38</b>
II.IV.I	Sink detection.....	38
II.IV.II	Data sorting and preparation .....	40
<b>II.V</b>	<b>Linear mixed effect models (LMMs) .....</b>	<b>41</b>
<b>III.</b>	<b>Results .....</b>	<b>43</b>
<b>III.I</b>	<b>Validation of VTA targeting.....</b>	<b>44</b>
III.I.I	Laser transmission properties of the used implants .....	46
III.I.II	Anatomical distance between fiber tip and VTA.....	47
III.I.III	Anatomical position of successful VTA stimulation by O-ICSS .....	48
<b>III.II</b>	<b>VTA projections into the ACx .....</b>	<b>49</b>
<b>III.III</b>	<b>Optogenetic stimulation of the VTA increases columnar processing.....</b>	<b>49</b>
III.III.I	Effects of laser stimulation without tone evoked processing .....	55
<b>III.IV</b>	<b>Effects of VTA stimulation on layer-specific synaptic processing .....</b>	<b>57</b>
III.IV.I	Changes in spectral tuning sharpness of cortical layers.....	60
<b>IV.</b>	<b>Discussion.....</b>	<b>64</b>
<b>IV.I</b>	<b>Effectiveness of VTA targeting in the Mongolian gerbil.....</b>	<b>65</b>
<b>IV.II</b>	<b>Effect associations of dopamine.....</b>	<b>68</b>
<b>IV.III</b>	<b>Dopamine increases corticocortical columnar communication.....</b>	<b>70</b>
<b>IV.IV</b>	<b>Layer specific changes due to dopaminergic influence .....</b>	<b>72</b>
<b>IV.V</b>	<b>Alterations of the cortical micro-circuitry .....</b>	<b>75</b>
<b>V.</b>	<b>Conclusion.....</b>	<b>76</b>
<b>V.I</b>	<b>Outlook.....</b>	<b>77</b>
<b>Literature .....</b>	<b>79</b>	
<b>Appendix .....</b>	<b>97</b>	
<b>Supplementary Figures.....</b>	<b>97</b>	
Laser-Fiber-Coupling Efficiencies of the used C1V1 animals .....	97	
Temporal stability of CSD signals.....	98	
Common initial granular BFs of the groups .....	98	
BF development and shift towards the granular sink (III/IV) for the Control group .....	99	
Lever presses of single animals .....	100	
AVREC and ResidualCSD traces of the YFP and Control animals .....	101	

Time course of C1V1 animals after SCH-23390 application .....	102
Close up of cortical region after viral VTA transduction.....	103
<b>Protocols.....</b>	<b>104</b>
Preparation of a head mount for an optic fiber for VTA-Stimulation in Gerbils 1.1.....	104
Nissl-staining protocol .....	107
TH-staining protocol for gerbils .....	108
<b>List of animals for the electrophysiological experiments.....</b>	<b>109</b>
<b>List of abbreviations .....</b>	<b>110</b>
<b>List of Figures .....</b>	<b>113</b>
<b>List of Supplementary Figures .....</b>	<b>113</b>
<b>List of tables.....</b>	<b>114</b>

## I. Introduction

### I.I The neocortex – The new trait to a conscious mind?

*"There is grandeur in this view of life, with its several powers, having been originally breathed into a few forms or into one; and that, whilst this planet has gone cycling on according to the fixed law of gravity, from so simple a beginning endless forms most beautiful and most wonderful have been, and are being, evolved."*

*-On the Origin of Species by Charles Darwin (1859)-*

With his closing remarks on his work “On the Origin of Species” Charles Darwin laid the groundwork for the theory of evolution (Darwin, 1859), which is still relevant today also in respect of the complexity of development from the central nervous system (CNS). This evolving complexity of the CNS coincides with the evolutionary appearance of species and the rising complexity of their environmental interactions. Whereas early species like the *Hydra* (phylum: *Cnidaria*; class: *Hydridae*) are lacking the necessity of a centralized coordination via a brain for muscle movements and only developed a rudimentary nerve net for environmental interactions, other, evolutionary higher, species like *Drosophila* (phylum: *Euarthropoda*; class: *Insecta*) developed brains for more complex environmental interactions involving sensory detection and controlled movements. In higher animals, the evolutionary emerging of the species overlaps with an increasing complexity of the CNS, especially the brain and its functions for instance in the aspect of vital controls (Galizia and Lledo, 2013). In spirit of Darwin’s theory, the German neuroanatomist Ludwig Edinger noted that the cerebral cortex of mammalian brains, compared to reptilian and avian brains, developed a new six-layered structure, which he called the neocortex, (“neo” ancient Greek for new, “cortex” Latin for bark) based on it being the newest evolutionary trait. Many researchers saw in the neocortex a potential explanation for the intelligence and higher cognitive functions, like goal-directed behavior, of the conscious mind. Especially since the brain’s appearance changes from a smoother cortical surface area (*lissencephaly*: “*lissos*” ancient Greek for smooth, “*encephalos*” ancient Greek for brain) in smaller animals like rodents, towards a more folded and much more complex surface area, consisting of gyri (Latin/ancient Greek for ridge) and sulci (Latin for furrow) for an increase of the surface area, in larger mammals (Galizia and Lledo, 2013).

In mammals, the evolutionary appearance of the neocortex led to the development of the functional areas, which numbers are increasing with the volume of the cortex (Galizia and Lledo, 2013; Merker, 2007; Molnár et al., 2014). Among those areas are the five primary sensory areas (somatosensory, gustatory, olfactory, visual and auditory) which share four common properties (Kandel et al., 2013, bk. Principles of neural science 5th Edition-Chapter 18: The Organization of Cognition):

1. Except for the olfactory cortex, they all receive thalamic inputs from corresponding sensory relay nuclei (Courtiol and Wilson, 2015).
2. Their neurons have small receptive fields arranged as topographic maps.
3. Injuries to those topographic maps cause a simple sensory loss in the corresponding contralateral sensory systems.
4. Connections to other cortical areas are limited and almost exclusively confined by nearby areas that process the same modality.

The last feature of those common properties is highly debatable, since studies about explicit memory formation have shown memory traces (engrams, see section I.II) within primary sensory areas (Moczulska et al., 2013; Weinberger, 2004), which, due to the complex nature of memory formation, hint at a long-distance communication between non-related modalities (Chen et al., 2013).

In recent years, the neocortex has been disproven as a sole trait mark of intelligence and consciousness (Kirsch et al., 2008; Molnár et al., 2014). Especially the avian research has proven that intelligent behavior is not solely linked towards the existence of a neocortex but rather the cell density (Jarvis et al., 2005; Kirsch et al., 2008; Olkowicz et al., 2016). Likewise, it was shown that the auditory pallium of birds displays a laminar and columnar organization as it was initially assumed to be an exclusive trait mark of the mammalian auditory cortex or other neocortical regions (Wang et al., 2010).

Even though the neocortex has lost its prestige of being the sole explanation for intelligence and consciousness, its unique appearance and exact purpose, like its involvement in memory formation and recall, are still a challenging puzzle, which needs to be solved by the endeavor of the neuroscientific community.

## I.II Engram formation and memory recall

The conscious individual is in steady interaction with its environment. The daily bombardment of sensual information raises the challenge for our brains to filter and store the necessary information in forms of a complex memory, which engage different areas of our neocortex (Brodt et al., 2018; Weinberger, 2004). Depending of the type of memory (e.g. long-term or short term), the complex sensation of all involved and necessary senses or modalities needs to be stored and represented in various regions of the brain—like the neocortex—in form of engrams (Tonegawa et al., 2015).

Still, the process of plastic changes within the neocortex like in the auditory cortex (Grosso et al., 2016; Weinberger, 2004) has not yet been described.

Literature has shown that electrical stimulation of the hypothalamus (Laxton et al., 2010) or the temporal neocortex can evoke memory recall (Figure 1). However, the unspecific nature of the electrical stimulation (“Method of the Year 2010,” 2011) complicates the investigation of engram formation and recall. New techniques like optogenetics (see I.VII) have already been utilized to create and recall “fake memories” (X. Liu et al., 2012).

Depending on the type of memory, various brain regions are involved in the formation and recall of engrams:

The working memory is rather of a transient nature and does not need to withhold information for a long time (seconds). Working memory related activity has been reported for the prefrontal cortex (Slotnick et al., 2003). Implicit memories are of an unconscious nature and include the recall for daily routines like bicycle riding or using a fork. Implicit memories acquire the cerebellum and the basal ganglia (Witt et al., 2002). The more conscious memory is the explicit memory, which engages the hippocampus, amygdala, and neocortex. Explicit memories are reinforced by a vast variety of teaching signals like physiological sensation (auditory, visual and somatosensory) and the release of various neurotransmitters (adrenaline, acetylcholine, serotonin and dopamine) (Agnati et al., 2004; Hasselmo, 2006; Martins and Froemke, 2015; Scheich et al., 1997; Shen, 2018; Stark and Scheich, 1997; Weinberger, 2004).

Especially dopamine is of an crucial interest due to its involvement of cortical plasticity, formation and adaption of memory (Bao et al., 2001; Hui et al., 2009; Reichenbach et al., 2015; Schicknick et al., 2012, 2008; Shohamy and Adcock, 2010), since it has been thoroughly shown to be involved as a teaching signal in reward-associated learning and event evaluation of prediction (Schicknick et al., 2008; Schultz, 2016, 2015, 1998; Stark et al., 2000).



*Figure 1: Deep brain stimulation of the hypothalamus for memory retrieval*

Screenshot from the House M.D. medical drama TV show. After a trauma-induced amnesia, Dr House undergoes a surgical procedure for deep brain stimulation of his hypothalamus to retrieve crucial information to help his patient.

In order to understand the mechanisms of memory formation and retrieval of engrams—especially on the observation level of the smallest functional cortical units (columns)—in the neocortex, a detailed knowledge of the cortical microarchitecture and its potential cortical microcircuits as well as the dopamine induced influence on these circuits are mandatory.

## I.III Microarchitecture of the auditory cortex

In general, roughly 80% of all neurons of the neocortex are of an excitatory glutamatergic nature, whereas the remaining 20% are rather of an inhibitory nature, very often utilizing gamma-aminobutyric acid (GABA) as their neurotransmitter (Noback et al., 2005). Nearly 50% of those inhibitory cells are basket cells (Budinger and Kanold, 2018). The auditory cortex (ACx) is located in the brain's temporal lobe (compare Figure 2 A) and displays a key role via its multiple connections towards other sensory and non-sensory brain areas, emphasizing its role for learning associated bottom-up and top-down processing whereas non-auditory inputs primarily target superficial and deeper layers (Budinger and Kanold, 2018). Like the entire neocortex, the ACx consists of six layers.

### I.III.I Properties of cortical layers

The entire microarchitecture of those layers is confined by the density distribution of distinct receptors (cf. Happel, 2016; Lidow, 1995; Radnikow and Feldmeyer, 2018; Santana and Artigas, 2017) as well as by the occurrences and different cellular properties (see staining methods in Figure 2 C) of three major cell types: interneurons, pyramidal, and glial cells.

The most prominent cell type among those three are the pyramidal cells. As indicated by their name, pyramidal cells can be identified by their triangular cell body. They display long axons and apical and basal dendrites. Pyramidal cells are usually of an excitatory nature by utilizing the neurotransmitter glutamate.

Interneurons (e.g. star-shaped stellate neurons) have short axons and are interconnected to other neurons, displaying excitatory but most of the time inhibitory effects at the post synapse.

Glial cells are supporting and protecting their neighboring cells by providing the homeostasis of the myelin (Jessen and Mirsky, 1980).

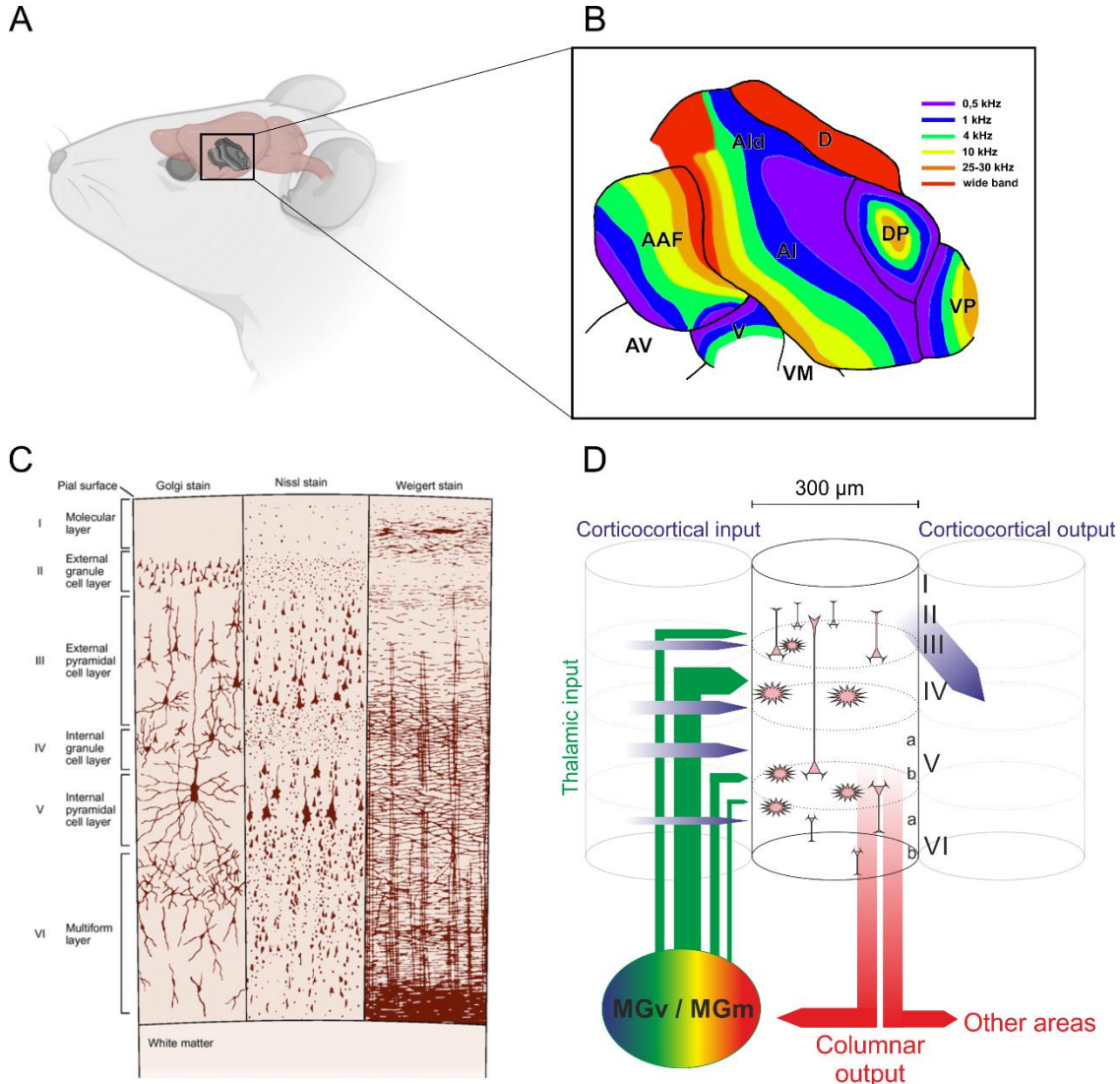


Figure 2: Column as the smallest unit of the auditory cortex

A) Schematic representation of the cortical location of the auditory cortex within the temporal lobe of the rodent brain. B) Schematic representation of tonotopic gradients and receptive fields (AI: primary auditory cortex, AAF: Anterior auditory field, DP: Dorsoposterior, AV: Anteroventral, V: Ventral, D: Dorsal, VP: ventroposterior) of the auditory cortex of the Mongolian gerbil. Courtesy of Dr Eike Budinger and adapted from Budinger et al., 2000. C) Cellular distribution across cortical layers. Differences in cortical microstructure can be shown by different staining methods: Golgi staining displays cell somas, axons and dendrites. Nissl staining reveals soma and dendrites. Weigert staining is used to stain myelinated fibers of the axons. (adapted from Kandel et al., 2013). D) Schematic sketch of a columnar unit (diameter  $\sim 300 \mu\text{m}$ ) along the cortical layers. Sensory thalamocortical input is provided by the medial and ventral division of the medial geniculate nucleus (MGv/MGm). Corticocortical inputs from neighboring columns and other cortical regions targets layer specifically in almost all layers. Dominant corticocortical connections from supragranular layer II/III affect granular layers of neighboring columns (Aru et al., 2019; Linden and Schreiner, 2003). Further columnar, corticoefferent output projects back towards the MGv/MGm and other subcortical structures (Aru et al., 2019; Budinger and Kanold, 2018; Happel, 2016; Kandel et al., 2013; Mitani et al., 1985; Mountcastle, 1998; Schaefer et al., 2015).

In the literature, there are two distinct ways to describe cortical layers:

- A) For a rough description, the cortex can be separated into three cortical layer regions:

Based on the prominent thalamic input in cortical layer IV, this layer is commonly used as a reference and referred to as the granular layer. All layers above the granular layer (I, II and III) are referred to as the supragranular layers and all layers underneath layer IV (V and VI) are stated as the infragranular layers. For the methodology of this thesis, the term granular layers referrs to layers III and IV.

- B) In a more detailed fashion, all cortical layers display different properties in respect of their distinct cell type distribution, cortical in-/output association and interlayer connectivity (Braak, 1974; Briggs, 2010; Budinger and Kanold, 2018; Crochet and Petersen, 2009; Deliano et al., 2018; Douglas et al., 1989; Douglas and Martin, 1991; Guy and Staiger, 2017; Lefort et al., 2009; Mountcastle, 1998; Oberlaender et al., 2012; Santana and Artigas, 2017; Schaefer et al., 2015; Schubert et al., 2006; Weiler et al., 2008):

**Layer I**, also known as the plexiform or molecular layer (Braak, 1974), consists mainly out of neuropil with dendrites and axons from deeper layer neurons in a horizontal arrangement. The plexiform layer is lacking any type of pyramidal cells. Instead, it mainly consists of more than 90% inhibitory GABAergic interneurons targeting layer I itself and layers II/III (Budinger and Kanold, 2018; Lefort et al., 2009). GABAergic cells in this layer have been demonstrated to also inhibit cortical activity of layer V. The only excitatory cell type within the plexiform layer are the Cajal-Retzius cells, which might project across multiple columns in layer I (Budinger and Kanold, 2018).

**Layer II**, the outer granular layer, mainly consists of small pyramidal cells as well as small stellate neurons. Pyramidal cells of layer II are branching primarily into layers I-III to serve for intracolumnar connections. Up to 24% of Layer II is made up by GABAergic interneurons (Budinger and Kanold, 2018). Output projections in layer II have been postulated to target ipsilateral cortices (Mountcastle, 1998). Layers I/II receive faint thalamic inputs from the medial division of the geniculate body (MGm). Whereas layer I primarily displays excitatory projections onto itself, layer II has been shown to excitatory project onto all supragranular layers and layer Va (Lefort et al., 2009; Oberlaender et al., 2012; Weiler et al., 2008). In general,

layer II has been shown to have inhibitory projections into all cortical layers. In monkeys, the presence of calbindin-positive cells in layers I/II was shown by the co-localization of the  $\alpha$ -subunit of the  $\text{Ca}^{2+}$ -calmodulin-dependent protein kinase II (CAMKII $\alpha$ ) (Jones, 2001).

**Layer III**, also known as the outer pyramidal layer, is made up by medium-sized and more complex pyramidal cells and small stellate neurons as in layer II. Like layer II, layer III consists to 24% of GABAergic cells (Budinger and Kanold, 2018). Output projections of layer III have been postulated to project into contralateral cortices. For the vibrissal cortex of rats, intracolumnar projections from layer III up to layer I have been reported, which are spreading across columnar borders (Budinger and Kanold, 2018). Those projections have been associated with cross-columnar interactions. Layer III has been reported to project onto large pyramidal cells in layers V (Guy and Staiger, 2017). There are no reports of excitatory projections of layers II/III towards the infragranular layer VI in rodents, yet inhibitory projections across all layers exist. In addition, according to literature, superficial inputs have been rarely reported for rodents. In general, layers II/III receive strong inputs from itself and layer IV (Douglas and Martin, 1991; Lefort et al., 2009). Some studies have claimed projections from layers Vb and VI towards layers II/III (Briggs, 2010; Budinger and Kanold, 2018; Lefort et al., 2009; Oberlaender et al., 2012). Excitatory inputs in layers II/III have been shown to be more excitatory signals from the tonotopic direction rather than from the iso-frequent direction, which is a prominent feature of A1 and might contribute to the tuning properties (Budinger and Kanold, 2018). Most inhibitory projections of layers II/III are originating from the layer itself with some additional inputs arising from layers IV and V (Briggs, 2010; Oberlaender et al., 2012).

**Layer IV**, also known as the granular layer, consists of numerous excitatory stellate neurons and is almost free of pyramidal cells (Budinger and Kanold, 2018). Granular stellate cells target layers III to V (Douglas et al., 1989; Guy and Staiger, 2017) and are driven by thalamo-, corticocortical and commissural stimulation, whereas branching in supragranular layers across columnar borders is given. The granular layer consists up to 26% of GABAergic cells (Budinger and Kanold, 2018). In comparison to the visual cortex, the granular layer of the ACx displays a weaker sub-lamination, which hints at a reduced intralaminar circuitry. Thalamocortical feedforward excitation by principal neurons targets primarily GABAergic neurons,

which results in a strong feedforward inhibition. The granular layer receives the main input from the thalamocortical projections (Crochet and Petersen, 2009) (compare section I.I). The strongest excitatory projections of layer IV have been reported to project onto layer IV itself. Layer Va has also been reported to project prominently onto layer IV (Budinger and Kanold, 2018). Various reports claimed further inputs to layer IV from layers II/III, Vb and VI, whereas the impact of cortical projections varies from faint inputs up to almost as strong as the inputs of layer IV itself (Briggs, 2010; Budinger and Kanold, 2018; Douglas and Martin, 1991; Lefort et al., 2009; Oberlaender et al., 2012; Weiler et al., 2008). Those reports also include *in vitro* studies, which have shown that the granular layer receives excitatory inputs from layers II/III, VI and itself (Briggs, 2010; Budinger and Kanold, 2018; Schubert et al., 2007). In general, excitatory and inhibitory inputs in layer IV have been stated as equally balanced (Budinger and Kanold, 2018) with similar tuning properties also in respect of their best frequencies (BFs, for definition read page 36).

**Layer V**, also named as the inner pyramidal or ganglion layer, can be divided into the two sublayers Va and Vb whereas layer Va has a lesser cell density than Vb (Budinger and Kanold, 2018). The ganglion layer consists of 27% of GABAergic interneurons, which are receiving strong inputs from the granular and supragranular layers but rather faint inputs from infragranular layers (Budinger and Kanold, 2018). Corticothalamic projections of layer V are among the primary excitatory and inhibitory corticofugal projections—projecting through other infragranular layers towards the thalamus and striatum—and target primarily the dorsal division of the medial geniculate nucleus (MGd) via inverted pyramidal cells. On the border of layers Va and Vb large pyramidal cells can be found that have been reported to project up to layer I (Budinger and Kanold, 2018; Lefort et al., 2009; Oberlaender et al., 2012; Weiler et al., 2008). For the rodent barrel cortex, a strong excitatory input of layer Va onto itself as well as fainter inputs from layers I/II, IV and Vb have been reported, whereas weak inhibitory inputs originate from layers IV and Va itself (Lefort et al., 2009; Schubert et al., 2007; Weiler et al., 2008). Pyramidal neurons in layer Vb receive strong excitatory inputs from layer Vb itself and layer VI. Other excitatory projections targeting layer Vb originate from layers II/III, IV and Va (Budinger and Kanold, 2018; Lefort et al., 2009). Inhibitory inputs towards layer Vb originate from layers II/III, IV and Va (Lefort et al., 2009). Recent electrophysiological studies have revealed two less prominent thalamic inputs in

layers Vb and VIa, which derive from the ventral and medial part of medial geniculate nucleus (MGv, MGm) (Constantinople and Bruno, 2013; Schaefer et al., 2015). Those inputs have been shown to be boosted in their relative activity by dopaminergic agonists (Happel et al., 2014a). However, due to the prominence of the layer IV as the main thalamic input, the physiological purpose of those infragranular inputs stays rather elusive in literature.

**Layer VI** is highly heterogeneous in its cell type distribution and cell sizes (pyramidal cells, fusiform cells and club-shaped neurons), and is therefore known as the multiform or polymorphic layer (Braak, 1974; Briggs, 2010). Layer VI has been reported to consist of 10–20% inhibitory neurons (Briggs, 2010; Budinger and Kanold, 2018). Taken together with the strong inhibitory loop action in this layer it is assumable that inhibitory neurons in layer VI strongly affect their neighboring cells. In addition, next to the inhibitory neurons, excitatory pyramidal neurons of layer VI have been shown to contribute to lateral connections. Like the ganglion layer, layer VI can be subdivided into layers VIa and VIb, whereas VIa is highly populated by pyramidal cells that have been reported to receive thalamic inputs from the MGm (Crochet and Petersen, 2009; Schaefer et al., 2015). In comparison, layer VIb accumulates more club-shaped and horizontally arranged fusiform neurons (Braak, 1974; Budinger and Kanold, 2018).

Some reports state that short pyramidal neurons in layer VI project towards excitatory and inhibitory cells in layer IV and therefore, perform in a modulatory role of the thalamic input (Briggs, 2010). However, for rodents, little to no excitatory inputs of layer VI towards the granular and superagranular layers have been reported. Yet, pyramidal and inhibitory neurons of layer VI have been stated to receive inhibitory inputs of superficial layers. Vertical fusiform neurons in layer VIa project up to layer IV whereas pyramidal cells of layer VIa even project up to layer III (Briggs, 2010; Oberlaender et al., 2012; Santana and Artigas, 2017). Many inhibitory neurons in layer VI are thought to be involved in different specialized local circuits, whereas most inhibitory neurons project onto excitatory neurons in layer VI itself (Briggs, 2010). Inhibitory basket neurons from layer VIa, for instance, have been described to have descending dendrites throughout layer VI as well as axons laterally extending through layers V and IV (Santana and Artigas, 2017). Some of the weaker and sparser spread cells in layer VI are suggested to play important roles in cortical information processing due to their projections to other cortical

areas and subcortical structures (Briggs, 2010). The latter is even more affected by large pyramidal cells, which are projecting into layer V, therefore affecting layer V output modulations (Briggs, 2010). Especially, the fusiform neurons of layer VIb have been reported to project towards ipsi- and contralateral regions as well as towards other subcortical structures (Braak, 1974; Briggs, 2010). Corticothalamic outputs are primarily projecting in an inhibitory and excitatory manner towards the thalamic nuclei. In general, infragranular layers V and VI are associated with afferent excitatory and inhibitory thalamic output projections - especially towards the MGd and MGv, respectively (Briggs, 2010; Budinger and Kanold, 2018; Schubert et al., 2007). Therefore, they are directly closing a thalamic input/output loop, indicating their role as thalamic feedback control of the active cortical side (Briggs, 2010; Budinger and Kanold, 2018; Guy and Staiger, 2017; Weiler et al., 2008). However, modulatory control mechanisms of this feedback loops have not been investigated in literature yet.

In addition, both layers can be additionally identified by the existence of giant boutons (Saldeitis et al., 2014).

All the above-described connections are summed up in the following layer associated projections summary. All vague projections i.e. layer III inhibition of layer V have been applied to all sublayers of V and vice versa.

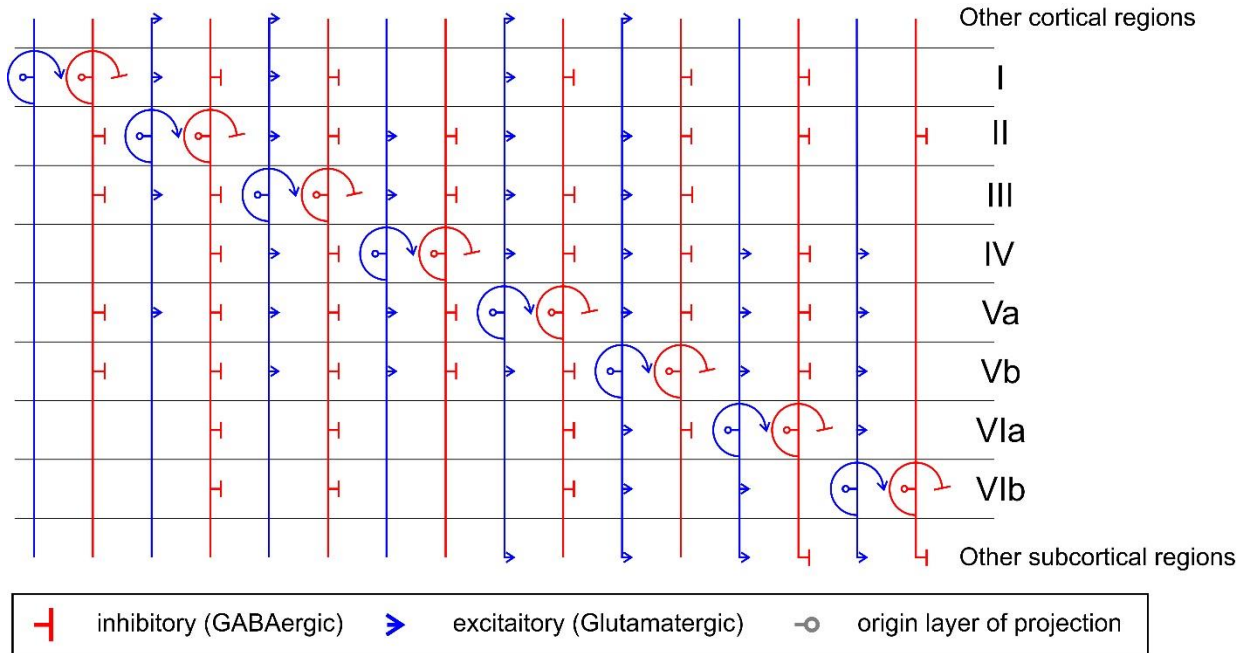


Figure 3: Summary of possible interlayer circuitry projections of the neocortex

This schematic sketch displays all above described interlayer projections for inhibitory and excitatory connections. It is based on the following references for neocortical descriptions and feedback by Eike Budinger; (Braak, 1974; Briggs, 2010; Budinger and Kanold, 2018; Crochet and Petersen, 2009; Deliano et al., 2018; Douglas et al., 1989; Douglas and Martin, 1991; Guy and Staiger, 2017; Lefort et al., 2009; Mountcastle, 1998; Oberlaender et al., 2012; Santana and Artigas, 2017; Schaefer et al., 2015; Schubert et al., 2006; Weiler et al., 2008).

Another, generalized, model of layer associated thalamic and non-thalamic in- and outputs as well as the cortical circuits is depicted in Figure 12 A on page 37.

The investigation of the various regions of the neocortices in *in vivo* and *ex vivo* electrophysiological experiments allowed to derive a common canonical microcircuit model based on the columnar organization of the cortex, which sums up the most prominent *feed-forward* and *feed-backward* connections between layers (Beul and Hilgetag, 2015; Bosman and Aboitiz, 2015; Dhruv, 2015; Douglas and Martin, 1991). However, those canonical microcircuits are primarily based on data from anesthetized animals and thus will differ in the awake state (Deane et al., 2019). Likewise, the presence of neuromodulators and neurotransmitters will affect the common canonical processing and thus might promote non-dominant interlaminar projections, which are enlisted in Figure 3.

### I.III.II Properties of cortical columns

The entire auditory cortex is involved in cortical processing of various tone evoked information derived from the medial geniculate nucleus of the auditory thalamus (MGm, MGv) via thalamic projections into various input layers.

Although, thalamic arbors from the auditory thalamus are projecting throughout all layers of the ACx, branching differences in layers as well as frequency selectivity of boutons results in a local heterogenous tuning within layers whereas the overall tuning of the entire column is more persistent contributing to the global tonotopy (Vasquez-Lopez et al., 2017). In addition, layers are affected by different excitatory and inhibitory layer projections, which causes different cortical frequency processing between layers by several octaves (Tischbirek et al., 2019) as also stated for other cortical regions (Ayaz et al., 2019).

On a single neuronal level, each cell displays a characteristic frequency as well as bandwidth and intensity levels, being heterogeneously distributed alongside the cortex (Bandyopadhyay et al., 2010). In their 2010 study, Bandyopadhyay et al. further showed that neurons not always respond to their characteristic frequencies contributing to the overall local heterogeneity. However, neurons with similar CFs properties are most likely clustered and respond with other neurons in close proximities ( $<100 \mu\text{m}$ ), leading to a common *modus operandi* for their regions, resulting in the gradients of global tonotopic bands (See Fig. Figure 2 B) (Bandyopadhyay et al., 2010; Rothschild et al., 2010; Tischbirek et al., 2019; Vasquez-Lopez et al., 2017).

Within those tonotopic bands functional units can be defined called columns (species dependent diameter: 200–600  $\mu\text{m}$ ), which are spanning across all cortical layers. Therefore, columns, within the frequency bands of the ACx display a population of neurons with similar receptive properties and display a common iso-frequent cortical processing (Figure 2 D) (Goldschmidt et al., 2010, 2004). The diameter of columns within the gerbil auditory cortex is around 300  $\mu\text{m}$  (Goldschmidt et al., 2004).

The electrophysiological properties of these columnar structures and the neuronal population activity in the corresponding layers of the neocortex can be investigated at two different levels:

The surface activity of multiple columns can be monitored by placing an ECoG-array on top of the exposed A1 to record electrocorticograms (Deliano et al., 2009), which allows to investigate changes in the global tonotopy of the cortex.

For cortical depth measurements—at a high precision— alongside all cortical layers, a multichannel shaft electrode can be inserted perpendicular in A1, capturing the tone evoked columnar activity (Happel et al., 2014a, 2010). This method has the advantage of capturing the cortical processes alongside all layers in a single column.

In order to investigate the influence of dopamine on cortical microcircuits on a columnar and layer-wise level, the usage of a shaft electrode was the method of choice for this thesis.

All recordings were performed using a 32-channel shaft electrode (NeuroNexus A1x32-50-413) with an inter-channel distance of 50 µm—spanning a total cortical depth of 1.6 mm— was used. Since the integrational cylinder of the shaft electrode integrates neuronal populations 100-250 µm around the electrode, the possibility of recording an entire column is given (Katzner et al., 2009).

#### I.IV The Mongolian gerbil and its auditory cortex as a model organism of choice for hearing research

In research, the usage of model organisms provides the foundation of principal investigation for certain biological aspects or phenomena as well as for the effects of the manipulation of the investigated parameters. For the research of cortical processes, the usage of small to medium-sized vertebrates like zebrafish, rodents (i.e. mice, rats, gerbils) and carnivores (i.e. ferrets, cats) is quite common.

The advantages of the Mongolian gerbil (*Meriones unguiculatus*) as a model organism of choice for experimental auditory investigations lays within its hearing range (0.1-43 kHz), which is covering the human hearing range (0.3-20 kHz), as well as its cheap maintenance costs (Thomas et al., 1993). Both auditory cortices within the Mongolian gerbil have been shown to be specialized for different purposes as shown by lesion experiments in auditory engaged perceptual tasks. Whereas the left ACx has been proven to be more involved in the temporal tone interval recognition (Deutscher et al., 2006; Wetzel et al., 2008), the right ACx is more engaged in distinguishing frequency-dependent differences between tones (Wetzel et al., 2008, 1998). Both cortices receive information from both ears with a leading contralateral processing (Kandel et al., 2013).

The ACx of the Mongolian gerbil can be subdivided into seven fields (Scheich et al., 1993; Thomas et al., 1993), which can be grouped as the primary and the secondary areas. In general, cortical fields can be identified alongside the vascular pattern and are designated by distinct features, like the cellular architecture (cyto-, fiber-, chemoarchitecture) and the cortical connections (thalamocortical, corticocortical and corticofugal). The primary area consists of the anterior auditory field (AAF) and the core of the primary auditory cortex (A1). Alongside the rostro-caudal axis of A1, the A1 displays a frequency-dependent gradient running from low to high frequencies, displaying a so-called tonotopy (Figure 2 B).

In young rodents, raised in acoustic environments, it was shown that their tonotopic mapping of A1 was specialized towards the environmental sounds (Kandel et al., 2013). This influence of passive sound exposure was not made in adult rodents, further strengthening the influence of the initial adaptation of tonotopic maps in the juvenile brain during the so-called critical period (Frischknecht and Happel, 2017; Patton et al., 2019). Especially during the maturation of the brain, formed synaptic connections become stabilized by a protein mesh called the extracellular matrix (ECM), which strengthens the built synaptic connections of the engrams (Frischknecht and Happel, 2017; Happel et al., 2014b; Happel and Frischknecht, 2016; Niekisch et al., 2019). The prior digestion of this protein-mesh in adult mice has been shown to improve learning associations in an auditory engaged reversal task, whereas non-treated animals did not improve in their performance (Happel et al., 2014b; Happel and Frischknecht, 2016; Niekisch et al., 2019). Tonotopic maps in awake adult rodents have been shown to be influenceable by stimulating neurotransmitter releasing brain structures like the nucleus basalis, in order to alter the tonotopic existing mapping in favor of a conditioned tone frequency (Kilgard, 1998). Likewise, in 2001 it was shown by Bao et al. that the electrical stimulation of the ventral tegmental area (VTA)—probably prompting the release of Dopamine (DA)—while playing 9 kHz pure tones caused an alteration in the tonotopic mapping of A1 over the time course of 20 days in adult rats (Bao et al., 2001). A recent study by Mitlöhner et al. further supports the influence of DA receptor activation—especially of D1 receptors—on the cleaving of the extracellular matrix (Mitlöhner et al., 2020). The latter two studies further promote the hypothesis that learning associations in a conceptual context can be supported by the release of neurotransmitters such like DA to alter stable tonotopic maps beyond the critical period, potentially forming new context related engrams in adult rodents.

## I.V Local field potentials and current source density

Cortical activity can be subdivided into two mesoscopic levels: Action potentials (APs) and local field potentials (LFPs).

Whereas APs reveal the immediate cellular response of inhibitory and excitatory neurons, LFPs reveal the overall population response of multiple cells at once. Henceforth, the LFP provides a more global output scale of cellular populations that share a common *modus operandi*.

Within cortices like the ACx, this recorded tone evoked layer-wise activity is based on the superposition of local extracellular sink (negative currents) and source (positive currents) activities within the recorded spatial column. Those currents are induced by—primarily—the cation influx in activated cell populations into the cells, leaving a netto negative charge in the extracellular room (sinks). The resulting unbalance enforces nearby cell populations to release cations into the extracellular room (sources) to counteract the activation in time. The overall summation of this electric current flow results in the LFPs, which are lacking the spatial information of their origins (Freeman and Nicholson, 1975; Mitzdorf, 1985). By calculating the current source density (CSD), the second spatial derivative of the LFP, it is possible to restore and measure the spatiotemporal information of cortical activity along the 32-channel shaft electrode and to define early thalamocortical inputs, and late corticocortical and intracortical processing events, to get further insides into the involved cortical microcircuitry (see Figure 2 D and Figure 12).

Based on anatomical knowledge of the neocortex (section I.III), corresponding sink and source activities can be associated with certain layers. The combination of the spatiotemporal CSD pattern and the possible laminar projections between layers (see Figure 3 on page 12), therefore, allowed to derive a common canonical microcircuit model within the neocortex (Atencio et al., 2009; Dhruv, 2015; Douglas and Martin, 2004). Alterations of those canonical microcircuits can be further analyzed by direct (within the cortices) and indirect manipulations (other subcortical structures) to get new insights into neocortical adaptions. Especially the interaction of various subcortical structures like the VTA with the neocortex allows for a better understanding of learning and memory related alterations of the circuitry and thus improves our understanding of the brain. From literature, it is known that the release of various neurotransmitters

orchestrates the cortical processing of the columnar microcircuits in different ways. Thus the close investigation of subset connections between subcortical structures, the associated neurotransmitters and the neocortical targets via spatiotemporal methods like the CSD analysis allows us to get new insights towards these subcortical-cortical connectomes.

## I.VI The origins and influence of cortical dopamine in the primary auditory cortex

As already introduced in section I.IV, DA is involved in the loosening of the extracellular matrix eventually allowing the formation of new context depending synaptic connections of new engrams. The described effects are the results over a time course of 20 days. Still the question arises, how does DA immediately affect cortical activity during tone evoked processing?

In 1997 Stark and Scheich published a microdialysis study in which they investigated the increase of cortical dopamine during a shuttle box avoidance task (Stark and Scheich, 1997). In this study, dopaminergic levels started increasing 15 min after the onset of the training and continued increasing for 15 min after the training, reaching more than 150% of the initial baseline levels. A subsequent set of studies (Stark et al., 2004, 2001, 2000, 1999) further verified the causal relation between the dopaminergic level increase in cortical regions and improvement of performance as well as the artificial mimicking of increased DA levels by the D1/D5 receptor agonist (SKF-38393) application prior to the training sessions (Schicknick et al., 2008).

The potential effects of DA on cortical processing were more thoroughly investigated by Happel et al. in 2014, by the systemic application of SKF-38393 and comparing pre- and post-recordings of sound-induced processing in anesthetized Mongolian gerbils (Happel et al., 2014a). Eventually, Happel et al. found that the agonist increased the infragranular processing, which is coinciding with the cortical receptor distribution of D1/D5-receptors in supra- and infragranular layers.

In general, the specific cortical distribution of dopaminergic D1/D5 receptors within supra- and infragranular layers (Happel, 2016; Lidow, 1995; Lidow et al., 1991; Radnikow and Feldmeyer, 2018) hint at a local necessity for a dopaminergic effect

modulation that might affect the efferent cortical bottom-up as well as the corticofugal top-down processing.

So far, two potential sources for the cortical dopamine have been identified: the ventral tegmental area (VTA) and, more recently, the locus coeruleus (LC).

The VTA has been closely linked with the release of dopamine since 1975 (Koob et al., 1975) as well as to addictive behavior (Gorelova et al., 2012; Hyman and Malenka, 2001; Kauer, 2003; Polter and Kauer, 2014). The VTA itself consists mainly (55-65% ~40.000 cells) of dopaminergic cells, followed by GABAergic (30-35%) and glutamatergic (2-5%) neurons (C. L. Liu et al., 2012; Ntamati and Lüscher, 2016; Polter and Kauer, 2014). The unequal distribution of cell types of the VTA is scattered across the seven regions of the VTA: The interfascicular nucleus (IF), the rostral and caudal linear regions (RL and CLI, respectively), paranigral nuclei (PN), parabrachial pigmented nuclei (PBP), parainterfascicular nucleus (PIF) and the rostral part of the VTA (VTAR) (Anderegg et al., 2015).

In 1996, Mirenowicz & Schultz described the reward prediction error (RPE), where the increase and decrease of spiking the spiking rate from dopaminergic neurons of the VTA were linked towards the error and reward prediction of a conditioned stimulus (Figure 4) (Mirenowicz and Schultz, 1996; Schultz, 1998). This local RPE phenomena is well described for the VTA. It has been shown that the RPE can also be found within cellular subpopulations of the PFC, striatum and amygdala (Schultz, 2016) as well as dopaminergic projections towards the nucleus accumbens and hippocampus (Russo and Nestler, 2013). Recent studies further proved that dopamine is co-released with glutamate and that the immediate response of the RPE is most likely of glutamatergic nature, whereas slow long lasting modulatory effects are related with DA (Lapish et al., 2006; Lavin et al., 2005).

DA related effects within the neocortex have been observed after an electrical burst stimulation of the VTA. Lavin et al showed in 2005 that the spiking rate within the PFC increases in an accumulative way leveling roughly 20 min after VTA stimulation in anesthetized rats (Lavin et al., 2005). The observed effects were contributed towards the activity of DA in the cortex since there was no increase in spiking rates seen for the same VTA stimulation protocol after a prior application of DA antagonist such like sulpiride, SCH23390 and reserpine. Based on the fact, that three out of four dopaminergic nerve tracts arise of the midbrain (substantia nigra pars compacta,

midbrain tegmentum and the VTA) (Kandel et al., 2013), it is highly likely that cortical DA arises from the VTA.

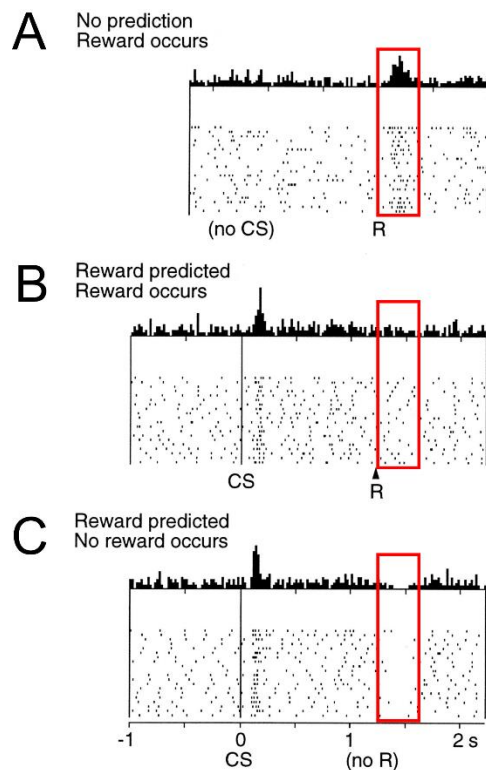


*Figure 4: Schematic representation of the reward prediction error within the neuronal population of the ventral tegmental area of monkeys*

Shown are the recorded spiking event within the VTA of an awake monkey as the sum of spike events as well as onset of the conditioned stimulus (CS) and reward (R) presentation. A) In the untrained state—without any stimulus conditioning—the spiking rate of dopaminergic VTA neurons increases shortly after the reward was given. B) In a trained animal the reward association is already linked to the conditioned stimulus presentation. Therefore, the spiking rate increases prior to the reward presentation. Since reward expectation was fulfilled, the spiking rate does not alter when the actual reward is presented. C) In a trained animal that does not receive any reward after the conditioned stimulus was presented, the spiking rate decreases around the time window when the associated reward should have occurred. Figure adapted from Schultz 1998.

The influence of the LC by neurotransmitters on the auditory cortex has been known since the 1970's (Foote et al., 1975), but it has been primarily associated with the release of noradrenaline. Recent studies show, that the time course of noradrenergic and dopaminergic effects coincide (Devoto et al., 2015, 2005, 2001). However, other studies indicate that stimulation of the LC also targets dopaminergic neurons of the VTA and vice versa, thus further prompting the central role of the VTA for influencing

the dopaminergic household of the brain (Guizard et al., 2008; Kim et al., 2016; Ornstein et al., 1987; Sara, 2009).

#### I.VI.I Is there a thalamo-cortical pathway between the ventral tegmental area and the auditory cortex?

Since the RPE reflects immediate learning associations within the VTA in terms of alterations in the spiking rates (Figure 4), the question remains if and how the dopaminergic signal is conveyed towards the auditory cortex.

Currently, in the widely accepted literature, the influence of the VTA towards the auditory cortex is rather neglected in favor of other more prominent projections (Figure 5 A) (Brocka et al., 2018; Kim et al., 2016). Most of those structures revealed immediate responses—within a few seconds—after optogenetic or electric VTA stimulations (Brocka et al., 2018) reflecting a RPE-like response. However, as indicated in the previous section I.VI, those immediate responses might rather be of a glutamatergic than of a dopaminergic nature.

For the first time Lou et al reported immediate effects after a prior electrical stimulation in the ACx of rats (Lou et al., 2014). In this study, it was revealed that the VTA stimulation resulted in a shortened time of the excitatory postsynaptic potentials on the level of neuronal firing, resulting in an increased strength and precision of A1 neurons. Yet, the dopaminergic nature of those signals was not verified by the prior application of dopaminergic agonists.

In 2008 Budinger et al performed one of the first studies verifying direct projections between the VTA and the ACx (Budinger et al., 2008). In this study, a fluorescent labeled retrograde tracer—dextran—was injected into the high- and low-frequency fields of A1. One week later, the animals were sacrificed and the cortical projections between A1 and various cortical regions were analyzed. Eventually Budinger et al. found that the non-sensory midbrain connections were the strongest (48.1%) with  $20.0 \pm 4.0\%$  deriving from the substantia nigra, the dorsal raphe nuclei (ipsi:  $9.5 \pm 2.7\%$ ; contra:  $3.8 \pm 1.3\%$ ), the VTA (ipsi:  $7.9 \pm 2.6\%$ ; contra:  $1.9 \pm 1.9\%$ ) and the LC (ipsi:  $3.7 \pm 1.4\%$ ; contra:  $1.3 \pm 1.3\%$ ). Thus, proving for the first time, that there are direct projections between the VTA and ACx (see Figure 5 BDC).

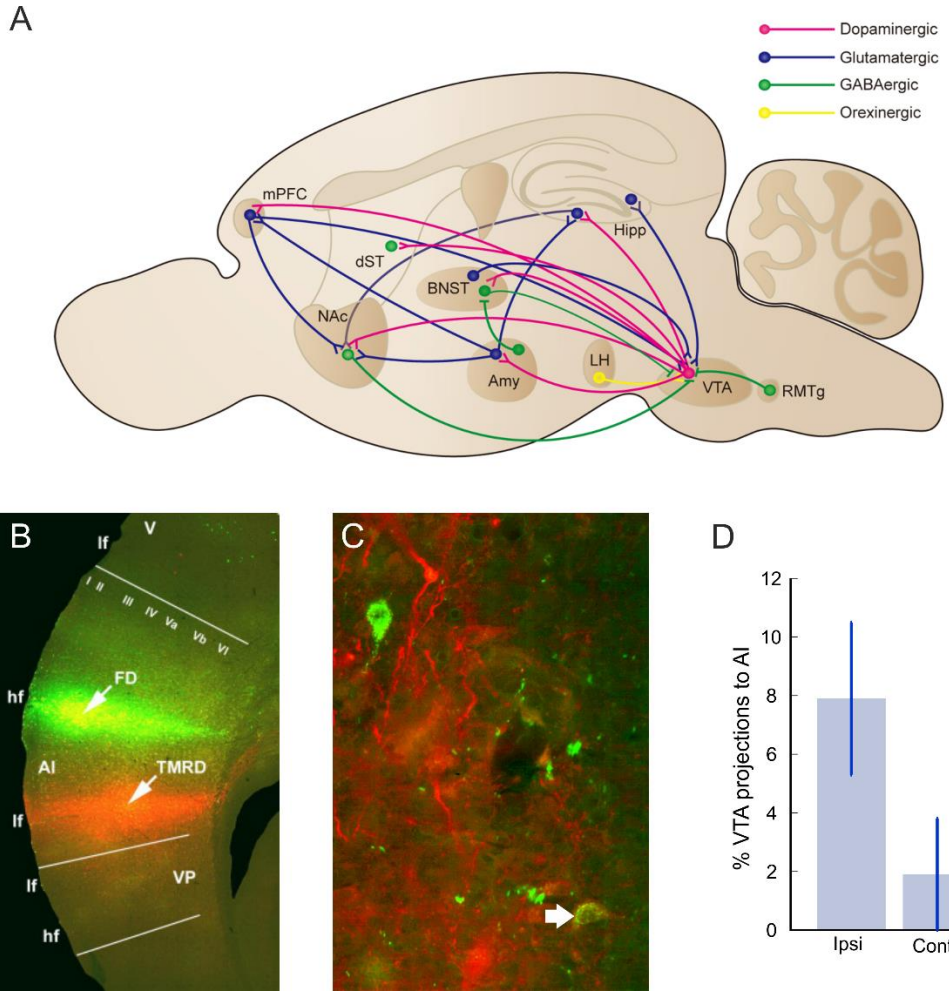


Figure 5: Verification of projections between the primary auditory cortex and the ventral tegmental area

A) Summary of the well-known and described projections within the brain. Especially dopaminergic projections from the VTA are known to project into the prefrontal cortex (PFC), nucleus accumbens (NAc), amygdala (Amy), Hippocampus (Hipp), dorsal striatum (dST) and the bed nucleus of the stria terminalis (BNST). B) Frontal cross section of A1 with fluorescent injections into high and low frequency field areas (hf and If corresponding) FD: fluorescein-labelled dextran (green) TMRD: tetramethylrhodamine-labelled dextran (red). C) Dopaminergic neuron projecting to AI identified (white arrow) by double staining of FD (green) and thyroxine hydroxylase (red) (Courtesy of Drs. Julia Henscke and Eike Budinger). D) Estimated percentage projections from ipsi- and contralateral VTA to AI (Cf. Budinger *et al.*, 2008). Figure A adapted from Kim *et al.* 2016; Figures B – D modified from Budinger *et al.*, 2008 and Budinger and Scheich, 2009.

Since the existence of the RPE in the ACx is a highly debatable topic (see previous section I.VI), and especially the slow and long-lasting effects of dopamine in the neocortex (Lavin *et al.*, 2005; Stark and Scheich, 1997) do not reflect the immediate response of VTA neurons (Lapish *et al.*, 2006; Mirenowicz and Schultz, 1996; Schultz, 1998), other theories should be taken in account for the cortical effect size of dopamine like the credit assignment problem (CAP).

The CAP can be subdivided into a structural (the single contribution of a specific structure) and a temporal aspect (Agogino and Turner, 2004). Unlike the RPE the temporal aspect of the CAP allows for the integration of relevant information within a prolonged time window (min, h and days), which would coincide with the previously described accumulative effects. Over a long repetitive time course, the release of dopamine might allow a loosening of the established ECM and allow for the formation of new context-related engram connections. This aspect can be combined with the theory of cortical plasticity of Ramón y Cajal.

In his theory Cajal states that a stimulus has two different effects (Kandel et al., 2013):

- 1) The excitability of nerve cells is affected by the stimulus itself.
- 2) It induces combinational plastic changes related to the stimulus.

The later point indicates that chemical synapses might display short-term physiological changes (seconds to hours) in which the synaptic effectiveness in-/decreases and long-term changes manifest in anatomical alterations.

As a summary, it can be concluded that direct dopaminergic projections between the VTA and the ACx are existing. However, due to the sparse nature of those connections and the unclear modality of the two involved neurotransmitters (glutamate and dopamine) the expected effects within electrophysiological measurements in the ACx are still rather elusive in the current literature. Effects from other dopaminergic structures affected by the VTA and eventually affecting the cortical processing in the ACx cannot be neglected.

## I.VII Optogenetics and its application for brain stimulation

The field of optogenetics mainly originates in the years 2002 and 2003 by the discovery of the two opsins, channelrhodopsins 1 and 2 (Nagel et al., 2003, 2002). The application of a light-controlled activation of transduced neurons and brain structures, yields in a potentially more precise and specific targeting than classical electrical stimulations (Deisseroth, 2011). By using viral transfecting agents like lenti- and/or AAVs, it is possible to include a promoter-sequence controlled copy of an opsin into cells with either a genomic integration (lentiviruses) or pseudochromosomes (AAV). The specificity of a promoter-controlled expression allows for a cell type specific expression of the opsin contributing to its precision. Verification of the expression of

the transduced opsins in the target regions is—in most cases—reported by the co-expression with fluorescent proteins like GFP, YFP and mCherry.

Stimulation of transduced cells within alive animals is achieved by the implantation of a light fiber to guide light (1-10 mW) towards the target region. Depending on the type of the used opsins, light stimulation will yield in either an activation or inhibition of cellular activity, eventually affecting behavior and transmitter induced neuromodulation. Based on the fiber properties, e.g. core radius and numerical aperture, as well as applied laser/light power, light transmission might yield into regional depth stimulation of more than 400  $\mu\text{m}$ , whereas within the first 200  $\mu\text{m}$  transmission power will decline by roughly 70% of its initial power<sup>1</sup>. The exact percentage loss of depth stimulation is still highly debated since the inhomogeneous nature of different cell types in respect of cell density and DNA condensation will affect the scattering of light within tissue and therefore does not allow for a defined generalization of the relation between depth and loss (Liu et al., 2015). For most opsins the required range of irradiance for a successful activation within tissue is assumed to lay between 1 – 5 mW/mm<sup>2</sup> (Senova et al., 2017).

However, the successful application of CamKII $\alpha$ -promotor driven approaches of the stimulation from excitatory neurons within the VTA have been shown on many occasions for an optogenetic intracranial self-stimulation paradigm (O-ICSS) in mice, gerbils and rats (Brocka et al., 2018; Guo et al., 2014; Lippert et al., 2018). For the O-ICSS, the rodents have been placed in a small box and were allowed to stimulate themselves by nose-poking a lever. This lever-pressing would result in a brief laser-pulse eventually exciting the transduced neurons of the VTA and leading to a reward associated addictive behavior. Depending on the proper placement of the fiber-implant within the VTA, animals would press the lever more than 50 times per minute.

Another advantage of the CamKII $\alpha$ -promotor sequence for the VTA stimulation is that—as already mentioned in section I.III.I—the CamKII $\alpha$ -promotor is associated with calbindin-positive cells in supragranular layers (Jones, 2001). Therefore, found expression of the co-expressed reporter proteins within the ACx of VTA transduced animals would further affirm the direct projections between the VTA and the ACx as reported by Budinger et al. 2008.

---

<sup>1</sup> Based on the calculations for the used parameters of our optogenetic stimulation paradigm ( $\lambda = 473\text{nm}$ , NA = 0.39, Power = 6.5 mW, fiber core = 200  $\mu\text{m}$ ) using Deisseroth's app on:  
<https://web.stanford.edu/group/dlab/cgi-bin/graph/chart.php>

In general, optogenetics is still a field that is rising in its importance and popularity, which is the reason why it has been declared as the method of the year in 2010 (“Method of the Year 2010,” 2011). Within the field, the research for new opsins, their functional roles and properties (Adam et al., 2018; Brunk et al., 2018; García-Martínez et al., 2015), as well as the mutagenesis of existing opsins (Dawydo et al., 2014) is still ongoing. Further research approaches yielded in the generation of new opsin based and inspired systems like luminopsins and chemical optogenetics (Berglund et al., 2016; Levitz et al., 2016) to surpass the—currently—invasive implantation of fiber implants into the brain.

## I.VIII Motivation and aims of this work

Learning associations beyond the critical period require the loosening of the existing physical structure of the engrams, an increase of the relevant signal representation as well as a corresponding teaching signal. Such roles can be fulfilled by neurotransmitters like Dopamine, which has been shown to affect the cortical plasticity over a time course of multiple days in favor of context driven stimuli. However, although the slow accumulative time course of released cortical dopamine has been shown for other cortical regions (Lavin et al., 2005), no investigation of the spatially induced changes in cortical layers during its release as well as the relatable changes of the stimuli representation of the cortical bottom-up and top-down processing have been reported yet.

The current literature mainly focuses on the RPE with respect to DA associated immediate time windows. However, clear evidence hints at two distinct events, which are the result of an early release of most likely glutamate followed by an accumulative increase of dopaminergic levels within the neocortex. Neither effects have yet been reported for the VTA-ACx pathway in a temporal manner.

Previous pharmacological studies have revealed that DA effects the cortical processing in a layer-specific fashion, potentially allowing for a boosted cortical integration of relevant information in a learning-related context (Happel et al., 2014a). Nonetheless, the origin of this context-bound DA levels have never been associated with the VTA, allowing room for the speculation of other structures potentially involved in the dopaminergic release. This aspect would be clarified by an optogenetic stimulation of the VTA and the resulting effects in the ACx.

Therefore the main questions, which will be answered in this thesis, are:

1. Does the VTA convey dopamine into the ACx?
2. Does dopamine have an immediate and/or long-lasting effect on the cortical processing?
3. Does dopamine allow an increase of the stimuli representation and how does it affect the cortical layers?

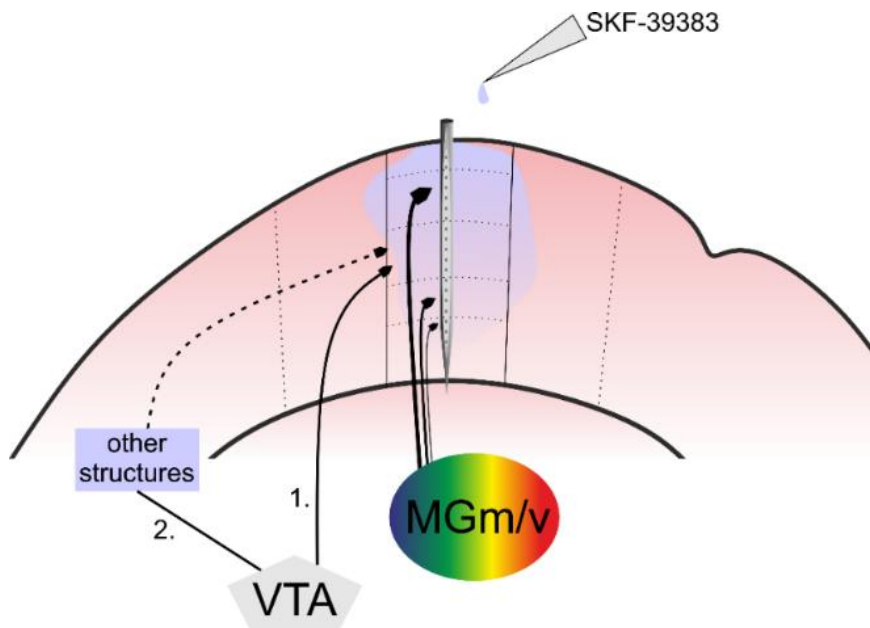


Figure 6: Summary of the underlying question and previous studies

In preliminary studies by Happel et al. (Happel, 2016; Happel et al., 2014a) it was shown that the topical application of SKF-39383, a dopaminergic agonist, is primarily affecting cortical input processing of infragranular layers. However, previous described effects did not mimic the existing transmission pathways from the midbrain and are therefore lacking the temporal time course from the activation of the VTA towards the effect side in the ACx. The existence of direct projections from the VTA indicates a direct pathway (1), whereas the indirect involvement of other structures cannot be neglected (2).

## II. Material and Methods

### II.I Optogenetic fiber implants

For optogenetic manipulation of the transduced VTA an inter-cranial fiber implant was required to conduct the laser-stimulation to deeper brain regions. Optogenetic fiber implants were manufactured according to the ‘Preparation of a head mount for an optic fiber for VTA-Stimulation in Gerbils 1.1’-protocol in the Protocol section of this thesis. Fiber implants have been checked for their light transmission properties at the acute setup before implantation (T0). Since transmission properties might differ between setups and manufactured implants, for instance due to reflections and entry angle of laser, the term laser-fiber-coupling efficiency (LFC) was used to describe the transmission properties at the acute setup. Note that the LFC in this context is valid for the implants, indicating the initial laser light power from the setup (10 mW) towards the, to be implanted, tip of the implant (~6.0-7.5 mW, compare Figure 15 B) and not for the entire setup as it is more commonly used in the literature (cf. Sidor *et al.*, 2015).

After optogenetic experiments and animal perfusions, the fiber implants have been removed from the animal skull and were measured for their LFCs a second time (T1). It is to be noted, that the loss of LFC between T0 and T1 does not exclusively result from the time of the experiment but also from the forceful removal from the skull. Yet, both values indicate the minimal and maximal values of laser power of the fiber tip, which were in the range of 160-214 mW/mm<sup>2</sup>. This range was calculated according to Ed Boyden’s home page<sup>2</sup>, including the mean LFCs of T0 and T1 from the C1V1 implants from the electrophysiological experiments (Appendix SFig 1).

Due to the fact that opsins are activated within an irradiance range from 1 – 5 mW/mm<sup>2</sup> (Senova *et al.*, 2017) and that this range is still the case up to 800 µm below the fiber tip for the experimental conditions<sup>3</sup>, one can assume that the entire VTA below the fiber tip is affected.

---

<sup>2</sup> <https://syntheticneurobiology.org/protocols/protocoldetail/35/9>

<sup>3</sup> Based on the calculations for the used parameters of our optogenetic stimulation paradigm ( $\lambda = 473\text{nm}$ , NA = 0.39, Power = 6.5 mW, fiber core = 200 µm ) using Deisseroth’s app on: <https://web.stanford.edu/group/dlab/cgi-bin/graph/chart.php>

### III.I.I Optogenetic preparation and intracranial self-stimulation

As described in Brunk et al. 2019, Mongolian gerbils (three months old, weights 60-100 g) have been anesthetized intraperitoneal (IP) by using an initial dose of 0.005 ml/g ketamine dilution (KD), consisting of 45% ketamine-hydrochlorid-solution (50 mg/ml, Ratiopharm GmbH), 5% xylazine (Rompun, 2%, Bayer Vital GmbH) and 50% of an isotonic 0.9% sodium-chloride (NaCl) solution (154 mmol/l, B. Braun AG). After initial KD injections, a butterfly catheter was placed IP for further injections to keep animals under stable anesthesia conditions. Based on the narcotic state of the animals, checked via breathing rate and foot-withdraw reflex, further doses (0.02-0.04 ml) of KD were applied in 10-20 min cycles. Previously chosen, self-manufactured, fiber implants (length 8 mm, Ø 230 µm, NA 0.39) with an LFC between ~60-75% (T0), were rinsed in excessive trypsin (Trypsin-EDTA solution, Sigma-Aldrich, T4049-500ML) just before implantation. Animals have been head-fixed in a stereotaxic device (DigiW Stereotaxic, Neurostar; Software: Stereo Device, Version 2.12.1) with ear and bite bars. The head angle of the animals has been re-adjusted until the anatomical position of bregma and lambda (Compare Figure 7 C) on the skull were planar to each other. The skull was drilled open at the target position -4.0 mm anterior-posterior (AP) and 0.5 mm medio-lateral (ML) towards the bregma reference (AP: 0.0; ML: 0.0 mm) (See Figure 7). 600-800 nl of a virus, containing an optogenetic construct, (*AAV5-CamKIIα-C1V1(E162T)-Ts-p2A-eYFP* or *AAV5-CamKIIα-eYFP*) were injected with a micropipette into the target region of the VTA in a dorso-ventral (DV) depth of 6.2 mm. Viral injection was performed with a steady flow of 100 nl/min (Micro injector pump, Model: UMC4, Worl Precision Instruments, Inc. Sarasota, FL USA). After an additional resting time of 5 min, the pipette was replaced by the fiber implant, which was lowered to the target position (AP: -4.0; ML: 0.5; DV: -5.8 mm). The implant was glued with UV-glue alongside two screws that were placed in the far parietal bone plates on the height of lambda. After surgery, the animals could awake and recover for 24h on a heated pad.

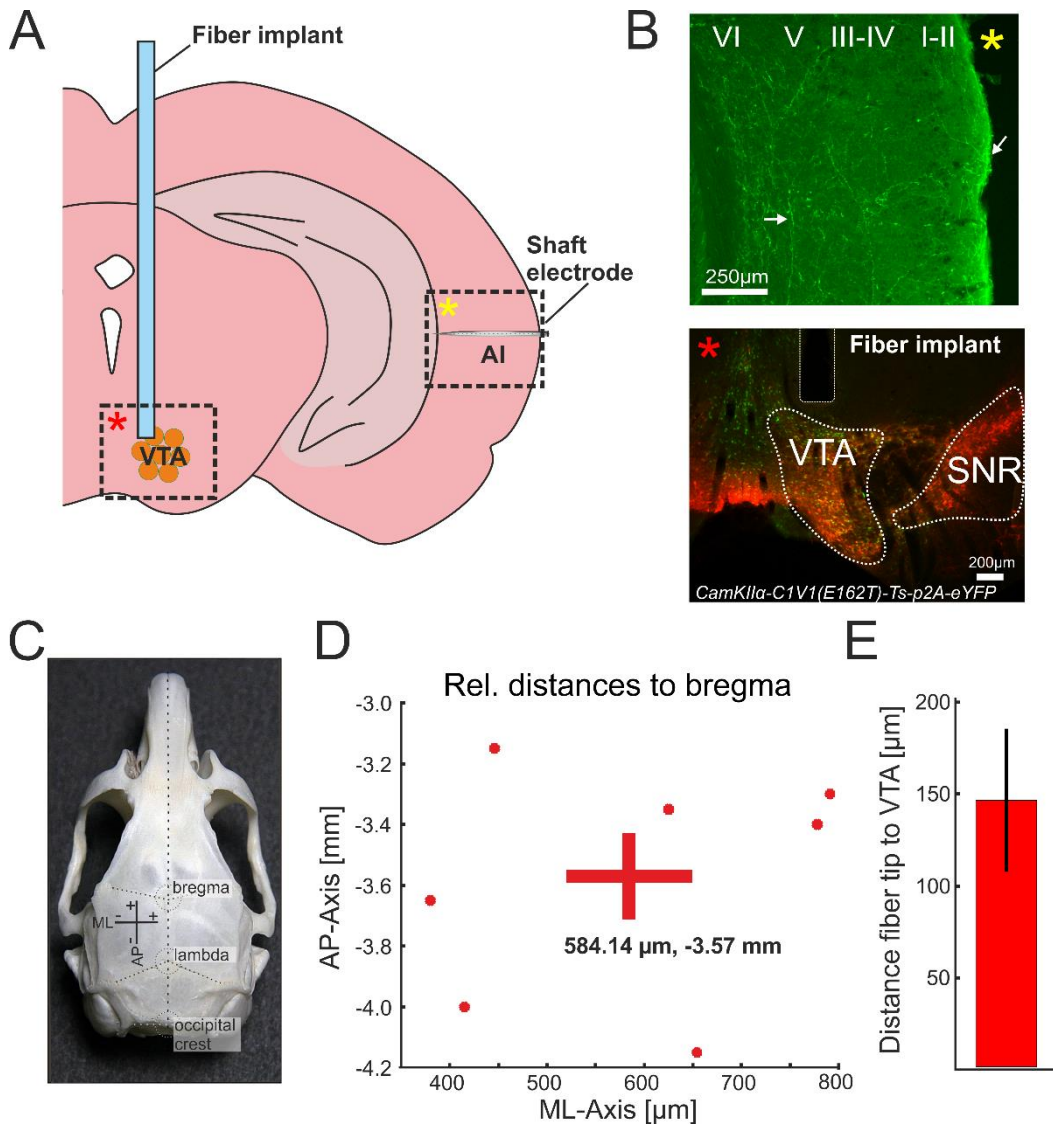


Figure 7: Anatomical locations and stereotactic verification

A) Hemispheric sketch of the optogenetic stimulation side of the transduced VTA and the implanted fiber as well as the recording side of AI and the insertion position of the shaft electrode. Corresponding anatomical example pictures were chosen for B) and are indicated with yellow<sup>4</sup> and red asterisks. B) The upper picture shows the cortical section corresponding to the region of A1 alongside cortical layers I-VI. YFP expression can be found mainly in supra- and infragranular layers (white arrows, layers I/II, V and VI, respectively). The VTA of this example animal was transduced with a CamKIIα-ChR(H134R)-eYFP construct. The observed fluorescence is a result of the thalamocortical projections between VTA and A1. The lower picture shows the co-fluorescence of the expressed CamKIIα-C1V1(E162T)-Ts-p2A-eYFP (green) with a tyrosine-hydroxylase antibody staining (red). The area of co-fluorescence is assumed to be the dopaminergic part of the VTA. In addition, the track of the fiber implant is to be seen above the VTA. C) Prominent landmarks (bregma, lambda and occipital crest) on the gerbil skull (modified from Radtke-Schuller et al., 2016). For the experiments, bregma has been used as the reference for medio-lateral (ML) and anterior-posterior (AP) position of the VTA. D) Anatomical positions of fiber implants of the C1V1 group ( $n=7$ ) relative to bregma. E)

<sup>4</sup> A detailed close up of the cortical section can be found in SFig 8.

Mean distance  $\pm$  SEM for the distance from the tip of the fiber track towards the area of co-fluorescence (Compare with B). Figures adapted from Brunk et al., 2019.

Three weeks after viral injection, the animals were placed into a 25 x 35 x 22cm<sup>3</sup> Plexiglas box for intracranial self-stimulation (ICSS). A fiber cable was attached to the animals' implants and kept in place via magnet (Visual example of acute setup in Figure 10). The animals were trained for 10 days with a session duration of 20 min. For ICSS the laser power of the laser (MBL-FN-473 100mW DPSS laser, CNI) was measured at the fiber cable with a laser power meter (PM100D, Thorlabs, sensor head: S120VC, Thorlabs) and adjusted to 10 mW. By nose poking the lever, at a height of 6 cm, the animals triggered a shutter device (SR 475 4-Channel Laser Shutter Driver Incl. Shutter heads, Stanford Research Systems) that was controlled via an analog-to-digital converter (USB-6009, National Instruments) by a LabVIEW program (32-bit 2009) (Lippert et al., 2018). The shutter pulsed the light stimulation with 10 pulses at 25 Hz. The stimulation was guided via collimator (KM100T, Thorlabs) and fiber cable into the animal's implant. Animals, that pressed the lever more than 850 times during one session (42.5 presses per minute) of the entire training, were used for further electrophysiological experimentation for the C1V1 group (Compare Section III.I). All animals expressing only an YFP-construct, except one, due to severe seizures during measurements, have been used for further electrophysiological experiments.

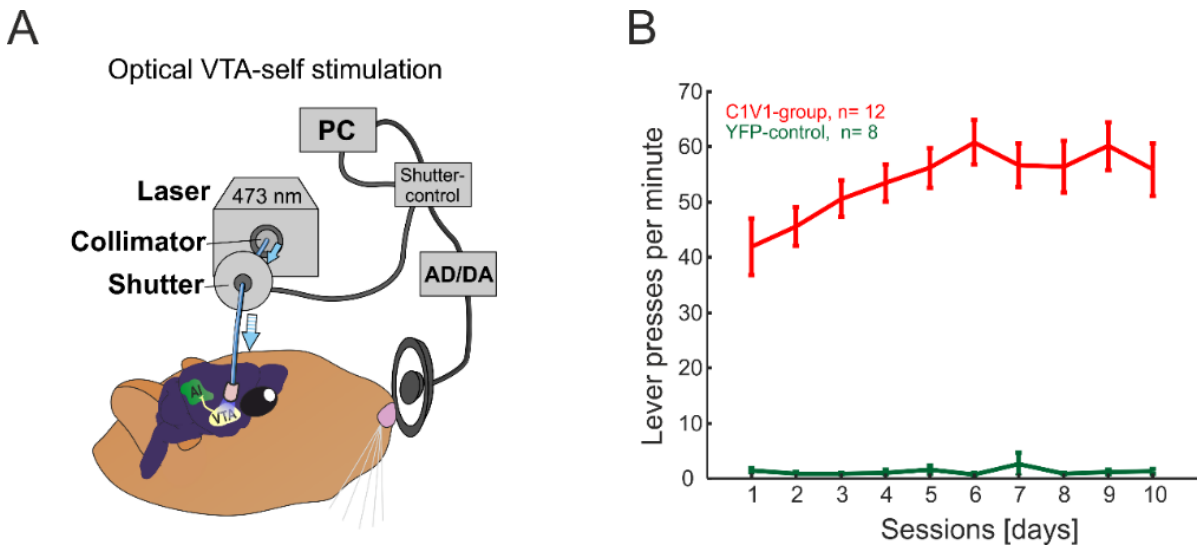


Figure 8: Intracranial self-stimulation and training performance

A) Schematic sketch of optogenetic ICSS. Each lever pressing was converted from an analog to a digital signal via analog-to-digital converter (AD/DA). The digital signal was transferred via the shutter-control into the computer, which was running the stimulation control program in LabView. The output of LabView was fed into the shutter-control to pulse the continuous laser light by the shutter. The pulsed laser light flash was guided via fiber implant towards the VTA eventually releasing dopamine, affecting potentially the A1 via thalamocortical projections. B) Average group results of lever presses per minute for a 10-day training. Each session took 20 minutes. C1V1 animals (red, n=12), YFP-animals (green, n=8). Figures adapted from Brunk et al., 2019.

### II.I.II Anatomical and histological validation of fiber position

For the anatomical and histological validation, the perfused brains were kept in 4% PFA overnight after the day of the experiment to allow for proper fixation. The medium was exchanged, and the brains were kept within a 30% sucrose solution until the swimming brains sunk down (1-3 days). The brains were indirectly deep-frozen (~25.0 °C) via Isopentan in liquid nitrogen for 2 minutes. The brains could now be used for the preparation of histological slices by a cryostat or stored at -20°C in a fridge. At the cryostat, the area around the VTA was cut in 50 µm thick coronal brain slices from which every second slice was used for histological staining against tyrosine hydroxylase (TH) and the remaining slices for Nissl staining (for details see protocols section).

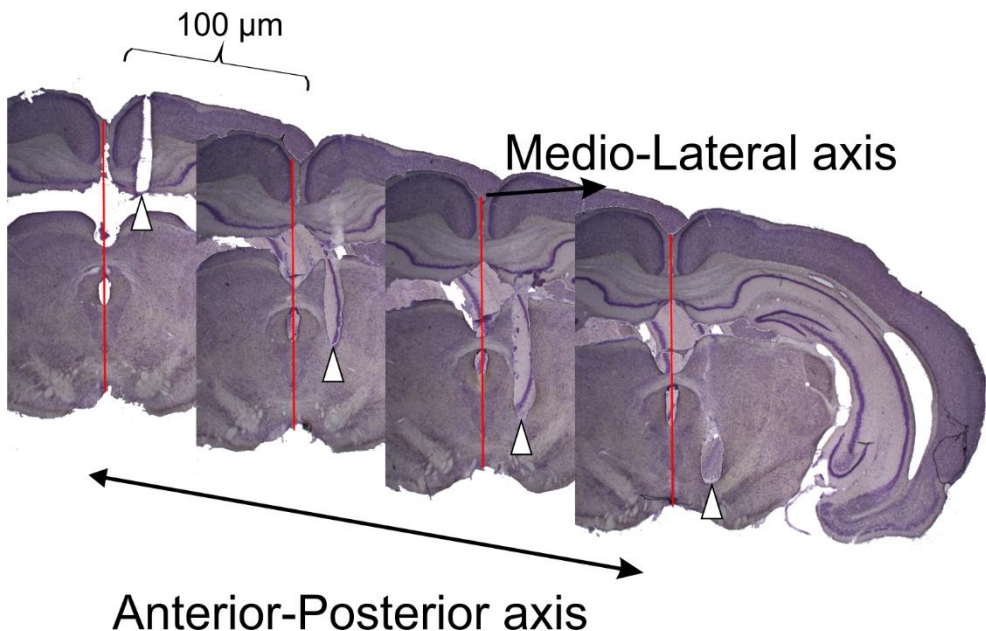


Figure 9: Conceptual visualization of anatomical estimations

Shown is a Nissl staining series of consecutive brain slice displaying the propagation of the fiber track (indicated by white arrows) alongside the anterior-posterior axis. The center of the slice is indicated by a red line and was used for the estimation of the medio-lateral distance of the fiber. The inter-slice distance was 100  $\mu\text{m}$ .

The Nissl stained slices were photographed at a Leica microscope (Axiocam 2, Leica GmbH) at a 1.25x fold magnification in histological order. The gerbil brain atlas (Radtke-Schuller et al., 2016) was used to estimate the position of the fiber track alongside the anterior-posterior axis relative to bregma (Compare Figure 9). For the fiber tip position, the slice with the deepest midbrain position was chosen. The central distance from the central line of the brain slice towards the central position of the wound was measured in FIJI ImageJ (Version 1.51g). For the histological examination, the corresponding slice of the fiber position was chosen in which the distance between fiber track and area of co-fluorescence was measured (Compare Figure 7 AB).

## II.II Acute setup for electrophysiological recordings

The used acute setup was built inside of a soundproofed chamber within a Faraday cage. The measuring station was placed on a vibration-free breadboard (PBH51510, Thorlabs, Inc). The animals have been head-fixed via a custom-made head holder in an open acoustic field with the animal facing away from the speaker (Tannoy arena satellite KI-8710-32) in 100 cm distance. Sound evoked LFPs within A1 were recorded

with a 32-channel linear shaft-electrode (Inter-channel distance 50 µm, NeuroNexus A1x32-50-413), which was attached to a self-made head stage. The recorded signal of the 32 channels was fed via an Omnetics connector (HST/32V-G2O LN 5V, 20x gain, Plexon Inc) into PBX2 preamplifier (Plexon, Inc), which band-pass filtered (0.7-300 Hz) and amplified 500-fold. A multichannel recording system (Multichannel Acquisition Processor, Plexon Inc) was used to digitize the data with a sampling frequency of 1 kHz. Pure tone sounds of 200 ms durations— spanning over eight octaves and ranging in between 125-32.000 Hz— were generated with Matlab (2006). The tonal presentations were pseudorandomized with 50 repetitions per tone and an inter stimulus intervals (ISI) from 600-800 ms. The generated sounds were sent into the setup as an analog signal by a data acquisition card (NI PCI-BNC2110, National Instruments). The used sound pressure level (SPL) was kept at 65 dB by a controllable attenuator (gPAH, Guger, Technologies) and amplified with an audio amplifier (Thomas Tech Amp75).

### II.II.I Acute measurements and experimental paradigm

At least three weeks after the initial operation, animals of the C1V1 or YFP group were used for the acute experiments. Animals have been anesthetized and were kept anesthetized the same way as previously described in section II.I.

Firstly, the regrown skin between the fiber implant and the area between eyes and nose as well as muscle, fat and binding tissue has been removed with a pair of scissors. The exposed skull was cleaned with 3% of hydrogen peroxide ( $H_2O_2$ ) and rinsed with 0.9% NaCl-solution. When the skull was clean and dry, an aluminum head bar was attached and glued with UV-glue onto the skull. In a second step, the skin above the temporal bone was cut open vertically along the cheek and kept open with bulldog clamps. The covering fascia was cut open alongside the edges of the chewing muscle like a pocket. The chewing muscle was carefully scratched off the temporal bone into the fascia pocket until the entire pocket could be removed in one piece. Then the temporal bone was trepanned with a dentil-drill to expose the covered ACx. A reference hole was drilled on the contralateral side of the open cortex to place and glue a reference wire (~ 5 cm, de-isolated stainless steel, Ø 200 µm) between the dura and the skull.

At the acute setup, the animal has been head-fixed with the head bar and rearranged until the ACx was most planar and easily accessible. For optogenetic manipulation, the

optogenetic cable was attached and kept in place to the fiber implant via magnets (Compare Figure 10). During the experiment the body temperature was kept stable at 34°C.

For cortical depth measurements of the tone evoked LFPs, a 32-channel shaft electrode was inserted perpendicular to the ACx, after a dura cut, in A1. The location for electrode implantation was chosen according to the vascular pattern of A1.

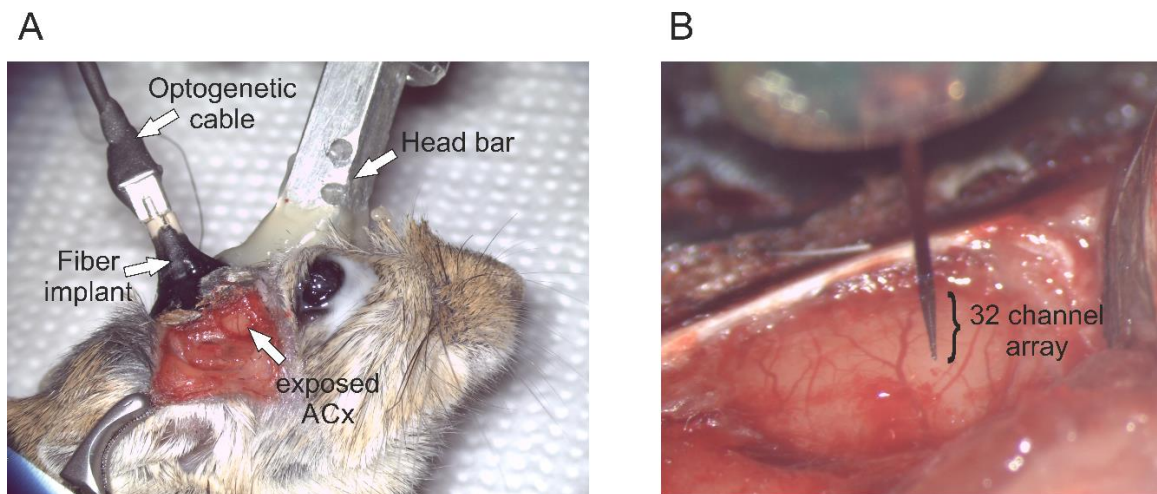


*Figure 10: Animal preparation for acute measurements*

A) After cleaning and drying the skull of the animal from muscle, fat, and binding tissue between the area of the implant and the eyes, an aluminum bar was glued on top of the area using UV-glue to fix the animal's head during the experiments. The ACx was exposed by removing the chewing muscle and trepanning the temporal bone. For optogenetic stimulation, an optogenetic cable was attached to the fiber implant and kept in place via magnets. B) 32 channel shaft electrode before the implantation. Localization of A1 was chosen based on the prominent vascular landmarks.

Laminar LFPs were measured, after implantation, for 45-75 min until CSD profiles had stabilized (baseline measurements, compare Figure 16 on page 50). From the pre-measurements the last three baseline recordings were taken as stable reference values for the data analysis. For the VTA stimulation within the C1V1 and YFP groups, the fiber implants were connected to a laser. The laser stimulation was synchronized and coupled for a single measurement with a pure tone presentation (25 Hz, 473 nm, estimated<sup>5</sup> irradiance at fiber tip ~160-214 mW/mm<sup>2</sup>; 350-400 repetitions in total). The phasic Laser stimulation of the VTA has been shown to result in increased spiking rates whereas a tonic stimulation yielded in comparable less spiking (Lippert et

<sup>5</sup> Based on mean T0 and T1 values from SFig 1

al., 2018). This measurement was taken as the laser-measurement, which was followed by a series of Post- measurements (>60 minutes) (Compare Figure 16 and SFig 2). The gerbils were perfused with 4% paraformaldehyde (PFA) at the end of the experiments as described in the literature (cf. Saldeitis et al., 2014) and brains have been removed for anatomical and histological validation (Figure 7). For the non-transduced Control group, a similar procedure was carried out except that no laser-measurement was performed. The entirety of the experimental procedure for the Control group was split into the initial 1h measurements (Pre) and the consecutive set of measurements (Post), whereas the first Post-measurement was used as a corresponding Laser measurement.

## II.III Mesoscopic investigation of cortical circuit functions using current-source-density recordings

As stated previously in section I.V, CSDs can be used in order describe cortical micro circuitry of neuronal populations within the recorded cortical columns of the recorded LFPs.

For spatial filtering, a so-called Hamming window with a kernel size of 300-400 µm (corresponding to 6-8 neighboring channels) is used, which allows for the influence integration of neighboring channels as well as the reduction of single channel noise while calculating the spatial derivative. Lower kernel sizes result in coarser CSD profiles allowing for a more detailed analysis especially of thalamocortical inputs, whereas higher kernel sizes result in much smoother CSD profiles eventually merging and/or erasing smaller events (cf. Figure 12 CD, Figure 13).

The CSD is calculated based on the relation of the LFP ( $\emptyset$ ), the coordinate of the single electrode ( $z$ ) and the inter-channel distance ( $\Delta z$ ) as follows:

$$(1) \quad -CSD = \frac{\emptyset(z+n\Delta z) - 2\emptyset(z) + \emptyset(z-\Delta z)}{(\Delta z)^2}$$

The average rectified CSD (AVREC) trace is a way to describe the overall evoked current flow within a column throughout the entire recorded time window (Compare with sketch Figure 17 A). Due to the positive current flow of sources and the negative current flow of sinks, the ideal mean of a CSD should be zero. To counter this, a

rectification is done to trace the overall current flow for all channels of the CSD resulting in the AVREC (2).

$$(2) \quad AVREC = \frac{\sum_{i=1}^n |CSD_i(t)|}{n}$$

Based on previous experiments with muscimol (Happel et al., 2010), which reduces corticocortical interaction, and the CSD quality check described by Harding (Harding, 1992), the residuum of the CSD (ResidualCSD) has become a stable to disentangle corticocortical from thalamocortical influence within a CSD pattern (Compare sketch for AVREC and ResidualCSD traces in Figure 11. Simplified, the ResidualCSD accounts for all non-local temporal unbalanced activities within the integrational cylinder around the electrode, which therefore can be associated with corticocortical input from nearby columns. Therefore, the ResidualCSD can be understood as a temporal imbalance within the spatiotemporal CSD pattern, which is unequal to zero if all channels are summed up (3).

$$(3) \quad \text{ResidualCSD} = \frac{\sum_{i=1}^n CSD_i(t)}{n}$$

Since previous studies were based on peak amplitudes of the AVREC and ResidualCSD traces, it was decided to also investigate changes in the peak amplitudes, especially since they displayed more stable and robust signals than the root mean square (RMS). A schematic representation of the AVREC and ResidualCSD signals is given in Figure 11.

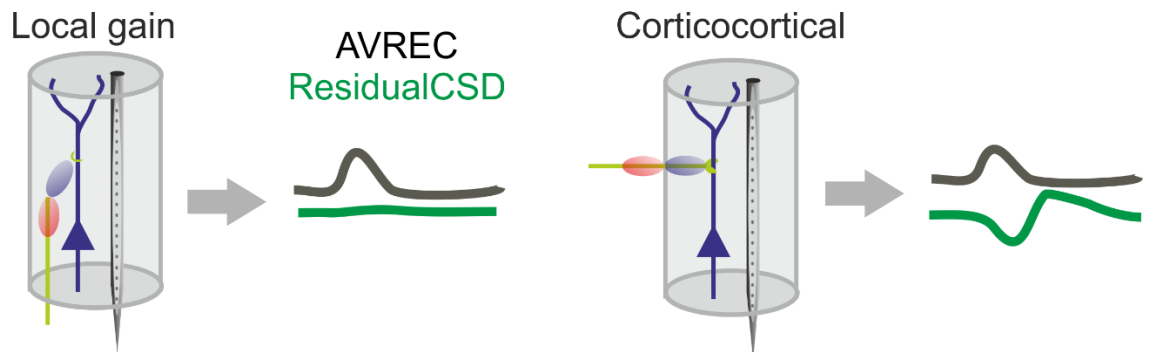


Figure 11: Schematic representation of AVREC and ResidualCSD signals

Left: Representation of thalamocortical input into the integrational cylinder of the electrode and column. The incoming sink (blue, negative current) and source (red, positive current) activities are temporally balanced and can only be detected by the rectification of the channel signals (AVREC) but not in the case of channel summation

(ResidualCSD). Right: Corticocortical integration of the incoming sink and source activities are temporally imbalanced since the signals need to invade the column. The signal contributes to the AVREC and the ResidualCSDs. Compare with Figure 2 D. Figure adapted from (Brunk et al., 2019).

Since CSD patterns display a spatio-temporal pattern of the cortical layers circuitry in terms of their specific cortical processing, certain layer associations can be assorbed based on the anatomical knowledge and electrophysiological data from previous studies (Saldeitis et al., 2014; Schaefer et al., 2015) (Figure 12).

For each animal channels have been chosen for a semi-automatic sink detection algorithm (see section II.IV.I), based on the generalized layer associations of Figure 12 C and D. Channel-based layer associations have been assigned according to common features as follows:

The strongest layer activation in layers III/IV derives from the lemniscal thalamocortical inputs of the MGv and were used as a primary indicator for layer associations. Depending on the individual anatomy and used kernel sizes one or two inputs of the infragranular layer can be found in layers Vb and VIa, receiving thalamocortical inputs from the MGm. All other non-input receiving layers were assigned accordingly.

Next to layer specific inputs, specific outputs can be associated to various layers. Especially layers V and VI are reported to project back into the MGd and MGv of the auditory thalamus potentially closing a feedback loop for thalamic inputs (Linden and Schreiner, 2003; Mitani et al., 1985; Schaefer et al., 2015). Linden and Schreiner hint at various ipsilateral projections from all layers from II to VI, whereas only layers III, V and VI have a contralateral contribution (Linden and Schreiner, 2003).

Evoked activity within the A1 can be plotted as a function of the tone evoked response power with respect to the played tones. Commonly, those functions display bell-shaped tuning curves, whereas the highest evoked power response is called the best frequency (BF). Therefore, the BF can be defined as a pure tone evoked processing, which triggers the maximal response of a neuron at the same stimulus intensity (Kaur et al., 2005). Next to the BF, the characteristic frequency (CF) is used in literature. The CF is defined as the frequency, which triggers the lowest firing rate within a neuron (Kaur et al., 2005). However, since the SPL was kept constant within the measurements the CF is not relevant in this thesis.

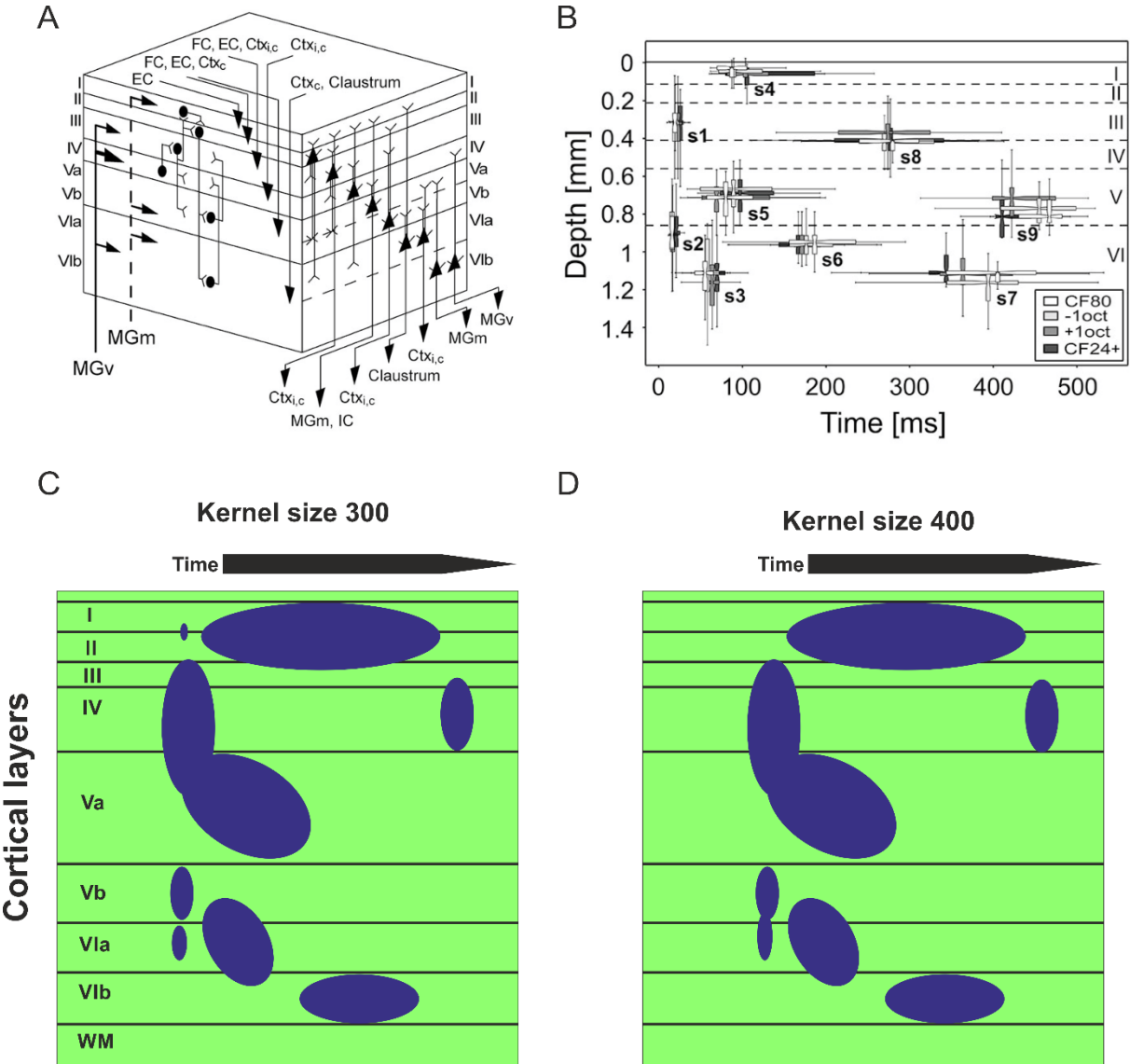


Figure 12: Cortical inputs and sink-layer association

A) Summary of cortical inputs (left side) from medial division of the medial geniculate nucleus (MGm, extralemniscal auditory pathway) and the ventral division of the medial geniculate nucleus (MGv, lemniscal auditory pathway) (adapted from Schaefer et al. 2015) and additional cortical inputs (EC: Entorhinal cortex ; FC: Frontal cortex; Ctx<sub>i/c</sub>: ipsi-/contralateral cortical hemisphere) as well as the cortical outputs (right side). B) Pure tone associated onset latencies according to automated sink detections (A and B adapted from Schaefer et al. 2015). C) Proposed schematic sink-layer association at a kernel size of 300 for a click condition for a 32-channel electrode with an inter channel distance of 50 µm at 65 dB SPL. Source associated activity has been omitted. Note the clear distinguishable inputs in layers Vb and VIa and the faint input in layers I/II (Compare Figure 20 A). D) Proposed sink-layer association for the same conditions of C at a kernel size of 400. Due to the excessive spatial smoothing, the inputs of layers Vb and VIa merge into a single infragranular input (Compare with actual data in Figure 13 on page 38). In addition, the faint input of layers I/II gets lost most of the time due to extensive spatial smoothing.

## II.IV Data processing and sorting

Due to the nature of the experimental design, big data analysis needed to be automatized to reduce the human factor. This automatization had to detect and sort data according to the following sections.

### II.IV.I Sink detection

Due to variability on a single animal level i.e. BF differences between sinks in different layers due to variances in input structures (Compare Figure 12 A) and specific onsets, stable parameters for sink detections on a layer-specific manner were not assumed to be suitable for data evaluation. Hence, the sheer amount of single measurements made it more time consuming to be processed on a manual level. Therefore, a layer-dependent sink-detection routine has been established in MATLAB (R2017b). This semiautomatic routine is based on the layer-wise channel definition by the user and therefore offers a broader range of investigative parameters like a coarser definition (early/late infra-, supra- and granular) or a more specific definition (early/late; layer I/II, III/IV, Va, Vb, VIa, Vb/VIa and VIb).

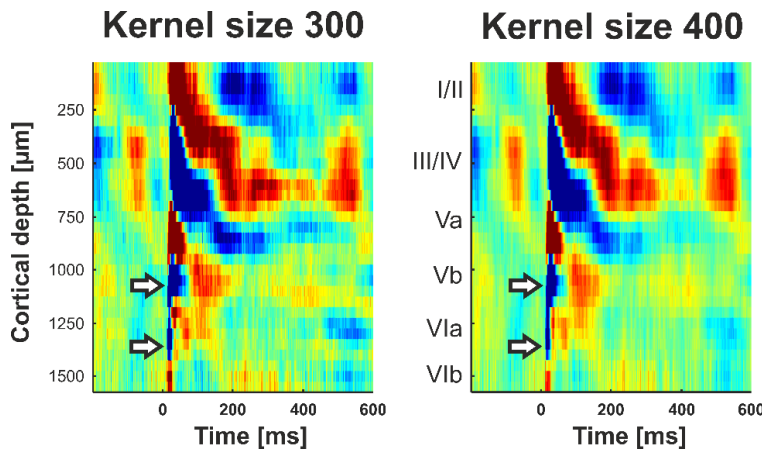


Figure 13: Comparison example of an evoked BF stimulation with different kernel sizes

Left: Kernel size 300, two different inputs in the infragranular layers become clearly distinguishable (indicated by white arrows). Right: Kernel size 400, the excess spatial smoothing merges the two distinguishable inputs of layer Vb and VIa into a single infragranular sink.

For initial layer definitions, the last pre-measurement of each animal was used and converted with a kernel size of 300  $\mu\text{m}$ . The coarser CSD image of the converted spatiotemporal pattern with a 300 kernel allows for a more defined spatial resolution compared to smoother CSDs with bigger kernel sizes (Compare Figure 13).

The layer-wise assorted channels have been applied for all animals to detect sinks of interest. For this study, the focus was set onto the early sink of layer III/IV, the early processing of Va, the combined early infragranular inputs of layers Vb/Vla, as well as the late processing of layers VIb and the supragranular layers I/II.

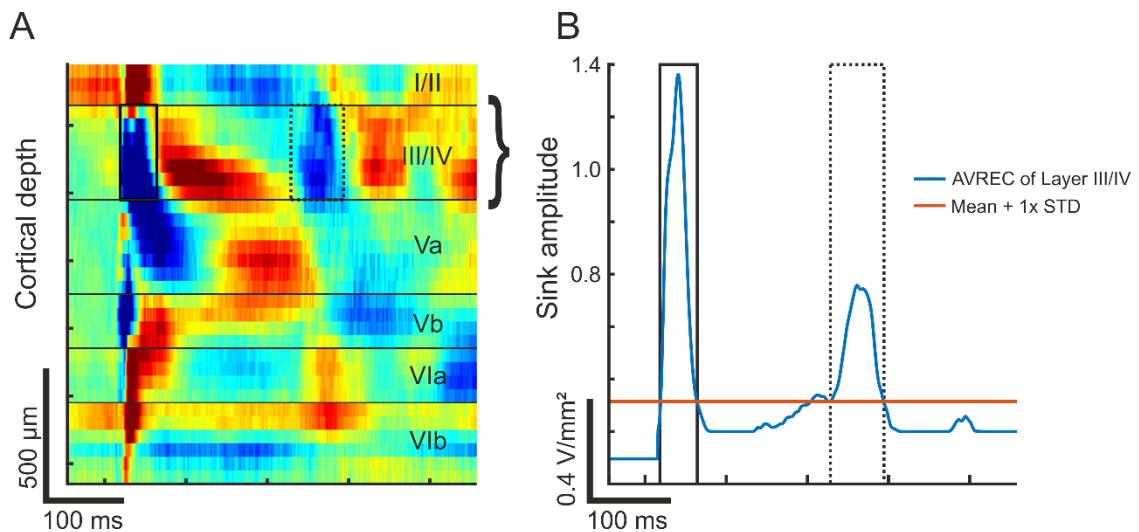


Figure 14: Layer depending sink detection

Exemplified detection of early and late granular sink. A) CSD measurement with layer indications. B) Source omitted rectified mean trace of layer III/IV. Based on the Pre-stimulus baseline, a mean and standard deviation (STD) was calculated to detect sink activity above the sum of both. Depending on sink onsets, early and late sinks can be detected within each defined layer.

The sink detection routine uses the overall mean and standard deviation (STD) from all baselines before tonal presentation from each measurement to have a steady reference value to check against the sink activity. Based on the assorted channels, the routine extracts the layers and omits source-associated activity. The mean value of the remaining sink-associated values is calculated and inverted to detect interceptions with the sum of the baseline mean and the corresponding STD. Depending on predefined stimulus onset limits ( $\leq 50$  ms: early,  $> 50$  ms: late), detected sink activity is deemed as early or late. In case of a multiple sink detections in the later phase, the sink activity of the highest peak activity is chosen by the MATLAB routine. Detected sink peak

amplitudes (PeakAmps), Peak-latencies, sink on-/offsets, durations and RMS values are stored within a structure to be processed in a later step. Since PeakAmps were used in previous studies (Happel et al., 2014a) and in general displayed the most stable parameter within animals as well as during measurements, the focus of this study was set on the temporal development of PeakAmps.

## II.IV.II Data sorting and preparation

With respect to the overall group analysis, the sheer amount of different measurements on a single animal level required a common methodology. Therefore, two different approaches for group data sorting on a single animal level have been implemented: The granular sink based (GS-based) sorting uses the direct input of the granular layers to calculate the PeakAmp tuning curve for the estimation of the columnar BF. All other data points are sorted accordingly around the early granular sink BF as center. The self-tuning based (ST-based) sorting is based around the idea of a layer independent tuning, due to other and/or additional thalamic and non-thalamic inputs (Compare Figure 12 A) (Rothschild et al., 2010; Tischbirek et al., 2019). Hence, BFs and tuning curve widths of, for instance, early infragranular and early granular inputs are not always coinciding in their activity and offer BF-shifts towards each other. Therefore, as an additional output for the ST-based sorting, a BF-shift plot is generated with the early granular PeakAmp BF as the 0-reference (Compare Table 1 & SFig 4).

Based on the fact, that the ST-based sorting omits potential effects of BF shifts within layers and provided the most stable time course within the Control groups (Compare SFig 4), it was decided to use a ST-based sorting to account for power increasing effects within all groups (C1V1, YFP and Control) to reveal associated effects of VTA stimulation within A1.

For further data reduction, a binning method was implemented that bins all octaves above and below the BF pairwise ( $\pm 1\text{-}2$  and  $\pm 3\text{-}4$  octaves). This would allow an equidistant analysis of near- and non-BFs and is in line with previous reports (O'Connell et al., 2014).

The ST-based sorting was applied to the entire time series of each single animal. For the group analysis, all single animal data were normalized by the mean value of the last three measurements before (Pre) the tone coupled optogenetic stimulation of the VTA (Laser). Time courses were plotted and analyzed on columnar and layer-wise

levels for the time from -22.5 min before (Pre) and 52.5 min after laser stimulation (Post). Since columnar activity is mainly driven by the layer III/IV input, it was decided to use the GS-based data for the overall columnar signals (AVREC, ResidualCSD), whereas ST-based sorting was used for the single layers.

Table 1: Layer associated BF-shift tendencies relative towards layer III/IV

<i>Layer sink</i>	<i>Mean Shift towards III/IV</i>	<i>Absolute mean shift towards III/IV</i>
I/II	-0.1818 ± 0.2451	1.7662 ± 0.1394
III/IV	0.0 ± 0.0	0.0 ± 0.0
Va	0.2078 ± 0.1698	1.1688 ± 0.1068
Vb	-0.5974 ± 0.1697	1.2727 ± 0.1104
Vla	-1.2857 ± 0.1196	1.4156 ± 0.0984
Vb/Vla	-1.2727 ± 0.1586	1.6364 ± 0.1061
VIb	-0.9610 ± 0.2144	1.7143 ± 0.1394

Relative BF-shifts in octaves of non-granular layers towards the BF of layer III/IV within the naïve Control group ( $n=7$ ). Mean shifts (mean ± SEM) reveal the overall tendencies of most layers, except layer Va, towards lower frequencies relative to the granular layer. Absolute mean shifts show the octaval distance tendencies independent of the shift tendencies.

On the single layer level, the resulting graphs were expected to be more stable unless an overall power increase changed the cortical processing independently from the current BF frequency. Significances were evaluated utilizing linear mixed effect models in R and a ± 10% criterion.

## II.V Linear mixed effect models (LMMs)

The principal concept of linear mixed effect models was first established by Ronald Fisher in 1919 (Fisher, 1919). Fisher envisaged including non-definable factors such like the environment into the classical Mendelian scheme of inheritance.

Common statistical analysis in neuroscience utilizes linear regressions to estimate significant effects. However, unlike LMMs, linear regressions do not take individual differences or non-defined parameters like the temporal development into account.

To get around the limitation of the before mentioned methods LMMs, therefore, increase the correlation by pooling the inter-individual differences of the random effects from the fixed effects of the population.

For the analysis within each animal group, all parameters of the recorded single trials, were animal-wise normalized by the mean value of the initial pre-measurements before the optogenetic manipulation of the VTA. The resulting time course of the measurements was treated as fixed effects for each group whereas the animals themselves are contributing to the random effects. The logic behind this methodology was to find differences between the animal groups (naïve control, YFP and C1V1) for the temporal signal development for each parameter of interest (early/late AVREC; early/late ResidualCSD; PeakAmps of late layers I/II, Va and VIb; PeakAmps of early layers III/IV and Vb/Vla) for each group, measurement and interaction between groups and measurements.

Significant differences of the C1V1 and YFP group have been calculated with respect of the naïve Control group. To further reduce the amount of significant differences towards the naïve Control group, an additional  $\pm 10\%$  criterion was applied, which needed to be exceeded as well.

Single trial data have been sorted within Matlab (2017) and exported as CSV-files to be further processed within R (R Studio; R 3.5.1). LMMs have been calculated with the lmerTest-package (3.0-1). Significances of the C1V1 and YFP groups towards the naïve Control group have been calculated using the car-package (3.0-2) by performing a Wald-Chi-square test for the group, measurements, and the group/measurements interactions.

For the calculation of LMMs of each parameter of interest in within each group during the time course of measurements, equation (4) was used for calculations of LMMs within R.

$$(4) \text{ Parameter} \sim \text{Group} + \text{Measurements} + \text{Measurements} * \text{Group} + (1 | \text{subjects})$$

This formula assumes a fixed slope for the LMMs but random intercepts on a single subject level.

### **III. Results**

The following sections enlist the results that contribute to driving questions stated in section I.VIII.

Although the Mongolian gerbil is a well-established model organism of choice for auditory investigations, it is a less favorable model for optogenetic experiments since—unlike for rats and mice—only wildtype strains are available. Also, the anatomical brain atlas for the Mongolian gerbil was only published rather recently (Radtke-Schuller et al., 2016). Therefore, the exact anatomical location of for VTA had to be found and validated on a more empirical level with the primary focus on a dopamine-driven behavior by optogenetic intracranial self-stimulation (O-ICSS).

Based on the O-ICSS performance, groups were assigned to derive the performance associated differences in lever pressing (high, medium and low, details in section III.I) to the fiber properties and anatomical position.

For the electrophysiological experiments, only animals of the high performing group were chosen to ensure a reasonable amount of released dopamine for the entire experimental time course. To affirm the VTA projection towards the auditory cortex the neocortical regions of the temporal lobe from two animals were analyzed for the co-found of YFP expression.

For the time course of the experiments the effects of the optogenetic C1V1 group needed to be compared towards an YFP and a naïve control group to account for laser induced effects as well as for the to be expected temporal development of the signal without any optogenetic manipulations. To reveal immediate effects of the direct projections from the VTA towards the ACx a set of only laser stimulations was performed without tonal presentation.

The temporal changes of the dopaminergic effects were investigated on the overall columnar level as well as on a layer-specific level for all groups. The dopaminergic nature of the VTA induced effects were further validated by the application of a dopaminergic antagonist, which would potentially reverse and block the associated effects.

### III.I Validation of VTA targeting

In literature, dopamine has been strongly associated with activation of the ventral tegmental area and thus provides a reasonable explanation as the primary source of cortical dopamine (section I.VI). Many experiments in rats and mice have shown that the electrical and optogenetic stimulation of the VTA can be utilized in an intracranial self-stimulation paradigm to induce an addictive lever-pressing behavior (Brocka et al., 2018; Fibiger et al., 1987; Fiorino, 1993; Lippert et al., 2018). Since the exact location of the VTA for the Mongolian gerbil was published more recently and due to the fact, that the opsinal expression in wild-type animals is rather unspecific, optogenetic intracranial self-stimulation (O-ICSS) was used to verify the effectiveness of the overall viral transduction. Another factor that might have influenced the efficiency of the O-ICSS was determined to be the properties of the used fiber implants.

Transduced animals (C1V1 n=35, YFP n=8) have been trained for 10 days within the O-ICSS setup (compare Figure 8 on page 30 and Figure 15 A on page 45) for 20 min sessions (described in section II.I.I).

Since all YFP animals did not show any addictive behavior all except one animal—due to severe seizures— were included in the electrophysiological experiments. The C1V1 animals were subdivided into three groups (single animal data in SFig 5):

1. High-Performer (HP): animals pressing the lever at least once more than 850 times during the time course of the 10 days
2. Medium-Performer (MP): animals that were pressing the lever at least twice more than 300 times during the time course of the 10 days
3. Low-Performer (LP): animals that did not show any improvement of performance during the time course of the 10 days

Potential performance drops were not taken into account for grouping, however in most cases—especially the in the HP subgroup—no drop in performance was present.

For the electrophysiological studies, only animals of the High-Performer C1V1 group were chosen since the robust pressing behavior was taken as indicator for sufficient DA release also potentially in the ACx.

The subgroups were used to investigate the influence from potential parameters (Figure 15 BCD) such like the LFC from the fiber, the distance between fiber tip and area of co-fluorescence and the actual fiber position in the following sections.

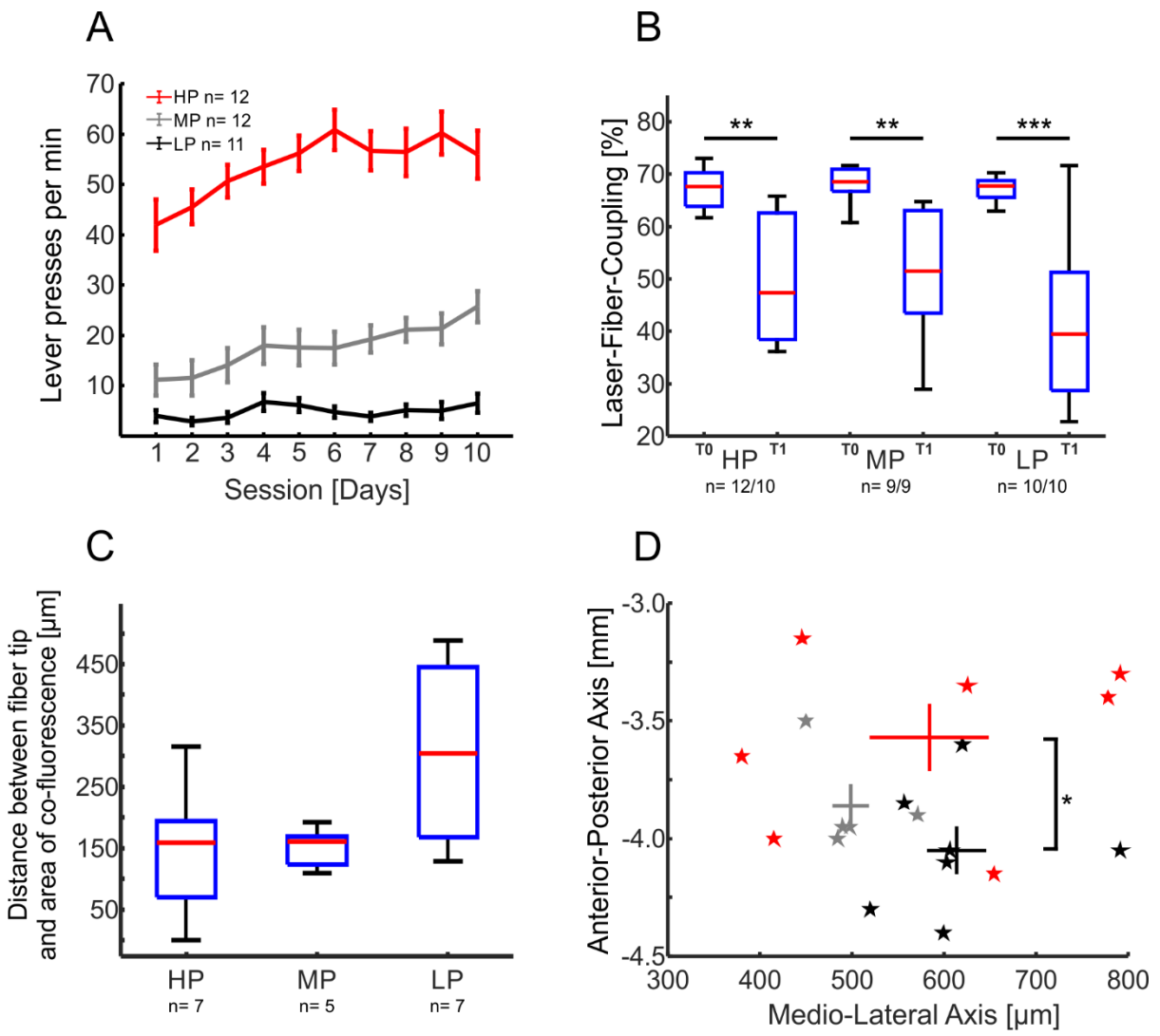


Figure 15: Anatomical validation based on initial C1V1 groups

Different aspects of animal performances for the initial C1V1 group. A) Averaged group lever pressing performances during a 10-day training course. Animals have been assorted afterwards according to their performances into High-, Medium- or Low-Performer (HP, MP and LP, respectively). B) Laser-Fiber-Coupling efficiencies (LFCs) of the manufactured fiber implants before the operation (T0; HP: n= 12, MP: n= 9, LP: n= 10) and after the experimental measurements (T1; HP: n= 10, MP: n= 9, LP: n= 10). The LFCs have also been sorted according to the animal groups (HP, MP and LP). Student t-tests between T0 and T1 values within groups were overall significant (HP: p= 0.0015, MP: p= 0.0061 and LP: p= 8.26e-04). C) Estimations of the distances between the tip of the fiber implant and the area of co-fluorescence (Compare Figure 7 AB) for each group (HP:  $146.84 \pm 38.92 \mu\text{m}$ , MP:  $150.5 \pm 14.38 \mu\text{m}$  and LP:  $306.43 \pm 83.46 \mu\text{m}$ ). D) Relative anatomical positions of the fiber implants (towards bregma) for the anterior-posterior (HP:  $-3.57 \pm 0.14 \text{ mm}$ , MP:  $-3.86 \pm 0.09 \text{ mm}$  and LP:  $-4.05 \pm 0.1 \text{ mm}$ ) and medio-lateral axis (HP:  $584.14 \pm 64.79 \mu\text{m}$ , MP:  $498.4 \pm 19.87 \mu\text{m}$  and LP:  $613.71 \pm 32.32 \mu\text{m}$ ). Boxplots display the medians (red), 25<sup>th</sup> and 75<sup>th</sup> percentiles (blue box) and the extreme data points as tails.

### III.I.I Laser transmission properties of the used implants

In section II.I, the term “Laser-Fiber-Coupling” was introduced as a quality check of the laser light transmission properties of the fiber implants at the acute setup. By measuring the initial transmission properties of the implants ( $T_0$ ,  $n= 31$ ), a certain quality was ensured before the implantation ranging from 60.8 – 73.0% (Figure 15 B). The initial  $T_0$  values were assorted according to the groups and compared using a one-way ANOVA. The  $T_0$  values for the HP ( $67.14 \pm 1.03\%$ ), MP ( $68.22 \pm 1.13\%$ ) and LP ( $67.14 \pm 0.69\%$ ) groups did not differ ( $F (2,28) = 0.38$ ,  $p=0.6856$ ), assuring that the initial quality for all groups was the same.

After the electrophysiological experiments, the implants were removed and re-measured for their LFCs at the same setup for all animals of the C1V1 group. The newly measured values ( $T_1$ ,  $n= 29$ ) were overall reduced, ranging from 25.5 – 65.8% evenly distributed among the groups (HP:  $50.18 \pm 3.88\%$ , MP  $50.49 \pm 4.22\%$  and LP:  $42.26 \pm 5.06\%$ ). A consecutive one-way ANOVA of all  $T_1$  values within groups confirmed that the overall reduction was of a homogenous nature ( $F (2,26) = 1.12$ ,  $p=0.3406$ ).

Details of the Bonferroni post hoc test of the one-way ANOVAs are enlisted in Table 2.

For a direct comparisons between the  $T_0$  and  $T_1$  values within each group a student t-test was used, resulting in very significant (\*\*) decreases within the HP ( $p= 0.0015$ ) and MP ( $p= 0.0061$ ) groups and an extremely significant (\*\*\*) decrease for the LP group ( $p= 8.26e-04$ ) (See Figure 15 B).

Table 2: Group comparisons of LFCs

Comparison	Bonferroni post-hoc test
HP $T_0$ vs MP $T_0$	$p= 1$
HP $T_0$ vs LP $T_0$	$p= 1$
MP $T_0$ vs LP $T_0$	$p= 1$
HP $T_1$ vs MP $T_1$	$p= 1$
HP $T_1$ vs LP $T_1$	$p= 0.6307$
MP $T_1$ vs LP $T_1$	$p= 0.6159$

All p-values of the Bonferroni post-hoc test for all LFCs within groups for  $T_0$  and  $T_1$ .

### III.I.II Anatomical distance between fiber tip and VTA

Next to the LFCs of the fibers the anatomical distance between the tip of the fiber and the area of eYFP and thyroxine-antibody staining were investigated (compare Figure 7 B on page 28). As indicated in section I.VII, the theoretical power of irradiance is declining exponentially, resulting in the loss of 70% of the initial power within the first 200 µm. Therefore, far more distant fiber tips do not transmit enough power to the area of co-fluorescence, resulting in lower performances.

The performance derived grouping was used to investigate whether differences were a result due to different stimulation depths.

Distances were measured between the tip of the fiber track towards the area of eYFP and TH-antibody co-fluorescence (for details see section II.I.II on page 30).

The estimated mean distances of the HP ( $n= 7$ ) and MP ( $n= 5$ ) groups are close to each other ( $146.84 \pm 38.92$  µm and  $150.5 \pm 14.38$  µm, respectively), whereas the LP ( $n= 7$ ) group had a mean distance of  $306.43 \pm 83.46$  µm (Figure 15 C).

A one-way ANOVA comparison revealed no significant differences between groups ( $F(2, 13) = 3.22$ ,  $p= 0.0731$ ).

Details of the Bonferroni post hoc test of the one-way ANOVAs are enlisted in Table 3.

The required irradiance power for a successful opsinal activation lays between 1-5 mW/mm<sup>2</sup> (Yizhar et al., 2011). For all C1V1 subgroups this range was reached within the fiber distance.

Table 3: Group comparison of fiber tip distance to area of co-fluorescence

Comparison	Bonferroni post-hoc test
HP vs MP	$p= 0.9340$
HP vs LP	$p= 0.1991$
MP vs LP	$p= 0.1197$

Calculated p-values for fiber tip to co-fluorescence distances between groups.

### III.I.III Anatomical position of successful VTA stimulation by O-ICSS

As a last denominator, the relative fiber positions towards bregma were investigated. Since differences between rostral and caudal VTA pathways have been stated in literature before (Li et al., 2019), it is assumable that effect sizes differ according to the VTA stimulation side. In order to investigate the potential effects of the AP and ML positions (Compare Figure 15 D).

The one-way ANOVA for the anterior-posterior fiber position is shown to be significant ( $F(2, 16) = 4.47, p= 0.0287$ ) between groups (HP:  $-3.57 \pm 0.14$  mm, MP:  $-3.86 \pm 0.09$  mm and LP:  $-4.05 \pm 0.1$  mm). A consecutive Bonferroni post-hoc test revealed a significant difference between the HP and LP groups ( $p= 0.0269$ ).

For the medio-lateral distances the one-way ANOVA does not show significant differences ( $F(2, 16) = 1.41, p= 0.2721$ ) for the groups (HP:  $584.14 \pm 64.79$   $\mu\text{m}$ , MP:  $498.4 \pm 19.87$   $\mu\text{m}$  and LP:  $613.71 \pm 32.32$   $\mu\text{m}$ ).

Details of the Bonferroni post hoc test of the one-way ANOVAs are enlisted in Table 4.

The higher pressing rates of the HP animals by a more rostral position of the VTA stimulation are in line with the study of Guo et al. in rats (Guo et al., 2014).

Table 4: Group comparisons of anatomical VTA position

Comparison	Bonferroni post-hoc test
ML HP vs MP	$p= 0.7132$
ML HP vs LP	$p= 1$
ML MP vs LP	$p= 0.3555$
AP HP vs MP	$p= 0.3638$
AP HP vs LP	$p= 0.0269 (*)$
AP MP vs LP	$p= 0.8918$

Calculated p-values for the Bonferroni post-hoc test for medio-lateral and anterior-posterior positions.

### III.II VTA projections into the ACx

To further solidify the background of direct and indirect pathway connections between the VTA and the auditory cortex, in a preliminary experiment the VTA of two animals have been transduced with an adeno-associated-virus (AAV), containing a *ChR2(H134R)-eYFP* construct, to search for YFP expression within the temporal cortex and eventually in A1 (Figure 7B on page 28). In both animals YFP expression within the temporal cortex was found, being indicative for a thalamocortical pathway from the VTA towards the ACx. Interestingly, the traces of YFP were dominantly found in supra- and infragranular layers. These findings are matching with the expression levels of D1/D5-receptors within the cortex (Happel, 2016; Jacob and Nienborg, 2018). This procedure was a *vice versa* approach towards the anatomical studies of Budinger et al. in which fluorescently labelled dextran was injected into the high and low frequency fields of A1 to track cortical connections (Budinger et al., 2008; Budinger and Scheich, 2009) (Compare Figure 5 ABC). Eventually, Budinger et al. found cortical projections within the VTA, confirmed by an overlay of thyroxine hydroxylase immunostaining, and quantified the percentage amount of VTA to A1 projections for the ipsi- and contralateral sides ( $7.9 \pm 2.6\%$  and  $1.9 \pm 1.9\%$ , respectively; see Figure 5 C). Also, Kandel et al. stated in their book that the VTA projects into the temporal cortex (Kandel et al., 2013).

Accounting the results with the existing literature, it is assumable that there are certain connections between the VTA and the ACx. However, it was not verified whether these connections are of a sole dopaminergic nature or whether they are of a direct and/or indirect nature.

### III.III Optogenetic stimulation of the VTA increases columnar processing

Electrical stimulation of the VTA has been shown to boost cortical activity in an accumulative way (Lavin et al., 2005), which—in its temporal time course—is matching the dopaminergic levels within the ACx (Scheich et al., 1997). Application of the dopaminergic agonist SKF-38393 has been shown to affect cortical processing and behavioral performance. However, in both approaches the effects of VTA activity was

not mimicked and therefore, they do not reveal any insights into the cortical changes during and after a VTA associated DA release.

To ensure prior stabilized signals before the combined laser stimulation, a set of pre-measurements was performed for 45 – 75 min (Figure 16) from which only the last three pre-measurements were used for data normalization. After the laser stimulation set of post-measurements was done for more than 60 min with the same settings as the pre-measurements to reveal DA associated long-term changes.

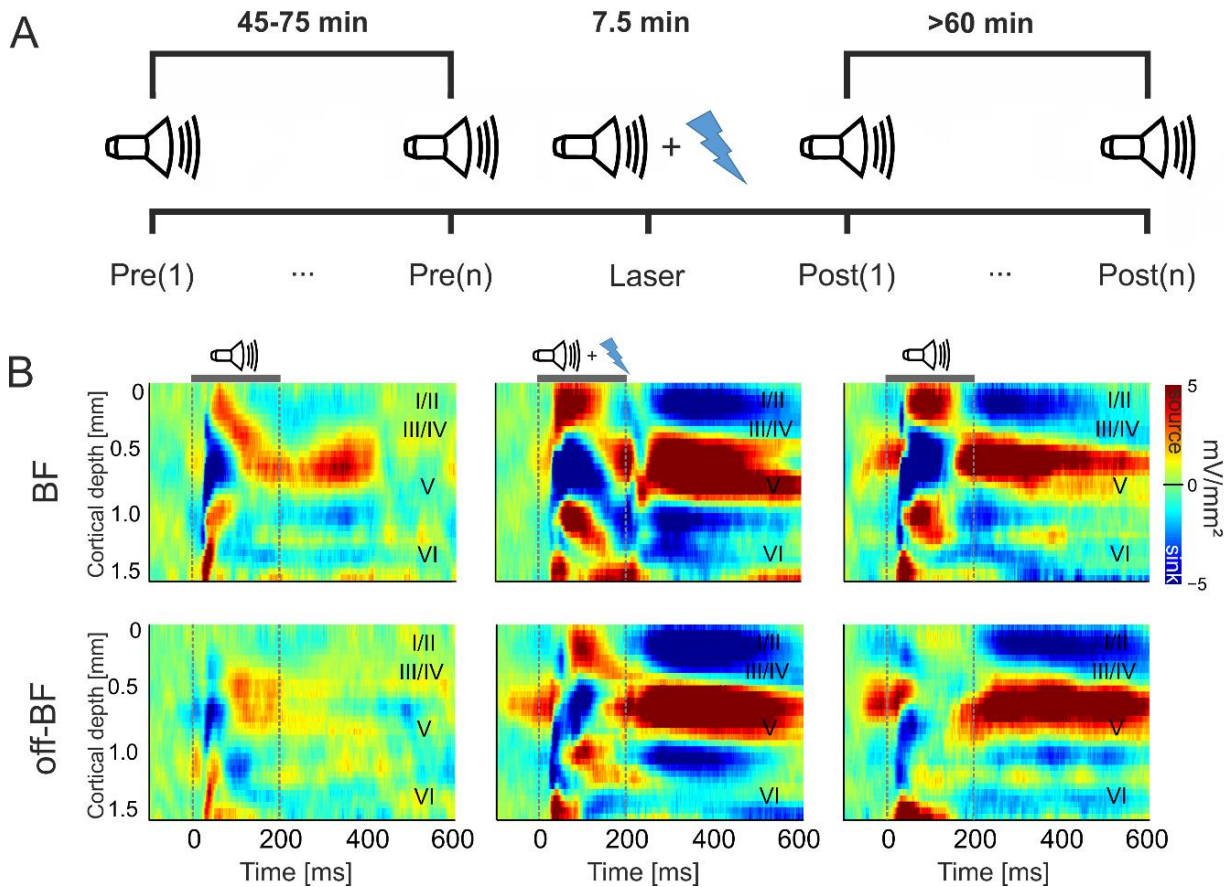


*Figure 16: Order of measurements and example measurement*

A) For temporal analysis of data, a common stable order of measurements was established, which included a set of Pre-measurements (randomized pure tones (7-8) with a duration of 200 ms, ranging from 125 Hz up to 32 kHz, 50 repetitions at SPL of 65 dB) till CSD pattern were deemed stable (45-75 min)(Compare SFig 2). For optogenetic animals (C1V1, YFP), a laser-measurement was applied consisting of the same stimuli as in the Pre-measurements, hence coupled with a 25 Hz laser-pulse for the duration of each tone with a final setup power of 10 mW. Afterwards a consecutive set of Post-measurements was applied, using the same stimulus conditions as for the Pre-measurements (>60 min). B) Exemplified CSD measurements from an animal of the C1V1 group for a BF (top) and an off-BF (bottom) for a Pre-, laser and a 30 min Post-measurement, respectively. Note the strong increase in sink activity in supra- and infragranular layers (I/II and V/VI, respectively). Figures adapted from Brunk et al., 2019.

For BF sorting on the columnar level the GS-based tuning was used, since the thalamic input of the granular layers in most cases was the most prominent activity and thus dominated the columnar processing.

Alongside the recording electrode, the overall cortical activity can be described on the level of two perspectives (compare section II.III).

For a brief recall, the rectification of all recording channels of the CSD is referred to as the average rectified CSD (AVREC) and reflects thalamocortical contributions whereas non-rectified contributions are used for the ResidualCSD, which reflects the corticocortical integration.

For this study, the early (0 – 50 ms) and later (80 – 300 ms) parts of the AVREC and ResidualCSDs were analyzed, whereas the early part represents the immediate tone evoked onset response and the later part the induced columnar processing for each group (C1V1: Figure 17 A, Control and YFP: SFig 6).

For an initial comparison, the root mean square (RMS) for the unbinned BFs was calculated within the given time windows of the averaged data and normalized by the mean of the last three pre-measurements. Therefore, it was possible to show the overall changes of the signal during the time course of the measurements (Figure 17 B). The most dominant course was found within the early ResidualCSDs. Here, the post-measurements showed three different stages, which would be used later for the temporal binning of the measurements: After the combined laser-stimulation (Laser), for the first 22.5 min the signal was steadily increasing (Post <30min). After an initial steady state 30 – 37.5 min after the laser stimulation (Post >30 min), the signal started declining again (Post >45min). The prior pre-measurements (-22.5 – -7.5 min) would also be used for binning (Pre).

In detail, the normalized RMS of the early AVREC, displayed a rather steady input strength of the thalamocortical inputs for YFP and naïve Control groups. With the naïve Control group as reference for the LMMs the C1V1 group reveals a significant increase ( $p < 0.001$  – 0.025) after the laser stimulation (15 – 52.5 min), hinting at an accumulative local gain increase of the thalamocortical inputs. Later cortical processing (80 – 300 ms) did not show any significant changes for all groups, yet a slight non-significant decrease for the YFP group is to be noted (Figure 17 B, upper right). The early ResidualCSD time courses also reveals two significant changes for the C1V1 group. The first significance can be found immediately while the laser stimulation

( $p= 0.04$ ) and during a later time course (22.5 – 37.5 min after laser,  $p= 0.014 – 0.039$ ) potentially hinting at two distinct events. Whereas the later increase is most likely related to DA, the immediate change most likely is a result of an immediate release of glutamate (Lapish et al., 2006; Lavin et al., 2005; Mylius et al., 2015). Both events are potentially boosting the early corticocortical integration of neighboring columns. The later part of the ResidualCSD reveals a mild increase of the C1V1 groups with a significant difference towards the naïve Control groups around 37.5 – 45 min ( $p= 0.008 – 0.033$ ).

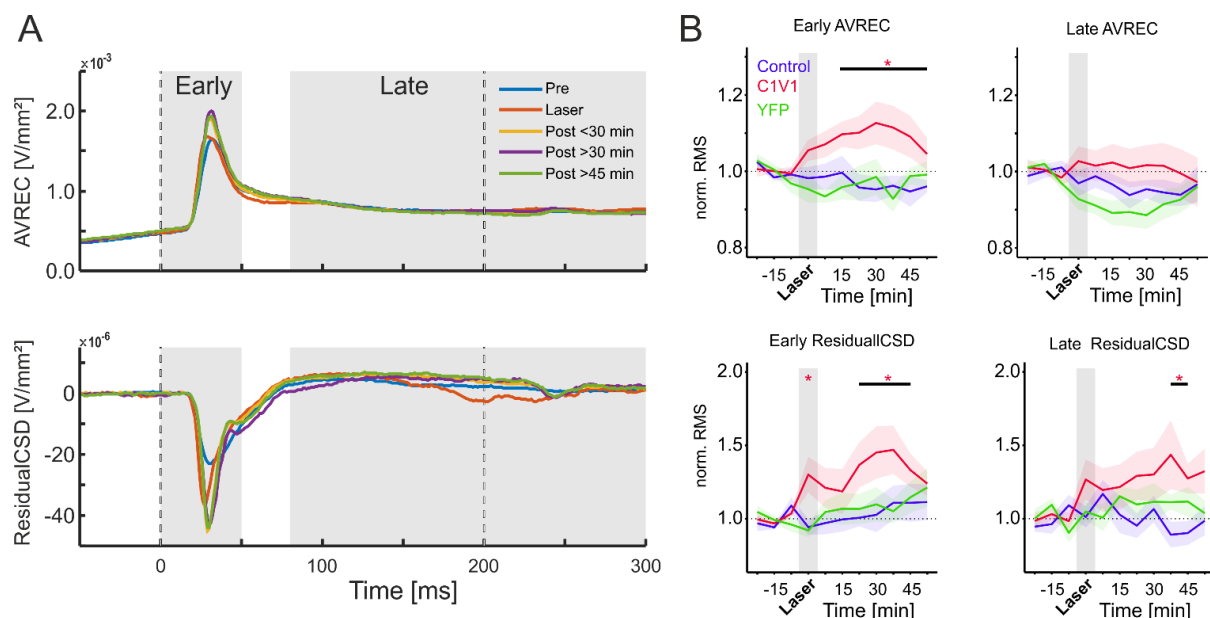


*Figure 17: Temporal changes of the early and late AVREC and ResidualCSD signals*

A) Average traces of the evoked BF responses for the AVREC and ResidualCSD signals (top and bottom, respectively) of the C1V1 group ( $n= 12$ ) for temporally binned measurements. B) Pre-normalized time courses of the BF for early and late AVREC as well as for early and late ResidualCSD traces (red: C1V1,  $n= 12$ ; blue: naïve Control,  $n= 7$ ; green: YFP,  $n= 7$ ). Significant changes towards the normalized data of the Control group are marked with asterisks (see Materials and Methods). Figure adapted from Brunk et al., 2019.

The previously proposed time bins (Pre, Laser, Post <30 min, Post >30 min and Post >45 min) were used for the average data, to investigate whether these local gain phenomena was only found for the BF presentation or whether also near- and non-BF frequencies were affected (Figure 18).

Early AVREC tunings hint at predominantly local gain increase of BF and near-BFs, while non-BF did not display an obvious gain increase. The tuning curves of the late AVREC do not display a prominent increase for any frequency. Mild tendencies within the  $\pm 10\%$  criterion might be seen for lower non-BFs (-3 – -4). Early and especially late ResidualCSDs display prominent increases for the corticocortical processing of all frequencies.

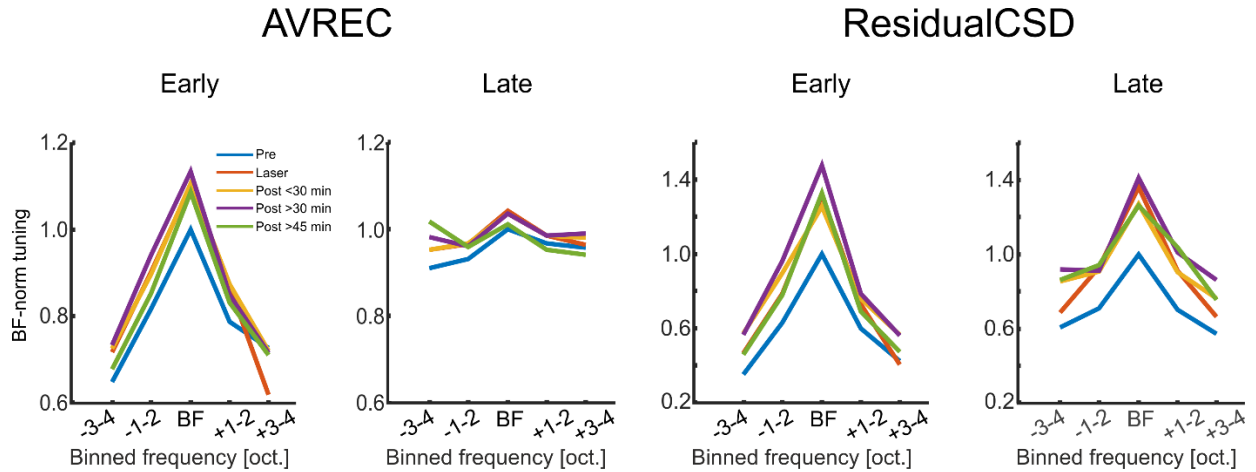


Figure 18: Tuning curves for early/late AVREC and ResidualCSD time bins

Pre-BF normalized time bins (Pre, Laser,  $<30$  min,  $>30$  min and  $>45$  min) for early/late AVREC and early/late ResidualCSD tuning. Figure adapted from Brunk et al., 2019.

To investigate the entire dataset in a simplified manner in respect of time points and frequencies while improving the statistical power for the LMMs, single-trial data have been binned for their frequencies (BF, near- and non-BF) as well as for the proposed time points (Pre, Laser, Post  $<30$ min, Post  $>30$ min and Post  $>45$  min) for all groups. The resulting time courses of the C1V1 and YFP groups have been compared with the course of the naïve Control group. Only significant changes towards the Control group that additionally surpassed the  $\pm 10\%$  criterion were deemed as real significant changes (Figure 19).

In general, the binned single-trial data confirm the observations from the average BF time courses in Figure 17 as well as the tuning properties from Figure 18.

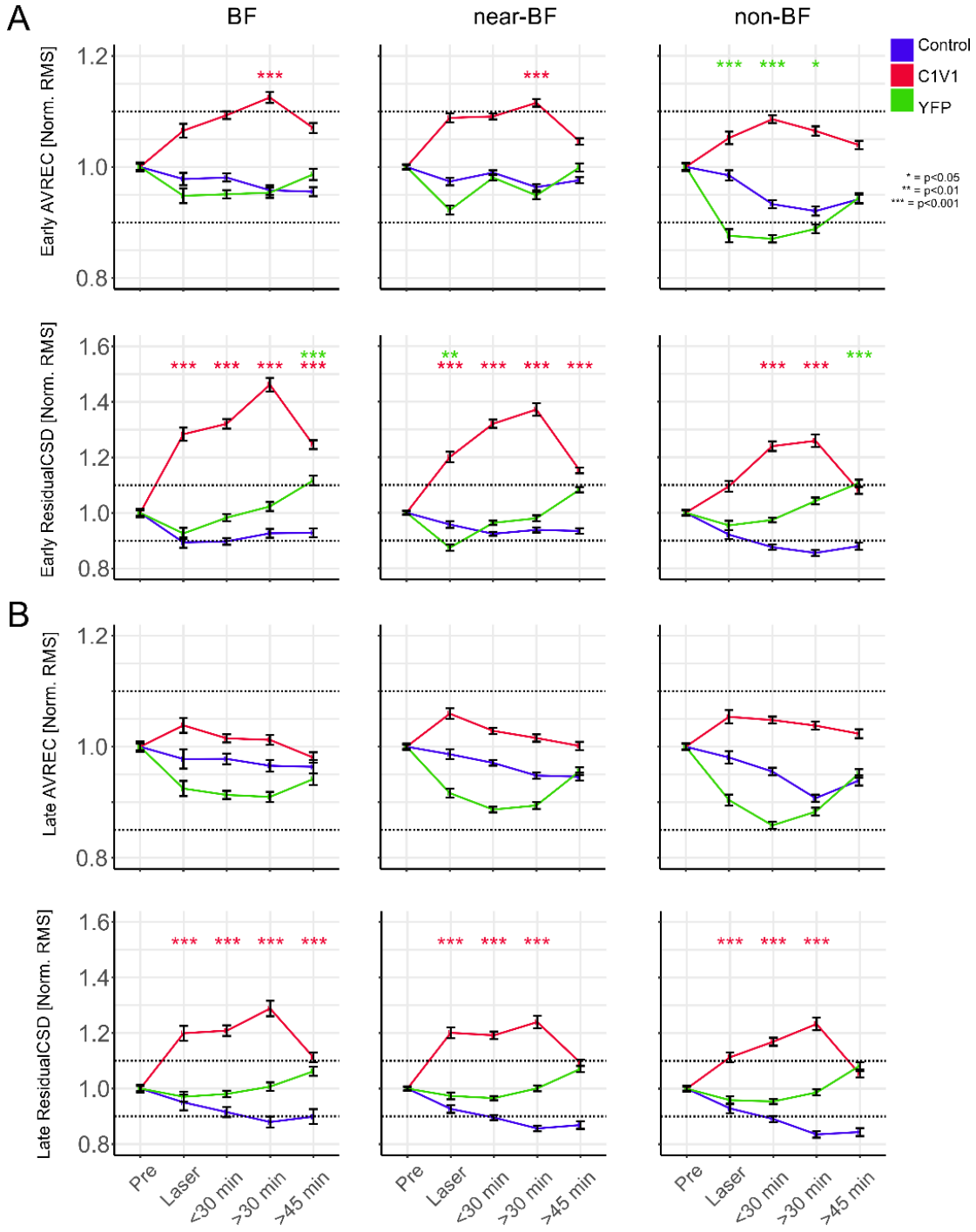


Figure 19: Binned time courses for normalized single-trial early and late AVREC and ResidualCSD

A) Temporal development of early Pre-normalized single-trial RMS AVREC (top) and ResidualCSD (bottom) values for best, near-best and non-best frequencies. Pre-, laser, and Post- measurements were binned for time points (<30 min, >30, >45 min) and octaval distances (near-BF:  $\pm 1-2$  oct, non-BF:  $\pm 3-4$  oct). B) Temporal development of late RMS AVREC and ResidualCSDs with the same temporal and frequency binning as in A). Asterisks indicate corresponding significances in comparison, verified by the Wald-Chi test, towards the Control group, utilizing LMMs. Additionally, changes had to surpass a  $\pm 10\%$  Pre-criterion. Red: C1V1, n=12; blue: naïve Control n=7; green: YFP, n=7. Figure adapted from Brunk et al., 2019.

In more detail, the early normalized RMS AVREC remained constant for the YFP and naïve control group for BF and near-BF bins, whereas the overall columnar activity of the C1V1 group increases, eventually becoming significant in the >30 min bin (12.5 %; p= 0.001 and 11.5 %; p< 0.001, respectively). For the non-BF bin, only a significant decrease for the YFP group is detected immediately while the laser condition and lasting until the >30 min bin (-12.9 – -11.1 %; p<0.001 – 0.046).

For the early ResidualCSD—reflecting the early tone evoked corticocortical integration—a more dominant increase of the C1V1 groups is to be seen within the BF and non-BF bins (15.3 – 46.2 %; p< 0.001). For the non-BF bin, the only significant increases are detected for the <30 min and >30 min time bins of the C1V1 group (24.0 – 25.9 %; p< 0.001). For the YFP group, non-unifiable significances were found for the >45 min time bin in the BF and non-BF bins (11.7 and 10.7 %; p< 0.001) and the laser condition of the near-BF bin (12.6 %; p= 0.003).

For the late AVREC signals, no significant changes were denoted that surpassed the ± 10% criterion, further affirming the initial observation of the time course (Figure 17 B) and tunings (Figure 18). Yet, it is to be noted that C1V1 animals showed a mild increase compared towards the naïve Control group, whereas YFP animals showed mild tendencies for a decreasing activity. On the other hand, the late ResidualCSDs display significant effects for the C1V1 group from the laser condition till the >30 min time bin in all frequencies with an additional significance in the >45 min bin of the BF (11.2 – 28.8 %; p< 0.001). No significant changes were found within the YFP group.

### III.III.I Effects of laser stimulation without tone evoked processing

Until now, all laser conditions were coupled with a sound presentation. However, this procedure does not reflect the sole effect of the direct projections from the VTA towards the ACx.

In order to investigate this aspect of the optogenetic stimulation, a subset of 5 animals was chosen from the C1V1 group in which a 1-minute laser stimulation without sound presentation (100 repetitions) was applied before the combined laser stimulation.

The result of this measurement (Laser only) was compared towards the corresponding Pre and Laser measurements, which included a tonal presentation, to unravel the potential influence of the VTA-ACx pathway within animals. Additionally, a Pause

condition from 5 Control animals (courtesy of Jing Ma) was also taken in account to potentially reveal slight changes, which might have been induced by the Laser only measurement. For the Laser and Pre-measurement, the BF presentations were chosen for analysis (Figure 20 A).

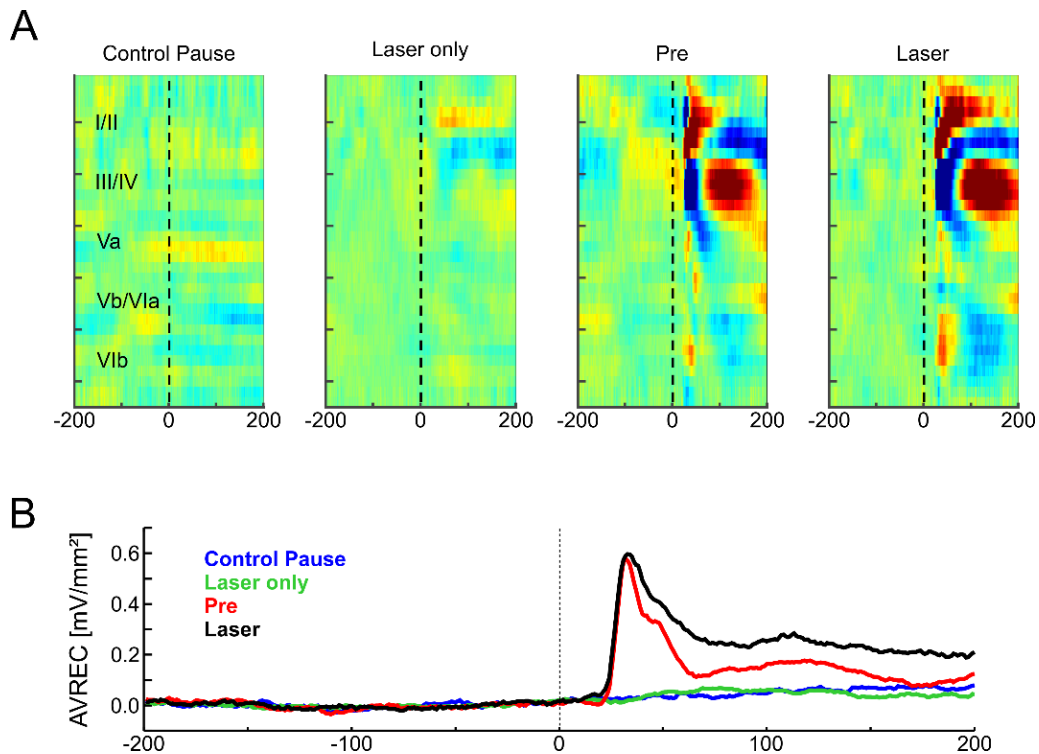


Figure 20: Comparison of immediate laser induced effects

Comparisons of CSDs for the time window from -200 ms before tone onset to 200 ms after tone onset. A) CSD examples for a pause condition in five Control animals and five animals of the C1V1 group for a Laser only, Pre and Laser conditions. B) AVREC traces of corresponding CSDs from A).

For comparisons, the RMS of the AVRECs was calculated for the time window (1-200 ms, Figure 20 B). The RMS values were then compared between the Pause and Laser only measurements via a two-sample students t-test on the single animal level. No significances were to be found. To further solidify whether immediate effects would be enhanced by the coupled tone presentation the same procedure was applied between the Pre and Laser measurements within animals. Also, no significant differences were to be found, further affirming that no immediate effects would be induced by direct projections.

### III.IV Effects of VTA stimulation on layer-specific synaptic processing

As already mentioned in the introduction, the microarchitecture of the neocortex can be investigated on the columnar and the layer-wise perspective (section I.III). Whereas the columnar point of view is well established in the current literature, the layer specific properties have barely been disclosed yet and if so, were rather focused at certain layers. Cell type specificity as well as validated projections between layer lay the foundation for the potential sound-evoked processing. A sole homogenous sound processing for all layers was not to be expected, since signal stability was not observed for a frequency-locked sorting as it was obtained for the GS-based sorting for the naïve Control group (Compare SFig 4 on page 99 and Table 1 on page 41). However, layer-specific tunings, which would allow for BF tuning shifts between layers resulted in much more stable signals for the entire time courses. Rejecting the aspect of a global stimulus-locked tuning within layers, therefore, would allow for describing the increase of activity related processing on an individual level of layer tuning. This type of sorting is also in line with the to be expected in-homogenous thalamic input differences between the prominent granular layers III/IV and infragranular layers Vb/Vla by the ventral and medial divisions of the medial geniculate nucleus (Compare Figure 12 A on page 37).

Applying the same procedure of the single-trial data binning from the columnar perspective, layer-wise PeakAmp data were assorted according to the averaged layer-specific response and binned in respect of frequencies (BF, near- and non-BF) as well as for specific time points (Pre, Laser, <30 min, >30 min and >45 min). Single animal data have been normalized by the mean of the final three measurements before the combined Laser measurement. The resulting time courses are displayed in Figure 21.

Most prominent layer-associated sink activities were chosen to be investigated (early: onset of sink <50 ms: granular layers III/IV, and infragranular layers Va, Vb/Vla; late: onset of sink>50 ms: supragranular layers I/II and infragranular layer VIb; Compare schematic sketch from Figure 12 CD on page 37).

LMMs were applied for all groups (C1V1, YFP and Control) and a Wald-Chi-square test was performed between the groups of interest (C1V1, YFP) towards the naïve Control group for each time bin. True significances were achieved, when values

derived significantly from the Control group while surpassing the additional  $\pm 10\%$  criterion.

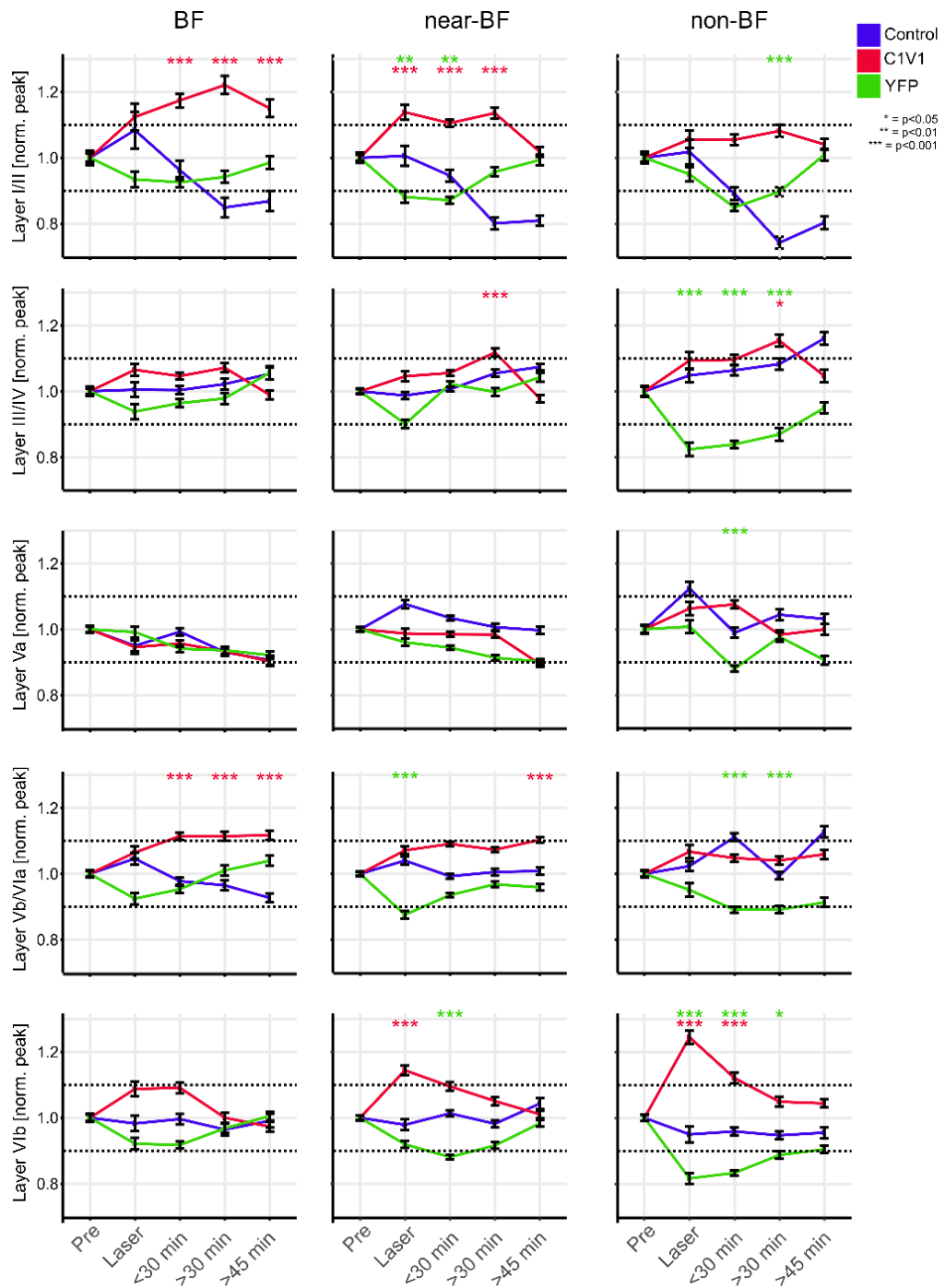


*Figure 21: Temporal development of time bins for the single-trial sink peak amplitude data of layer-specific CSD-traces*

Temporal development of early (onset  $<50$  ms) and late (sink onset  $>50$  ms) sink peak amplitudes for single-trial data. Data have been binned for frequencies and time points (See explanation Figure 19). Data have been normalized by the mean of the corresponding Pre measurements of each frequency bin. Significances have been calculated utilizing LMMs and a performing Wald-Chi test between groups of interest (YFP, C1V1) and the naïve Control group. Significant changes additionally had to exceed a  $\pm 10\%$  Pre-criterion to account for a general variance in the data sets. Figure adapted from Brunk et al., 2019.

Layer specificity is a keen aspect of the cortical micro circuitry as it hints towards the evoked thalamocortical and corticocortical processes. Therefore, DA or VTA mediated changes within layers were expected within the consecutive time course after an optogenetic stimulation of the VTA.

Most dominant effects were observed within the supragranular **layers I/II**. Within the C1V1 group, high significances were to be found for the layer specific BF stimulation after the VTA stimulation (Laser) lasting for more than 45 min (11.1 – 19.4 %,  $p < 0.001$ ). A similar trend was found starting during the Laser measurement and lasting for more than 30 min (10.5 – 13.8 %,  $p < 0.001$ ). In general, the YFP group displayed declining tendencies starting during the combined Laser presentation, which fully recovered within 45 min. For the layer specific BFs this relative decrease was not significant, whereas very significant changes are found for the near-BFs during the Laser stimulation and lasting less than 30 min (-12.9 – -11.9 %,  $p < 0.01$ ). Within non-BFs, the relative activity within the YFP group declined after the Laser stimulation (-15.1%) for less than 30 min (-10.3%), yet significant differences towards the naïve Control group were only obtained for the <30 min bin ( $p < 0.001$ ). Interestingly, the overall tendencies for the naïve Control group started declining during the time course, although no manipulation was applied to this group in any form.

Interestingly, the most prominent granular **layers III/IV** did not display significant changes for the layer specific BF presentation of the C1V1 group. The only significances for the C1V1 group were to be found in the >30 min time bins of the near- and non-BF frequencies (+11.8 % and + 15.4 %,  $p < 0.001$  and  $p < 0.01$ , respectively). On the other hand, the YFP group showed a significant decrease within the non-BFs starting at the time of the Laser stimulation and lasting for more than 30 min (-17.6 – -13.1 %,  $p < 0.001$ ).

With exception for the >30 min time bin of the non-BF of the YFP group (-12.0 %,  $p < 0.001$ ), **Layer Va** did not reveal any significant changes during the entire time course.

The thalamocortical inputs of **layers Vb/Vla**, on the other hand, showed an increase for their specific BFs after the Laser stimulation and lasting for more than 45 min (11.5 – 11.7 %,  $p < 0.001$ ). An additional increase within the C1V1 group was also noted in the late >45 min time bin of the near-BFs (10.3 %,  $p < 0.001$ ). The YFP animal group displayed a decrease in relative activity for the near-BF during the Laser measurement

(-12.4 %, Laser,  $p < 0.001$ ) and in the non-BFs after the Laser measurement lasting for more than 30 min (-10.9 % for each,  $p < 0.001$ ).

Layer specific changes of **layer VIb** display group specific changes within frequencies. Whereas the signals of the Control group remain stable, the C1V1 group shows overall increasing tendencies during the Laser stimulation and lasting for less than <30 min. On the other hand, the YFP group shows a decrease of activity for the same time bins as the C1V1 animals. In detail, the increase of relative activity of the C1V1 group was highly significant for the Laser stimulation of the near-BF (14.4 %,  $p < 0.001$ ) as well as for the non-BFs from the time of combined Laser stimulation and lasting for less than 30 min (12.1 – 24.5 %,  $p < 0.001$ ). The YFP group shows a highly significant decrease within the near-BFs, 30 min after the VTA stimulation (-11.9 %,  $p < 0.001$ ). For the non-BFs, the signals of the YFP group declined during the VTA stimulation and lasted for more than 30 min (-18.4 – -11.3%,  $p < 0.001$  – 0.01).

### III.IV.I Changes in spectral tuning sharpness of cortical layers

Reorganization of the tonotopic map requires a re-tuning of the columns towards the relevant stimuli. DA is thoroughly thought to be involved in this process as indicated by various studies, showing the cortical reorganization of the ACx after VTA stimulation (Bao et al., 2001; Hui et al., 2009) by DA potentially loosening the existing ECM from established synaptic connections eventually allowing the formation of new engrams (Frischknecht and Happel, 2017; Happel et al., 2014b; Mitlöhner et al., 2020; Niekisch et al., 2019). As previously shown, the stimulation of the VTA increases the relative cortical processing of each frequency. Yet, the question remained, if DA simply boosts existing cortical integration or even opens up the columnar integration for far more non-BFs. This aspect, normally, is investigated for experimental data with varying attenuations for investigating the corresponding CFs of the cortical bandwidth integration (Happel and Ohl, 2017). However, since experimental data were obtained from a steady SPL of 65 dB another approach was to be sought for.

To show whether a layer specific alteration of the bandwidth integration was given, the single animal data of the PeakAmps of the most prominent time points (Pre, Laser and Post >30 min) were normalized by the initial BF values of the Pre-measurements. By this approach it was possible to not only show the gain increase but also investigate changes in the existing tunings slopes from non-BFs towards BFs (Figure 22).

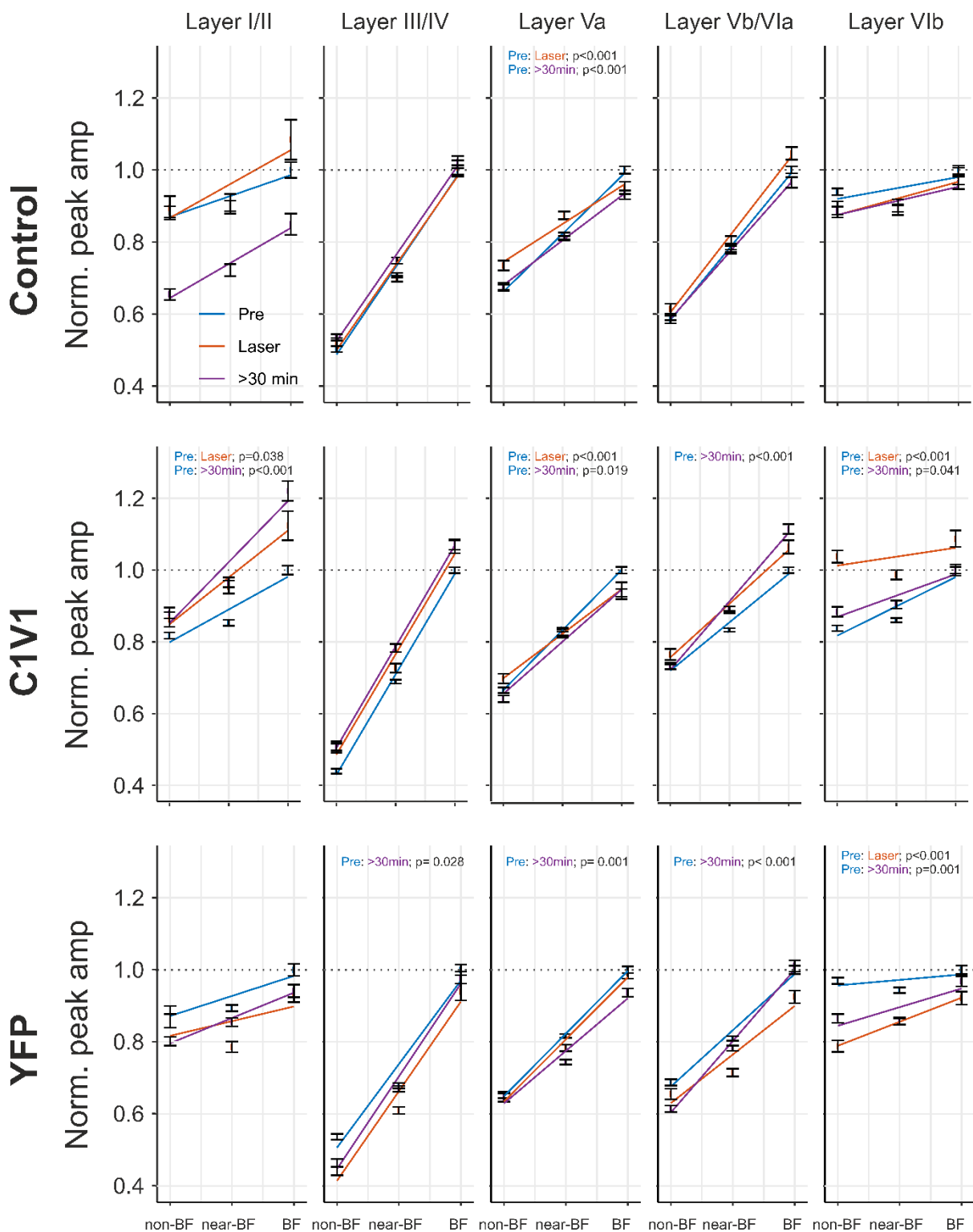


Figure 22: Layer-specific changes of tuning sharpness

Slope comparisons of the Pre BF normalized single-trial based sink tunings of the Pre, Laser and >30 min conditions of all groups. p-values correspond to comparison between slopes based on the Satterthwaite's degrees of freedom method (lmerTest-package, RStudio, 3.0–1). Corresponding slopes are enlisted in Figure 23. Figure adapted from Brunk et al., 2019.

In order to investigate significant changes in the tuning slopes of the LMMs, a least square linear fit was estimated across the evoked responses of the BF-, near-BF- and non-BF bins using the lsmeans package in R (version 2.27-62). Significant slope changes were calculated by comparisons between the initial slope steepness of the corresponding Pre measurements with steepness of the consecutive Laser and Post (>30 min) measurements using the ImerTest-package (3.0-2) in R, providing the p-values (type I, II or III) via a Satterthwaite's degrees of freedom method. With this methodology, slope steepness can be used to estimate whether, in comparison towards the initial Pre-measurements, the relative bandwidth narrows down (steep slopes) or opens up for further frequency integration (shallower slopes). To account for the repeated measurements during and across time points, animals were used as "by-subject" random effects, whereas, for the explanation of physiological data, measurements and groups were used as fixed effects.

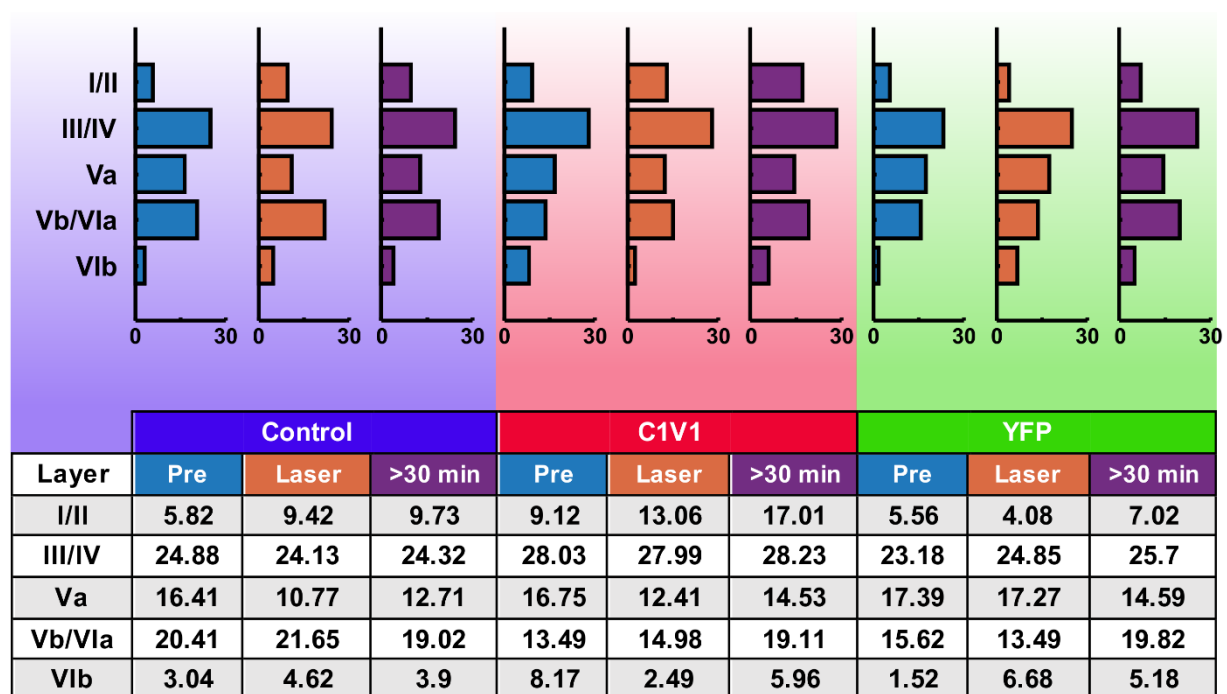


Figure 23: Slopes of layer tuning

Slope values in percentage corresponding to Figure 22. For visualization, slope values have been plotted as bar charts above the table.

In general, the sharpest tuning properties of PeakAmps are found in layers III/IV with slopes between 23 – 29 % (see Figure 23), corresponding to differences between BF- and non-BF-evoked peak amplitudes of up to almost 60% (Compare Figure 22). The

second sharpest tuning properties are found within the infragranular input layers Vb/Vla with varying values between 13.49 – 21.65%. Slope steepness for other non-thalamic input layers ranged between 1.52 – 17.39% (Details in Figure 23).

Yet, since frequency integration is a combined process of the layer specific change in slope and the overall gain de-/increase, both aspects need to be combined to reveal changes of cortical frequency representation within layers.

Although the naïve Control group showed a decrease of the supragranular **layers I/II** no significant changes within slope steepness are found. Likewise, the slope steepness of the YFP animals did not change. The C1V1 group, on the other hand, not only reveals a significant increase of steepness for the Laser stimulation ( $p= 0.038$ ) but also a highly significant increase of steepness for Post >30 min measurement ( $p< 0.001$ ), whilst undergoing an overall gain increase.

Granular **layers III/IV** do not show changes of slope steepness for the naïve Control group and the C1V1 animals. However, a very significant change in slope is found for the >30 min Post-measurement in the YFP group. Yet, at the same time no gain increase is observed, hinting at a narrowing of the bandwidth integration.

Within **layer Va**, up to highly significant slope changes ( $p= 0.019 – <0.001$ ) are found within all animal groups while no significant gain increase is given (Compare with time course of Figure 21). The overall tendencies for the layer Va tents towards shallower slopes.

Infragranular input **layers Vb/Vla** do not reveal significant changes for the Control group. Highly significant slope changes ( $p< 0.001$ ) are found in for the animals of the C1V1 and YFP groups with steeper slopes. Yet, while YFP animals show no gain increase, C1V1 animals show an additional gain increase around the BF and near-BFs. Which might hint at an increase of cortical integration of the layer specific BF and near-BF representations.

Infragranular **layer VIb** shows no significant changes of slopes for the Control group. Yet, while slope steepness for the Laser and >30 min Post-measurement become shallower for C1V1 group, YFP animals reveal an increase of slope steepness. The Laser stimulation within the C1V1 animals leads to a massive gain increase and a shallower slope ( $p< 0.001$ ), which in its combination almost nullifies the tuning differences within layer VIb. The >30 min Post-measurements also reveals a significant shallowing of the slope ( $p= 0.041$ ), which leads to an increased processing of non-BF

compared towards the initial processing of the Pre-measurement. YFP animals reveal steeper slopes whilst an overall gain decrease for the Laser ( $p < 0.001$ ) and Post measurements ( $p = 0.001$ ).

## IV. Discussion

Consistent interactions of the individual and their immediate environment require a certain amount of cortical plasticity to allow the new formation of learning-associated engrams. However, while learning improvements and engram formations are most efficient during an early age—due to the critical period—the adult brain is still capable, although less efficient, in creating new memory associations (Blundon and Zakharenko, 2013; Mowery et al., 2016; Patton et al., 2019).

During the critical period, the maturing of the brain and the essential engram formations between frequently required cortical and subcortical pathways involves a stabilizing protein mesh called the extracellular matrix (ECM) (Frischknecht and Happel, 2017; Happel and Frischknecht, 2016). Within the juvenile brain, the ECM is still maturing around frequently activated synaptic pathways, while other—non-frequently activated—pathways are not supported by the ECM formation building the essential basis for memory engram formations. It has been shown in adult rodents that a loosening of the established ECMs within the auditory cortex can be acquired by digesting this mesh with hyaluronidase in order to recreate a more juvenile state of the brain. In combination with an auditory avoidance task in mice it was later shown that hyaluronidase treated animals were much more efficient in relearning the reversal of the initial task than naïve control animals and hence indicate that the digestion of the ECM promotes new learning associations (Happel et al., 2014b). The natural ECM digestion, however, seems to be induced by dopamine (DA) activity and thus makes DA an essential teaching signal for new learning associations within the adult brain (Mitlöhner et al., 2020).

The Impact of DA release during an auditory task engagement (Stark and Scheich, 1997) was measured via microdialysis within the primary auditory cortex (A1) and revealed an accumulative increase during the training. The prior mimicking of DA by an artificial application of a dopaminergic agonist (SKF-38393) prior to training resulted in learning improvements and thus further confirmed the effects of DA during learning associated engram formation.

As a potential origin of cortical DA the ventral tegmental area (VTA) has been identified as an essential key structure that conveys DA as a teaching signal for the salience and value of a stimulus for all involved brain areas during the awake state. The A1 areal of the ACx, therefore, is a suitable target structure to investigate the integration of bottom-up and top-down processing during a reinforced auditory learning task.

For this study, I focused on the initial aspects of reward associated cortical processing in anesthetized Mongolian gerbils. The rationale of this procedure was to find immediate consequences of reward associated DA on the cortical processing within the A1 on a columnar level, since long-term (~20 days) effects have been shown to alter tonotopic mapping in favor of the reward associated stimulus in awake and anesthetized animals (Bao et al., 2001; Hui et al., 2009). Those long-term studies were severely lacking the descriptions of the immediate effects, opening up a black box for the DA associated principles that would allow for a context-driven reorganization on a columnar as well as a layer-specific level. The comparison of the C1V1 animals from the HP subgroup with naïve control and YFP animals would further allow me to disentangle time (naïve Control) and laser-related (YFP) effects, for the specific time points of interest before, during and after the VTA stimulation. Those changes would allow me to conclude for the immediate changes in cortical micro circuitry, potentially allowing for the columnar reorganization of relevant stimuli.

#### IV.I Effectiveness of VTA targeting in the Mongolian gerbil

By utilizing the aspect of VTA activity and DA release in addiction (Aransay et al., 2015; Bao et al., 2001; Ciccarelli et al., 2012; Holly and Miczek, 2016; Lippert et al., 2018; Salinas-Hernández et al., 2018), transduced animals have been trained in an O-ICCS to verify successful VTA transductions. Only a third of all C1V1 animals (Figure 15 A) displayed the expected behavior that is associated with DA whereas the rest was rejected from further studies (cf. Brocka et al., 2018).

Although, the relative targeting locations of the VTA towards bregma are well known (AP: -4.0, ML: ± 0.5, DV: -6.2 mm; Lippert et al., 2018) and are coinciding with the anatomy of the Mongolian gerbil's brain (AP: -3.75 – -5.15 mm, plate increment: 350 µm for 4 month old gerbils) (Radtke-Schuller et al., 2016), the effectiveness of the optogenetic ICSS was not always granted. Consecutive anatomical evaluations of the actual fiber positions of the lever pressing performance-based High-, Medium- and

Low-performer (HP, MP and LP, respectively) subgroups of all the C1V1 animals (section III.I ff.) revealed no significant differences between the HP and MP animals in respect of relative fiber positions, fiber distance and LFCs (Compare Figure 15 on page 45). The only significant differences ( $p= 0.0269$ ) have been found between the AP positions of the HP ( $-3.57 \pm 0.14$  mm) and LP ( $-4.05 \pm 0.1$  mm) animals, indicating that more rostral positions were more effective for the O-ICSS paradigm. This observation is in line with previous studies that used stimulation of the medial forebrain bundle and the rostral VTA to upregulate the locomotor activity in rats by dopamine (Guo et al., 2014; Talwar et al., 2002). In general, the more complex nature of the VTA and its seven regions (Anderegg et al., 2015) even further complicates the targeting of the correct position as for this day no specific projections between the ACx and the corresponding VTA regions have been described in detail.

Although at a first glance, the relative distances between the fiber tip towards the area of opsinal and TH-antibody staining co-fluorescence seem to differ drastically between the HP and LP animals, no significances are found. This coincides with the expected relative irradiances within those depths as calculated with the ‘Brain tissue light transmission calculator’ at T1 (see footnote 3 on page 26) as those irradiance cover the range of successful opsinal activations ( $1 – 5$  mW/mm $^2$ ) within tissues up to 800  $\mu$ m underneath the tip (Senova et al., 2017). Even LFCs at T1 seem to fulfill the required light intensities within brain depths of 700 – 750  $\mu$ m for all groups indicating that, although, the quality loss within groups is very/highly significant, the expected light penetration fully covered the depth of the VTA. Yet, one aspect that has not been taken in account is the declining spread in the geometric loss within cortical depths, which might additionally have resulted in lesser numbers of transduced cells activated by the laser for the LP group. However, this theoretical aspect does not account for reasonable differences between LP and MP animals.

For compensation of performance differences between LP and MP animals during the O-ICSS, one could have increased the applied laser power until lever pressing performances would have reached equal levels (Evans et al., 2018; Lippert et al., 2018; Weidner et al., 2019) and consecutively applied the same laser power during the electrophysiological experiments. However, this might have resulted into an increase of heat related side effects and photo damaging of the VTA further complicating the disentangling of heat and DA associated effects as the applied powers are in the

common range of optogenetic experiments (1 – 10 mW) (Arias-Gil et al., 2016; Chernov et al., 2014; Stujenske et al., 2015; Yizhar et al., 2011).

Furthermore, one could have tried to optimize the effectiveness of the O-ICCS by changing from a blue light laser stimulation ( $\lambda$  473 nm) to a green light stimulation ( $\lambda$  532 nm), since the optimum wavelength absorption of the chimeric C1V1 opsin has been stated to be between a wavelength of 535 – 540 nm (Batabyal et al., 2015; Wietek and Prigge, 2016). Light-induced activity at a wavelength of 473 nm of the C1V1 opsin lingers around 80% of its reported optimal performance. Those opsinal relative activity spectra are derived from single cell recordings (Adam et al., 2018; García-Martínez et al., 2015) and do not account for further influences such as pH and blood, which also might affect the effectiveness of the O-ICSS.

Although the used fiber implants are cheap and easy to produce, they offer another downside to the tissue light spread. Within the last years a new type of fiber was established which is referred to as tapered fibers. Unlike the classical flat tip fibers—the ones that have been used for this study—tapered fibers allow for a more evenly spread of light alongside the tapered fiber tip whereas flat tips are more locally emitting light (Pisanello et al., 2017, 2018; Vogt, 2017). But to this day tapered fibers have only been used for cortical layer specific stimulations and are not available for deep brain stimulations.

Next to analysis of the anatomical positions and fiber properties, one could have analyzed the expression levels of eYFP in all nearby slices or estimated the amount of eYFP expressing cells for each brain slice to account the total numbers and areas of successfully transduced cells—but this would have shifted the focus of the project onto more basic molecular aspects that should have been explored in advance and which in general has not been investigated for optogenetic experiments.

To the current state, it assumed that roughly 8% of the ipsilateral VTA project directly into the ACx (Budinger et al., 2008). Yet, as the VTA consists of seven regions (Anderegg et al., 2015), it needs to be investigated much more thoroughly, whether those direct projections originate from one or more specific regions of the VTA and if the same regions projecting into the ACx are also involved reward reinforcement. As the sole laser presentation indicates, there are no direct effects obtained within the ACx by VTA stimulation (Figure 20 on page 56). Based on the dominant eYFP expression in infra- and supragranular layers (Compare Figure 7 on page 28) direct projections would have been expected to terminate in those layers. This might be an

indication that the direct projections of the VTA towards the ACx do not originate from the rostral part of the VTA (mesocortical pathway) as there is also no immediate response as it has been described for glutamate (Gorelova et al., 2012; Lapish et al., 2006; Lavin et al., 2005; Mylius et al., 2015). Long-term accumulative effect associations, therefore, might be the predominately result of indirect projections via the ventral striatum and the nucleus accumbens in the mesolimbic pathway (Bariselli et al., 2016).

As a résumé of the results from section III.I, one can conclude that targeting the correct region for a successful O-ICSS of the VTA within the Mongolian gerbil to the current state is partially a gambling game, yet more rostral positions seem to be more efficient for reward associated lever pressing behavior. This finding is confirmed by the usage of rostral VTA stimulation by Guo et al. who promoted the locomotor activity in rats for traveling distances (Guo et al., 2014). Although the Mongolian gerbil is a suitable model organism of choice for hearing research—unlike other widely used rodent model organisms (e.g. rats and mice)—no specific gerbil strains (like DAT and Cre lines of rats/mice) are currently available. Therefore, VTA cell targeting in gerbils is currently only achievable by promotor driven transduction approaches, which are leaky in the specificity of cell targeting, yet do not evoke as strong evoked responses as observed for electrical stimulation (Brocka et al., 2018). Yet, all current results of this study can be used to reflect the influence of reward associated DA, triggered by a VTA stimulation, and its effects on cortical processing.

## IV.II Effect associations of dopamine

A common misconception in literature is that DA has an immediate response in the target structures as it has been described for the reward prediction error (RPE) within the VTA (Mirenowicz and Schultz, 1996; Schultz, 1998). For instance one of the immediate effects observed by the stimulation of the VTA was a rapid depolarization within neurons of the prefrontal cortex (Gorelova et al., 2012). Likewise, it was shown by Lavin et al. that the burst stimulation of the VTA leads to an immediate transient increase of the nM concentration of DA within the PFC, which would recover back to baseline levels within 2 – 6 s (Lavin et al., 2005). However, electrophysiological changes in the spiking rates would slowly accumulate after VTA burst stimulation over

more than 45 min. Those later accumulative effects would eventually be blocked by a prior dopaminergic antagonist application, verifying their dopaminergic nature.

In a small batch of two animals from the C1V1 animals (HP), I also investigated whether the observed accumulative effects were of dopaminergic nature (see SFig 7 on page 102). Just as described before, the Laser stimulation of the VTA yielded a relative increase of the columnar activity. This increase was immediately reversed after the application of a dopaminergic antagonist (SCH-23390) and eventually did not yield in a second increase after an additional Laser stimulation (indicated by blue arrow), further confirming that the observed changes are indeed of dopaminergic nature.

Recently, Brocka et al have shown that an O-ICSS of the VTA in rats triggers a co-release with glutamate, which results in a similar self-stimulating rate as in a more specific manner of sole dopamine. Based on their comparative studies of specific (Cre) and non-specific (WT) VTA stimulation in rats, Brocka et al. concluded that the observed responses are not primarily of a dopaminergic nature but could be the result alternative routes like glutamatergic transmissions (Brocka et al., 2018). This non-specific stimulation eventually affected also other brain areas like the PFC, the ipsi- and contralateral striatum as well as the ipsilateral NAc, which might result in additional brain area interactions, contributing to the corticocortical integration.

In order to predominately relate cortical changes with DA, I used the lever pressing rates as a criterion to select highly addictive animals since DA has been related to addiction on many occasions (Aransay et al., 2015; Keiflin and Janak, 2015; Lewis and Sesack, 1997; Lippert et al., 2018; Schultz, 1998; Sponaugle et al., 2008). Therefore, only animals from the HP subgroup were used for the C1V1 animals within the electrophysiological experiments while other performance groups were rejected as it is a common procedure (Brocka et al., 2018). This further simplified the DA associated effect estimation as other non-specific influences of the MP and LP animals would have further complicated the analysis. However, it cannot be rejected whether those animals would have shown similar effects to an equal or lesser degree.

It needs to be recalled at this point that DA is always co-released with glutamate and thus the observed effects are likewise always influenced by glutamate (Gorelova et al., 2012; Mylius et al., 2015).

#### IV.III Dopamine increases corticocortical columnar communication

Columns are the smallest functional units within the neocortex in which cortical micro circuitry can be observed on a mesoscopic level across all cortical layers (Goldschmidt et al., 2010, 2004). Within the range of the integrational cylinder of the implanted 32 channel shaft-electrodes, it is possible to observe thalamocortical gain amplification of afferent inputs from the corresponding thalamic nuclei by investigating the local early tone evoked AVREC as well as the consecutive late AVREC for the evoked micro circuital processing. Additionally, the ResidualCSD can be used in order to describe the global influence of corticocortical interaction during the initial thalamocortical and the micro circuital processing (cf. Figure 11 on page 35). The later can be used in combination with the layer specific sink activity to draw conclusions about potential efferent corticothalamic and long-range corticocortical feedbacks (Happel, 2016).

I investigated the columnar integration for three different groups. For the investigation of the temporal stability I used a naïve control group (Control) without optogenetic implant, which eventually would be used for comparisons of the dopaminergic (C1V1) and laser induced effects (YFP). Effects of laser stimulation on non-transduced cells have been reported to increase the neuronal firing rates by up to 42.9% (Stujenske et al., 2015) and thus additionally affect the recorded cortical processing. Even the transduction of sole reporter proteins like GFP and YFP can affect the absorption of light, since those proteins can affect the efficiency of nearby proteins by phenomena like Förster Resonance Energy Transfer (FRET) (Berglund et al., 2019; Ghisaidoobe and Chung, 2014). Since aromatic amino acids like histidine, phenylalanine, tyrosine and tryptophan also display the property of auto-fluorescence, they can be used for internal quenching studies from proteins and thus are potential FRET interaction partners in nearby proteins (Möller and Denicola, 2002). Therefore, the YFP group was included to investigate the unspecific effects of naïve and C1V1 animals.

On the columnar level, the control group displayed the most stable time courses for early and late AVREC and ResidualCSD signals. However, it is to be mentioned that over time both signals of the naïve animals declined on the columnar level without any additional manipulation, especially in for the ResidualCSD signal of the non-BFs (cf. Figure 19 on page 54), indicating that, over time the bandwidth of the columnar tuning sharpened due to less corticocortical integration of non-BF columns. This naïve event

might hint at a potential lock down of cortical integration in order to preserve the established BFs on the columnar level. This sharpening of frequency tuning might be a result of sideband inhibition (O'Connell et al., 2014).

Interestingly, YFP animals showed a decrease in the AVREC signals after VTA stimulation whilst ResidualCSDs started increasing, probably compensating the sudden lack of thalamocortical input integration. Since an excitatory release from dopamine was not expected by those animals, as confirmed by the lever pressing rates (Figure 8 on page 30), this effects were most likely induced by the laser stimulation (Stujenske et al., 2015) and probably a result of a decrease in the neuronal firing rates from the VTA. It has been reported before that dopaminergic neurons from the VTA can have two distinct different modes: a more tonic firing under normal conditions (~5 Hz) or more phasic firing (>20 Hz) for attentional signaling (Ellwood et al., 2017). Assuming that a more tonic firing was present for the Control group, one might assume that the laser stimulation of the VTA increased the activity of the GABAergic cells within the VTA, which further inhibited the existing tonic firing below 5 Hz by an internal GABAergic feedback within the VTA. Additionally, one can assume that a slight decrease in the tonic neuronal firing can have immense effects on the recorded signals as it has been reported for dopaminergic neurons from the substantia nigra that an increase of the tonic firing from 1 Hz to 6 Hz resulted in a five-fold higher calcium signal as initially predicted (Hage and Khaliq, 2015). Yet, to my current knowledge, no literature is available confirming similar effects for a decrease of neuronal firing rates within the VTA below 5 Hz.

For the C1V1 animals, I observed a general increase in the early AVREC as well as for the early and late ResidualCSD signals. While the early AVREC signal for BF and near-BFs became stronger and, eventually, were peaking significantly 30 min after the VTA stimulation, the early ResidualCSDs for all frequency bins was increased already during the VTA stimulation indicating a boost of corticocortical integration from most likely neighboring columns and other cortical regions (Roland et al., 2014). The prolonged corticocortical activity of the ResidualCSDs as the result of optogenetic stimulation from the VTA is not only matching with the behavioral outcome and dopaminergic levels within ACx from Stark and Scheich (Stark and Scheich, 1997) but also for the increased prefrontal activity after a single burst VTA stimulation (Lavin et al., 2005), indicating that DA primarily boosts the corticocortical integration on the

columnar level, which might be a foundation for the tonotopic remapping of relevant stimuli over multiple repetitive presentations (Bao et al., 2001; Hui et al., 2009).

Yet, direct stimulation of the VTA without tonal presentation does not initiate dopaminergic cortical processing on its own as shown for the pure laser stimulations (see Figure 20 on page 56). However, the accumulative nature of the cortical signals maybe a hint for the involvement of more indirect, mesolimbic, pathways almost neglecting the influence of the direct VTA projections towards the ACx, which in first place seems to be dominated by a glutamatergic nature. This conclusion can be drawn on the one hand side from the initial significant increase in the early ResidualCSDs (Figure 17 B on page 52) and the mild peaking in a Post-measurement after a second VTA-stimulation in presence of the dopaminergic antagonist SCH-23390, which not only reversed the DA associated power increase after application but suppressed it in a consecutive set of measurements (SFig 7 on page 102).

The DA gated increase of corticocortical integration—as shown by the early and late ResidualCSDs—probably allows for context associations of relevant stimuli, which validation is boosted via the reward center by increasing the sensitivity of stimulus representations eventually allowing for a columnar remapping of the engram encoded columnar BF.

#### IV.IV Layer specific changes due to dopaminergic influence

Layer specificity for cortical processing is based on a far more complex interaction as on the columnar level. Not only do cortical layers display differences in the cellular architecture (cyto-, fiber-, chemoarchitecture) and the cortical connections (thalamocortical, corticocortical and corticofugal) but also in their layer-wise tuning properties (compare Table 1 on page 41 and SFig 4 on page 99), which did not display unifiable tendencies in respect of time point and shift tendencies in relation to the prominent input of granular layers III/IV. However, by assuming individual layer differences and non-stable BF contributions, I introduced a layer-wise self-tuning based (ST-based) sorting and compared the time course of the signal with a granular sink based (GS-based) sorting. Interestingly, ST-based data did display the most stable signals for the naïve control group, indicating that tuning properties are present, yet, the probability of layer-specific tunings differs between single measurements and between layers, which is in line with other studies even revealing changes in the BF

under different sound pressure levels (Guo et al., 2012; Rothschild et al., 2010; Tischbirek et al., 2019). By omitting potential BF-shifts between layers; I therefore ensured to reveal gain related effects of DA for each layer, since it has been stated in literature before, that neurons in different layers have different firing rates and therefore, layers display different tuning properties (Crochet and Petersen, 2009; Rothschild et al., 2010; Tischbirek et al., 2019). Henceforth, non-stable tuning shifts within layers might be a result of spontaneous firing, which might add to non-stable BFs within the consecutive cortical processing.

By the validation of the VTA projections towards the ACx (section III.II), I found prominent fluorescence in supra- and infragranular layers. Those results quite strongly confirm the interaction of the layers I/II, Vb and VI with dopamine by matching with cortical receptor distribution from D1/D5 receptors (Happel, 2016; Lidow, 1995; Lidow et al., 1991; Radnikow and Feldmeyer, 2018). The DA layer interaction can be further validated by accounting the used CAMKII $\alpha$ -promotor sequence for the viral transductions, since the CAMKII $\alpha$  subunit is found within calbindin-positive cells (Jones, 2001), which are primarily found in supra- and infragranular layers. Calbindin is a calcium binding protein that has been reported to influence the release probability of DA (Anderegg et al., 2015), therefore the found fluorescence of the CAMKII $\alpha$  controlled protein expression additionally hints at DA associated activity in those layers.

As already hinted by the burst VTA stimulation for spiking activity in the PFC by Lavin et al, DA is associated with an increase of the relative cortical activity after the event of VTA stimulation. I found similar trends in the ST-sorted layer data for more than 30 min after the VTA stimulation. Especially, the supragranular (I/II) and infragranular layers (Vb/Vla and VIb) were affected in different time constraints. Whereas, the supragranular layers I/II and the infragranular input layers Vb/Vla follow a similar temporal course as reported by Stark and Scheich (Stark and Scheich, 1997) in the BF and near-BFs, layer VIb displays a strong increase in the off-BFs during the VTA stimulation. In general layer VI is associated with a glutamate guided thalamocortical feedback. This corticothalamic feedback has been reported for the visual cortex of the cat (Cudeiro and Sillito, 2006). Assuming, that the initially observed relative increase in cortical activity is facilitated by the glutamate from the glutamate/DA co-release of the VTA, it is assumable that this initial response serves as an attentional signal for the potential increase of salience and valence for off-BFs to boost thalamic inputs in a

behavioral relevant driven context before physical alterations of the engrams manifestation. This hypothesis could be investigated in a follow up study in which the laminar effects—especially the ones in the infragranular layer VI—of topical applied glutamate would be investigated in respect of the induced tuning and bandwidth effects. Additionally, activity of the auditory nuclei should be monitored to correlate the potential glutamatergic corticothalamic feed with the activity of layer VI.

The DA associated gain increase of infragranular layers Vb/Vla and supragranular layers I/II is coinciding with the principle idea of long-term memory consolidation and learning associated plasticity (Happel, 2016). Although previous studies indicate that the artificial application of SKF-38393 as a DA agonist also facilitates in a relative gain increase due to infragranular input activity as proven by depth stimulation in infragranular layers (Happel et al., 2014a), I did not find any significant increase of granular activity, which deviates from the naïve control animals (Brunk et al., 2019). Therefore, I assume that DA boosts the infragranular layers Vb and Vla in order to promote the trajectory from layer Vb towards the supragranular layers as no such excitatory projections have been found in layer Vla in the current literature (Compare Figure 3 on page 12).

In order to estimate the changes of cortical integration within layers, I derived the tuning slopes for BF, near- and non-BF bins in a layer-wise fashion. Interestingly, although the naïve Control group revealed a decline in cortical tuning properties for layer I/II, over time, those changes did not alter in their slopes indicating that the relative corticocortical communication still remained constant.

The manipulation of the VTA clearly affected thalamocortical input layers Vb/Vla as well as changes in slope and gain amplification were solely found in the optogenetic groups (C1V1 and YFP), yet steeper slopes and gain amplification were only found within the C1V1 animals and thus coincide within the effects found in supragranular layers, potentially laying a foundation for a mechanism of intratelencephalic neurons in the layers Vb/Vla which may provide a translaminar gain control of reward based sensory representation (Brunk et al., 2019). Sharpening of supragranular tuning has also been associated with attention and task engagement in the ACx of humans (De Martino et al., 2015).

The observed DA boosted increase of the supragranular activity most likely contributes to the ResidualCSDs and thus may reflect the increase of ipsilateral communication between columns by the overall gain increase in the cortical tuning for off-BFs. This

columnar communication would be a result of the corticocortical interaction from supragranular layers towards the granular layers of neighboring columns, which is in line with the work from Linden and Schreiner who showed in their 2003 publication that ipsilateral contributions mainly target in layers III/IV whereas contralateral projections target all layers except for layer I (Linden and Schreiner, 2003). Therefore, one can conclude that DA enhances the infragranular thalamic input and the corticothalamic output as well as the cortical processing of the supragranular layers, probably to prepare the column for an non-conscious engram related remapping of salient stimuli (Aru et al., 2019).

#### IV.V Alterations of the cortical micro-circuitry

In literature, the established canonical cortical circuitry is described to originate from the leminesel thalamocortical pathway in granular layers III/IV towards supragranular layers I/II before its trajectory terminates into infragranular layers V/VI (Constantinople and Bruno, 2013; Linden and Schreiner, 2003; Mitani et al., 1985). Yet, this generalization of cortical micro-circuitry is only valid for the anesthetized state and does not hold to be true in awake animals since those animals display a stronger thalamic input activity in infragranular layers (Deane et al., 2019; Zempeltzi et al., 2019).

In their 2019 review Aru et al. state that there are two distinct thalamocortical pathways, which are engaged differently according to the conscious state of the individual. They describe a so-called specific thalamic input, which dominantly targets the granular layer IV as well as more mildly the infragranular layers Vb/Vla. The second non-specific thalamic input engages cells in layer Vb and the supragranular layers and thus emphasizes the central role of layer Vb for both circuits as well as for the corticothalamic feedback (Aru et al., 2019). The authors state that the corticothalamic feedback is vital for the conscious perception and further states that only parts of the layer Vb guided information becomes eventually conscious. In perspective of my results this further increases the importance of the infragranular layers in respect of thalamic input and corticothalamic feedback propagation in learning associations.

Similar evidence was shown in our lab by direct stimulations of supra-, infra- and granular layers during an active auditory avoidance task, further solidifying the importance of the infragranular layers during learning associations of salient stimuli (Happel et al., 2014a).

Assuming that we investigate two different cortical loop systems at the same time the disentangling and relating of either system towards the observed changes displays a challenging task.

Yet, since animals have been deeply anesthetized during the recording and the conscious state of the animals has been frequently checked via the paw-withdraw-reflex, it can be assumed that changes within infragranular layers are primarily results of increased DA boosted cortical processing. This boost is most likely guided via cortical layer Va—without affecting the gain of layer Va processing—towards layers I/II increasing the corticocortical columnar processing of the unconscious state (Aru et al., 2019). Likewise, Va projects also into infragranular layers Vb and VI, promoting corticothalamic feedback towards the MGm/MGd as corticothalamic feedbacks have been associated with motor planning (Collins and Anastasiades, 2019) and are more dominant in the awake state (Deane et al., 2019; Zempeltzi et al., 2019).

In order to understand cortical circuits, *in vivo* studies in anesthetized and awake animals are essential, especially to improve the understanding of the cortical effects in an active listening state during early and late training stages (Budinger and Kanold, 2018).

## V. Conclusion

In this thesis I showed the temporal changes of cortical processing within the ACx of the Mongolian gerbil before and after a reward associated stimulation of the VTA in a naïve control, an YFP control and an optogenetic C1V1 group. Increased cortical processing in infra- and supragranular layers, was found to be matching with DA receptor distributions and found YFP expression originating from the transduced VTA. Furthermore, I showed that YFP animals are not sufficient to relate optogenetic experiments with since non-specific effects reduced the power of cortical processing below the level of the naïve, non-manipulated, control group and that more rostral stimulation sides within the VTA yield in higher lever pressing. These findings lay a potential foundation for the initial effects for cortical remapping on a columnar level for context associated stimuli (Bao et al., 2001; Hui et al., 2009). The findings of my thesis revealed dopaminergic effects beyond the well-established immediate scope of the RPE, which rather serve as an explanation of the scope of the credit assignment problem or Cajal's theory of cortical plasticity.

The potential observed changes of the micro-circuit mechanisms, evoked by VTA associated DA, within the cortical column of the ACx are summarized in Figure 24.

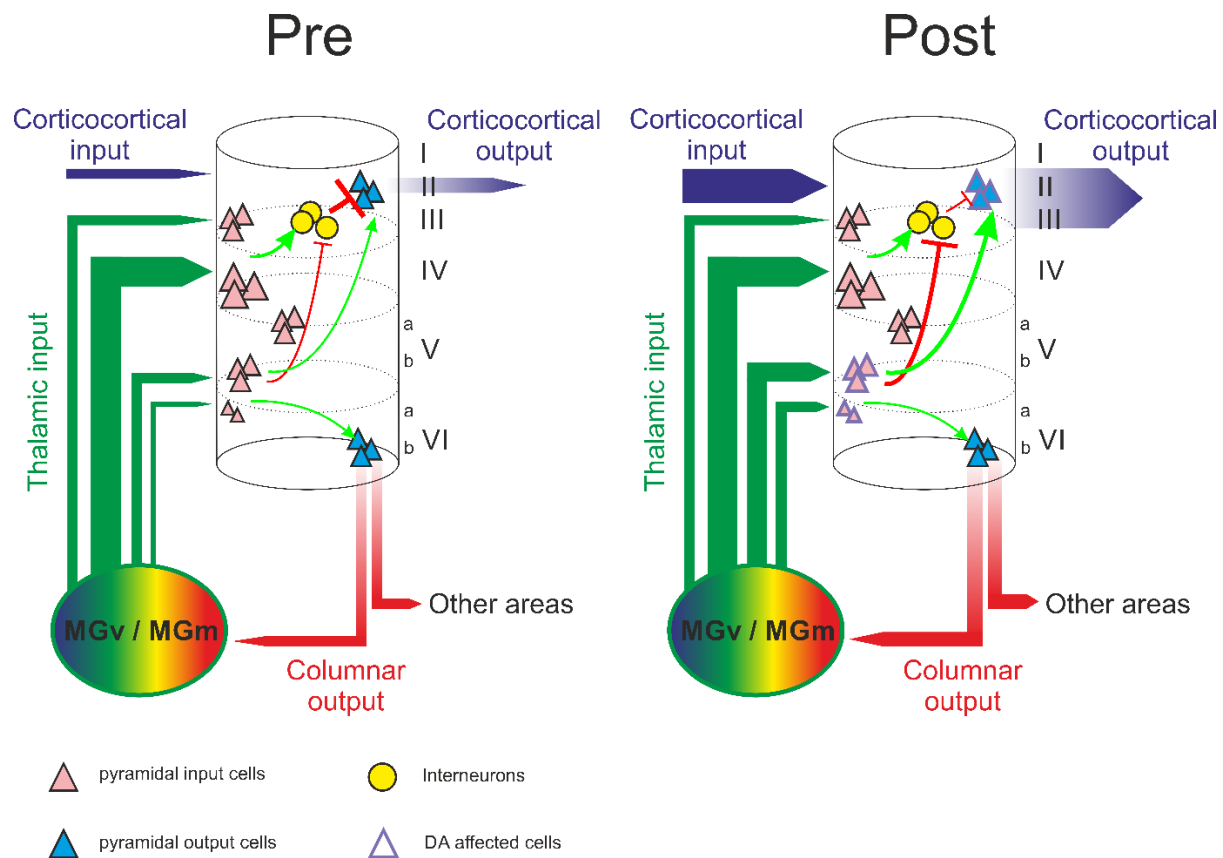


Figure 24: Summary of VTA stimulation effects on cortical layers

Prominent thalamocortical projections from the ventral and medial divisions of the MGB terminate predominantly into the granular and infragranular layers III/IV and Vb/Vla, respectively. DA associated effects after VTA stimulation (Post) are found within supragranular (I/II) and infragranular layers (Vb/Vla). VTA associated DA, therefore, performs in a bimodal fashion: Firstly, there is frequency-specific gain amplification within the sensory-evoked responses of the infragranular input layers Vb/Vla. This gain enhancement surpasses granular inputs and effectuates the spectral tuning of supragranular layers I/II. Linewidth indicates conceptual effects sizes. Based on Brunk et al., 2019; Deane et al., 2019; Happel, 2016.

## V.I Outlook

Dopamine is among one of the most important neurotransmitters involved in engram formation by inducing and thus its investigation thoroughly contributes to the understanding of cortical remapping. The current study merely scratched the surface of the investigative scope and thus allows for future experiments to further investigate the influence of contra- and ipsilateral stimulation of the VTA within an awake and task engaged animal. Whether the cortical origin of DA truly emerges from the direct

projections of the VTA or rather of an indirect pathway can be further explored with anatomical connectome studies. Likewise other candidate brain structures, which might contribute towards the indirect dopaminergic projections like the substantia nigra, locus coeruleus, amygdala and nucleus accumbens could be manipulated via optogenetic manipulation to reveal time effects within cortical electrode measurements or microdialysis during the animal training. Limitations of the stimulation side, as implied by higher lever pressing rates by more rostral VTA stimulation side could be avoided by changing from the classical optogenetic stimulation of opsins towards bioluminescent optogenetics of luminopsins (Berglund et al., 2019, 2016; Prakash et al., 2018), since luminopsins are expressing their own light source, which can be activated by an intravenous drug application of luciferins.

Although gerbils are an excellent model organism of choice when it comes towards learning experiments and the investigation of human like hearing ranges, to the current stage gerbils are not the most suitable model organism of choice for optogenetic manipulations of specific brain structures due to the lack of specific strains. Therefore, it is to be recommended to change to Cre- or Dat- rat strains for future experiments, since the gain specificity would allow for more unifiable outcomes by avoiding the intermingled effects of the unspecific stimulations sides.

However, the new-insights gained from this thesis provide an initial estimate about the, to be expected, effects and therefore, lay the foundation for future experiments further expanding our knowledge of the process of cortical plasticity.

## Literature

- Adam A, Deimel S, Pardo-Medina J, García-Martínez J, Konte T, Limón MC, Avalos J, Terpitz U. 2018. Protein Activity of the Fusarium fujikuroi Rhodopsins CarO and OpsA and Their Relation to Fungus-Plant Interaction. *Int J Mol Sci* **19**. doi:10.3390/ijms19010215
- Agnati LF, Ferré S, Leo G, Lluis C, Canela EI, Franco R, Fuxe K. 2004. On the Molecular Basis of the Receptor Mosaic Hypothesis of the Engram. *Cell Mol Neurobiol* **24**:501–516. doi:10.1023/B:CEMN.0000023626.35717.5d
- Agogino AK, Tumer K. 2004. Unifying Temporal and Structural Credit Assignment Problems. *Proc Third Int Jt Conf Auton Agents Multiagent Syst - Vol 2* 980–987. doi:10.1109/aamas.2004.289
- Anderegg A, Poulin J-F, Awatramani R. 2015. Molecular heterogeneity of midbrain dopaminergic neurons – Moving toward single cell resolution. *FEBS Lett* **589**:3714–3726. doi:10.1016/J.FEBSLET.2015.10.022
- Aransay A, Rodríguez-López C, García-Amado M, Clascá F, Prensa L. 2015. Long-range projection neurons of the mouse ventral tegmental area: a single-cell axon tracing analysis. *Front Neuroanat* **9**:59. doi:10.3389/fnana.2015.00059
- Arias-Gil G, Ohl FW, Takagaki K, Lippert MT. 2016. Measurement, modeling, and prediction of temperature rise due to optogenetic brain stimulation. *Neurophotonics* **3**:045007. doi:10.11117/1.NPh.3.4.045007
- Aru J, Suzuki M, Rutiku R, Larkum ME, Bachmann T. 2019. Coupling the State and Contents of Consciousness. *Front Syst Neurosci* **13**:1–9. doi:10.3389/fnsys.2019.00043
- Atencio CA, Sharpee TO, Schreiner CE. 2009. Hierarchical computation in the canonical auditory cortical circuit. *Proc Natl Acad Sci U S A* **106**:21894–9. doi:10.1073/pnas.0908383106
- Ayaz A, Stäuble A, Hamada M, Wulf M-A, Saleem AB, Helmchen F. 2019. Layer-specific integration of locomotion and sensory information in mouse barrel cortex. *Nat Commun* **10**:2585. doi:10.1038/s41467-019-10564-8
- Bandyopadhyay S, Shamma SA, Kanold PO. 2010. Dichotomy of functional organization in the mouse auditory cortex. *Nat Neurosci* **13**:361–368.

doi:10.1038/nn.2490

- Bao S, Chan VT, Merzenich MM. 2001. Cortical remodelling induced by activity of ventral tegmental dopamine neurons. *Nature* **412**:79–83. doi:10.1038/35083586
- Bariselli S, Gланетас C, Tzanoulinou S, Bellone C. 2016. Ventral tegmental area subcircuits process rewarding and aversive experiences. *J Neurochem* **139**:1071–1080. doi:10.1111/jnc.13779
- Batabyal S, Cervenka G, Ha JH, Kim YT, Mohanty S, Davies WIL. 2015. Broad-band activatable white-opsin. *PLoS One* **10**:1–13. doi:10.1371/journal.pone.0136958
- Berglund K, Clissold K, Li HE, Wen L, Park SY, Gleixner J, Klein ME, Lu D, Barter JW, Rossi MA, Augustine GJ, Yin HH, Hochgeschwender U. 2016. Luminopsins integrate opto- and chemogenetics by using physical and biological light sources for opsin activation. *Proc Natl Acad Sci U S A* **113**:E358-67. doi:10.1073/pnas.1510899113
- Berglund K, Fernandez AM, Gutekunst CAN, Hochgeschwender U, Gross RE. 2019. Step-function luminopsins for bimodal prolonged neuromodulation. *J Neurosci Res*. doi:10.1002/jnr.24424
- Beul SF, Hilgetag CC. 2015. Towards a “canonical” agranular cortical microcircuit. *Front Neuroanat* **8**:1–8. doi:10.3389/fnana.2014.00165
- Blundon JA, Zakharenko SS. 2013. Presynaptic Gating of Postsynaptic Synaptic Plasticity at thalamocortical synapses: a plasticity filter in the adult auditory cortex. *Neurosci* **19**:465–478. doi:10.1177/1073858413482983
- Bosman CA, Aboitiz F. 2015. Functional constraints in the evolution of brain circuits. *Front Neurosci* **9**:303. doi:10.3389/FNINS.2015.00303
- Braak H. 1974. On club-shaped neurons establishing part of the deep moiety of layer VI in the human isocortex. *Cell Tissue Res* **156**:113–125. doi:10.1007/BF00220105
- Briggs F. 2010. Organizing principles of cortical layer 6. *Front Neural Circuits* **4**:3. doi:10.3389/neuro.04.003.2010
- Brocka M, Helbing C, Vincenz D, Scherf T, Montag D, Goldschmidt J, Angenstein F, Lippert M. 2018. Contributions of dopaminergic and non-dopaminergic neurons to VTA-stimulation induced neurovascular responses in brain reward circuits.

Brodt S, Gais S, Beck J, Erb M, Scheffler K, Schönauer M. 2018. Fast track to the neocortex: A memory engram in the posterior parietal cortex. *Science* **362**:1045–1048. doi:10.1126/science.aau2528

Brunk M, Sputh S, Doose S, van de Linde S, Terpitz U. 2018. HyphaTracker: An ImageJ toolbox for time-resolved analysis of spore germination in filamentous fungi. *Sci Rep* **8**:605. doi:10.1038/s41598-017-19103-1

Brunk MGK, Deane KE, Kisse M, Deliano M, Vieweg S, Ohl FW, Lippert MT, Happel MFK. 2019. Optogenetic stimulation of the VTA modulates a frequency-specific gain of thalamocortical inputs in infragranular layers of the auditory cortex. *Sci Rep* **9**:20385. doi:10.1038/s41598-019-56926-6

Budinger E, Heil P, Scheich H. 2000. Functional organization of auditory cortex in the Mongolian gerbil (*Meriones unguiculatus*). III. Anatomical subdivisions and corticocortical connections. *Eur J Neurosci* **12**:2425–2451. doi:10.1046/j.1460-9568.2000.00142.x

Budinger E, Kanold PO. 2018. Auditory Cortex CircuitsBrain Mapping. pp. 199–233. doi:10.1007/978-3-319-71798-2\_8

Budinger E, Laszcz A, Lison H, Scheich H, Ohl FW. 2008. Non-sensory cortical and subcortical connections of the primary auditory cortex in Mongolian gerbils: bottom-up and top-down processing of neuronal information via field AI. *Brain Res* **1220**:2–32. doi:10.1016/j.brainres.2007.07.084

Budinger E, Scheich H. 2009. Anatomical connections suitable for the direct processing of neuronal information of different modalities via the rodent primary auditory cortex. *Hear Res* **258**:16–27. doi:10.1016/j.heares.2009.04.021

Chen X, Guo Y, Feng J, Liao Z, Li Xinjian, Wang H, Li Xiao, He J. 2013. Encoding and retrieval of artificial visuoauditory memory traces in the auditory cortex requires the entorhinal cortex. *J Neurosci* **33**:9963–74. doi:10.1523/JNEUROSCI.4078-12.2013

Chernov MM, Chen G, Roe AW. 2014. Histological assessment of thermal damage in the brain following infrared neural stimulation. *Brain Stimul* **7**:476–82. doi:10.1016/j.brs.2014.01.006

- Ciccarelli A, Calza A, Panzanelli P, Concas A, Giustetto M, Sassoè-Pognetto M. 2012. Organization of GABAergic Synaptic Circuits in the Rat Ventral Tegmental Area. *PLoS One* **7**:e46250. doi:10.1371/journal.pone.0046250
- Collins DP, Anastasiades PG. 2019. Cellular specificity of cortico-thalamic loops for motor planning. *J Neurosci* **39**:2577–2580. doi:10.1523/JNEUROSCI.2964-18.2019
- Constantinople CM, Bruno RM. 2013. Deep Cortical Layers Are Activated Directly by Thalamus. *Science (80- )* **340**:1591–1594. doi:10.1126/science.1236425
- Courtiol E, Wilson DA. 2015. The olfactory thalamus: unanswered questions about the role of the mediodorsal thalamic nucleus in olfaction. *Front Neural Circuits* **9**:49. doi:10.3389/fncir.2015.00049
- Crochet S, Petersen CCH. 2009. Cortical Dynamics by Layers. *Neuron* **64**:298–300. doi:10.1016/J.NEURON.2009.10.024
- Cudeiro J, Sillito AM. 2006. Looking back: corticothalamic feedback and early visual processing. *Trends Neurosci.* doi:10.1016/j.tins.2006.05.002
- Darwin C. 1859. On the Origin of the Species, Darwin.
- Dawydow A, Gueta R, Ljaschenko D, Ullrich S, Hermann M, Ehmann N, Gao S, Fiala A, Langenhan T, Nagel G, Kittel RJ. 2014. Channelrhodopsin-2-XXL, a powerful optogenetic tool for low-light applications. *Proc Natl Acad Sci U S A* **111**:13972–7. doi:10.1073/pnas.1408269111
- De Martino F, Moerel M, Ugurbil K, Goebel R, Yacoub E, Formisano E. 2015. Frequency preference and attention effects across cortical depths in the human primary auditory cortex. *Proc Natl Acad Sci U S A* **112**:16036–41. doi:10.1073/pnas.1507552112
- Deane KE, Brunk MGK, Curran AW, Zempeltzi MM, Ma J, Lin X, Abela F, Aksit S, Deliano M, Ohl FW, Happel MFK. 2019. Ketamine anesthesia induces gain enhancement via recurrent excitation in granular input layers of the auditory cortex. doi:10.1101/810978
- Deisseroth K. 2011. Optogenetics. *Nat Methods* **8**:26–29. doi:10.1038/nmeth.f.324
- Deliano M, Brunk MGK, El-Tabbal M, Zempeltzi MM, Happel MFK, Ohl FW. 2018. Dopaminergic neuromodulation of high gamma stimulus phase-locking in gerbil

primary auditory cortex mediated by D1/D5-receptors. *Eur J Neurosci*. doi:10.1111/ejn.13898

Deliano M, Scheich H, Ohl FW. 2009. Auditory cortical activity after intracortical microstimulation and its role for sensory processing and learning. *J Neurosci* **29**:15898–15909. doi:10.1523/JNEUROSCI.1949-09.2009

Deutscher A, Kurt S, Scheich H, Schulze H. 2006. Cortical and subcortical sides of auditory rhythms and pitches. *Neuroreport* **17**:853–856. doi:10.1097/01.wnr.0000221837.20255.62

Devoto P, Flore G, Pani L, Gessa GL. 2001. Evidence for co-release of noradrenaline and dopamine from noradrenergic neurons in the cerebral cortex. *Mol Psychiatry* **6**:657–664. doi:10.1038/sj.mp.4000904

Devoto P, Flore G, Saba P, Fà M, Gessa G. 2005. Co-release of noradrenaline and dopamine in the cerebral cortex elicited by single train and repeated train stimulation of the locus coeruleus. *BMC Neurosci* **6**:31. doi:10.1186/1471-2202-6-31

Devoto P, Flore G, Saba P, Frau R, Gessa GL. 2015. Selective inhibition of dopamine-beta-hydroxylase enhances dopamine release from noradrenergic terminals in the medial prefrontal cortex. *Brain Behav* **5**:n/a-n/a. doi:10.1002/brb3.393

Dhruv NT. 2015. Rethinking canonical cortical circuits. *Nat Neurosci* **18**:1538–1538. doi:10.1038/nn1115-1538

Douglas RJ, Martin KA. 1991. A functional microcircuit for cat visual cortex. *J Physiol* **440**:735–69. doi:10.1113/jphysiol.1991.sp018733

Douglas RJ, Martin KAC. 2004. Neuronal Circuits of the Neocortex. *Annu Rev Neurosci* **27**:419–451. doi:10.1146/annurev.neuro.27.070203.144152

Douglas RJ, Martin KAC, Whitteridge D. 1989. Microcircuit for Neocortex. *Neural Comput* **1**:480–488.

Ellwood IT, Patel T, Wadia V, Lee AT, Liptak AT, Bender KJ, Sohal VS. 2017. Tonic or Phasic Stimulation of Dopaminergic Projections to Prefrontal Cortex Causes Mice to Maintain or Deviate from Previously Learned Behavioral Strategies. *J Neurosci* **37**:8315–8329. doi:10.1523/JNEUROSCI.1221-17.2017

Evans DA, Stempel AV, Vale R, Ruehle S, Lefler Y, Branco T. 2018. A synaptic

threshold mechanism for computing escape decisions. *Nature* **558**:590–594. doi:10.1038/s41586-018-0244-6

Fibiger HC, LePiane FG, Jakubovic A, Phillips AG. 1987. The role of dopamine in intracranial self-stimulation of the ventral tegmental area 1. *JNeurosci* **7**:3888–3896.

Fiorino DF. 1993. Electrical stimulation of reward sites in the ventral tegmental area. Vol.55, *Behavioural Brain Research* **55**:131–141.

Fisher RA. 1919. XV.—The Correlation between Relatives on the Supposition of Mendelian Inheritance. *Trans R Soc Edinburgh* **52**:399–433. doi:10.1017/S0080456800012163

Foote SL, Freedman R, Oliver AP. 1975. Effects of putative neurotransmitters on neuronal activity in monkey auditory cortex. *Brain Res* **86**:229–242. doi:10.1016/0006-8993(75)90699-X

Freeman JA, Nicholson C. 1975. Experimental optimization of current source-density technique for anuran cerebellum. *J Neurophysiol* **38**:369–82.

Frischknecht R, Happel MFK. 2017. Impact of the extracellular matrix on plasticity in juvenile and adult brains. *e-Neuroforum* **22**:1–6. doi:10.1515/s13295-015-0021-z

Galizia CG, Lledo P-M. 2013. Neurosciences - From Molecule to Behavior: a university textbook. Springer Verlag. doi:10.1007/978-3-642-10769-6

García-Martínez J, Brunk M, Avalos J, Terpitz U. 2015. The CarO rhodopsin of the fungus Fusarium fujikuroi is a light-driven proton pump that retards spore germination. *Sci Rep* **5**:1–11. doi:10.1038/srep07798

Ghisaidoobe ABT, Chung SJ. 2014. Intrinsic tryptophan fluorescence in the detection and analysis of proteins: A focus on förster resonance energy transfer techniques. *Int J Mol Sci* **15**:22518–22538. doi:10.3390/ijms151222518

Goldschmidt J, Wanger T, Engelhorn A, Friedrich H, Happel M, Ilango A, Engelmann M, Stuermer IW, Ohl FW, Scheich H. 2010. High-resolution mapping of neuronal activity using the lipophilic thallium chelate complex TIDDC: Protocol and validation of the method. *Neuroimage* **49**:303–315. doi:10.1016/j.neuroimage.2009.08.012

Goldschmidt J, Zuschratter W, Scheich H. 2004. High-resolution mapping of neuronal

activity by thallium autometallography. *Neuroimage* **23**:638–647. doi:10.1016/j.neuroimage.2004.05.023

Gorelova N, Mulholland PJ, Chandler LJ, Seamans JK. 2012. The glutamatergic component of the mesocortical pathway emanating from different subregions of the ventral midbrain. *Cereb Cortex* **22**:327–36. doi:10.1093/cercor/bhr107

Grosso A, Cambiaghi M, Milano L, Renna A, Sacco T, Sacchetti B. 2016. Region- and Layer-Specific Activation of the Higher Order Auditory Cortex Te2 after Remote Retrieval of Fear or Appetitive Memories. *Cereb Cortex* **27**:bhw159. doi:10.1093/cercor/bhw159

Guillard BP, El Mansari M, Blier P. 2008. Cross-talk between dopaminergic and noradrenergic systems in the rat ventral tegmental area, locus caeruleus, and dorsal hippocampus. *Mol Pharmacol* **74**:1463–75. doi:10.1124/mol.108.048033

Guo S, Chen S, Zhang Q, Wang Y, Xu K, Zheng X. 2014. Optogenetic activation of the excitatory neurons expressing CaMKIIα in the ventral tegmental area upregulates the locomotor activity of free behaving rats. *Biomed Res Int* **2014**:687469. doi:10.1155/2014/687469

Guo W, Chambers AR, Darrow KN, Hancock KE, Shinn-Cunningham BG, Polley DB. 2012. Robustness of cortical topography across fields, laminae, anesthetic states, and neurophysiological signal types. *J Neurosci* **32**:9159–9172. doi:10.1523/JNEUROSCI.0065-12.2012

Guy J, Staiger JF. 2017. The Functioning of a Cortex without Layers. *Front Neuroanat* **11**:54. doi:10.3389/fnana.2017.00054

Hage TA, Khaliq ZM. 2015. Tonic firing rate controls dendritic Ca<sup>2+</sup> signaling and synaptic gain in substantia nigra dopamine neurons. *J Neurosci* **35**:5823–5836. doi:10.1523/JNEUROSCI.3904-14.2015

Happel MFK. 2016. Dopaminergic impact on local and global cortical circuit processing during learning. *Behav Brain Res* **299**:32–41. doi:10.1016/j.bbr.2015.11.016

Happel MFK, Deliano M, Handschuh J, Ohl FW. 2014a. Dopamine-Modulated Recurrent Corticoefferent Feedback in Primary Sensory Cortex Promotes Detection of Behaviorally Relevant Stimuli. *J Neurosci* **34**:1234–1247. doi:10.1523/JNEUROSCI.1990-13.2014

- Happel MFK, Frischknecht R. 2016. Neuronal Plasticity in the Juvenile and Adult Brain Regulated by the Extracellular MatrixComposition and Function of the Extracellular Matrix in the Human Body. doi:10.5772/62452
- Happel MFK, Jeschke M, Ohl FW. 2010. Spectral Integration in Primary Auditory Cortex Attributable to Temporally Precise Convergence of Thalamocortical and Intracortical Input. *J Neurosci* **30**:11114–11127. doi:10.1523/JNEUROSCI.0689-10.2010
- Happel MFK, Niekisch H, Castiblanco Rivera LL, Ohl FW, Deliano M, Frischknecht R. 2014b. Enhanced cognitive flexibility in reversal learning induced by removal of the extracellular matrix in auditory cortex. *Proc Natl Acad Sci* **111**:2800–2805. doi:10.1073/pnas.1310272111
- Happel MFK, Ohl FW. 2017. Compensating Level-Dependent Frequency Representation in Auditory Cortex by Synaptic Integration of Corticocortical Input. *PLoS One* **12**:e0169461. doi:10.1371/journal.pone.0169461
- Harding GW. 1992. The currents that flow in the somatosensory cortex during the direct cortical response. *Exp Brain Res* **90**:29–39. doi:10.1007/BF00229253
- Hasselmo ME. 2006. The role of acetylcholine in learning and memory. *Curr Opin Neurobiol* **16**:710–5. doi:10.1016/j.conb.2006.09.002
- Holly EN, Miczek KA. 2016. Ventral tegmental area dopamine revisited: effects of acute and repeated stress. *Psychopharmacology (Berl)* **233**:163–86. doi:10.1007/s00213-015-4151-3
- Hui GK, Wong KL, Chavez CM, Leon MI, Robin KM, Weinberger NM. 2009. Conditioned tone control of brain reward behavior produces highly specific representational gain in the primary auditory cortex. *Neurobiol Learn Mem* **92**:27–34. doi:10.1016/J.NLM.2009.02.008
- Hyman SE, Malenka RC. 2001. Addiction and the brain: The neurobiology of compulsion and its persistence. *Nat Rev Neurosci* **2**:695–703. doi:10.1038/35094560
- Jacob SN, Nienborg H. 2018. Monoaminergic Neuromodulation of Sensory Processing. *Front Neural Circuits* **12**:51. doi:10.3389/fncir.2018.00051
- Jarvis ED, Güntürkün O, Bruce L, Csillag A, Karten H, Kuenzel W, Medina L, Paxinos

G, Perkel DJ, Shimizu T, Striedter G, Wild JM, Ball GF, Dugas-Ford J, Durand SE, Hough GE, Husband S, Kubikova L, Lee DW, Mello C V, Powers A, Siang C, Smulders T V, Wada K, White SA, Yamamoto K, Yu J, Reiner A, Butler AB, Avian Brain Nomenclature Consortium. 2005. Avian brains and a new understanding of vertebrate brain evolution. *Nat Rev Neurosci* **6**:151–9. doi:10.1038/nrn1606

Jessen KR, Mirsky R. 1980. Glial cells in the enteric nervous system contain glial fibrillary acidic protein. *Nature* **286**:736–737. doi:10.1038/286736a0

Jones EG. 2001. The thalamic matrix and thalamocortical synchrony. *Trends Neurosci* **24**:595–601. doi:10.1016/S0166-2236(00)01922-6

Kandel ER, Schwartz JH, Jessell TM, Siegelbaum SA, Hudspeth AJ. 2013. Principles of neural science, 5th Editio. ed. McGraw-Hill.

Katzner S, Nauhaus I, Benucci A, Bonin V, Ringach DL, Carandini M. 2009. Local Origin of Field Potentials in Visual Cortex. *Neuron* **61**:35–41. doi:10.1016/j.neuron.2008.11.016

Kauer JA. 2003. Addictive Drugs and Stress Trigger a Common Change at VTA Synapses. *Neuron* **37**:549–550. doi:10.1016/S0896-6273(03)00087-4

Kaur S, Rose HJ, Lazar R, Liang K, Metherate R. 2005. Spectral integration in primary auditory cortex: Laminar processing of afferent input, *in vivo* and *in vitro*. *Neuroscience* **134**:1033–1045. doi:10.1016/J.NEUROSCIENCE.2005.04.052

Keiflin R, Janak PH. 2015. Dopamine Prediction Errors in Reward Learning and Addiction: From Theory to Neural Circuitry. *Neuron*. doi:10.1016/j.neuron.2015.08.037

Kilgard MP. 1998. Cortical Map Reorganization Enabled by Nucleus Basalis Activity. *Science (80- )* **279**:1714–1718. doi:10.1126/science.279.5357.1714

Kim J, Ham S, Hong H, Moon C, Im H-I. 2016. Brain Reward Circuits in Morphine Addiction. *Mol Cells* **39**:645–653. doi:10.14348/molcells.2016.0137

Kirsch JA, Güntürkün O, Rose J. 2008. Insight without cortex: Lessons from the avian brain. *Conscious Cogn* **17**:475–483. doi:10.1016/J.CONCOG.2008.03.018

Koob GF, Balcom GJ, Meyerhoff JL. 1975. Dopamine and norepinephrine levels in the nucleus accumbens, olfactory tubercle and corpus striatum following lesions in the ventral tegmental area. *Brain Res* **94**:45–55. doi:10.1016/0006-8993(75)90875-6

Lapish CC, Seamans JK, Judson Chandler L. 2006. Glutamate-Dopamine Cotransmission and Reward Processing in Addiction. *Alcohol Clin Exp Res* **30**:1451–1465. doi:10.1111/j.1530-0277.2006.00176.x

Lavin A, Nogueira L, Lapish CC, Wightman RM, Phillips PEM, Seamans JK. 2005. Mesocortical dopamine neurons operate in distinct temporal domains using multimodal signaling. *J Neurosci* **25**:5013–23. doi:10.1523/JNEUROSCI.0557-05.2005

Laxton AW, Tang-Wai DF, McAndrews MP, Zumsteg D, Wennberg R, Keren R, Wherrett J, Naglie G, Hamani C, Smith GS, Lozano AM. 2010. A phase I trial of deep brain stimulation of memory circuits in Alzheimer's disease. *Ann Neurol* **68**:521–534. doi:10.1002/ana.22089

Lefort S, Tomm C, Floyd Sarria J-C, Petersen CCH. 2009. The excitatory neuronal network of the C2 barrel column in mouse primary somatosensory cortex. *Neuron* **61**:301–16. doi:10.1016/j.neuron.2008.12.020

Levitz J, Popescu AT, Reiner A, Isacoff EY. 2016. A Toolkit for Orthogonal and in vivo Optical Manipulation of Ionotropic Glutamate Receptors. *Front Mol Neurosci* **9**:2. doi:10.3389/fnmol.2016.00002

Lewis DA, Sesack SR. 1997. Chapter VI Dopamine systems in the primate brain. *Handb Chem Neuroanat* **13**:263–375. doi:10.1016/S0924-8196(97)80008-5

Li Y, Li C-Y, Xi W, Jin S, Wu Z-H, Jiang P, Dong P, He X-B, Xu F-Q, Duan S, Zhou Y-D, Li X-M. 2019. Rostral and Caudal Ventral Tegmental Area GABAergic Inputs to Different Dorsal Raphe Neurons Participate in Opioid Dependence. *Neuron* **101**:748-761.e5. doi:10.1016/j.neuron.2018.12.012

Lidow MS. 1995. D1- and D2 dopaminergic receptors in the developing cerebral cortex of macaque monkey: A film autoradiographic study. *Neuroscience* **65**:439–452. doi:10.1016/0306-4522(94)00475-K

Lidow MS, Goldman-Rakic PS, Gallager DW, Rakic P. 1991. Distribution of dopaminergic receptors in the primate cerebral cortex: Quantitative autoradiographic analysis using [<sup>3</sup>H]raclopride, [<sup>3</sup>H]spiperone and [<sup>3</sup>H]SCH23390. *Neuroscience* **40**:657–671. doi:10.1016/0306-4522(91)90003-7

Linden JF, Schreiner CE. 2003. Columnar Transformations in Auditory Cortex? A Comparison to Visual and Somatosensory Cortices. *Cereb Cortex* **13**:83–89.

doi:10.1093/cercor/13.1.83

- Lippert MT, Takagaki K, Weidner T, Brocka M, Tegtmeyer J, Ohl FW. 2018. Optogenetic Intracranial Self-Stimulation as a Method to Study the Plasticity-Inducing Effects of DopamineHandbook of Behavioral Neuroscience. pp. 311–326. doi:10.1016/B978-0-12-812028-6.00017-3
- Liu CL, Gao M, Jin GZ, Zhen X. 2012. GABA Neurons in the Ventral Tegmental Area Responding to Peripheral Sensory Input. *PLoS One* **7**:1–8. doi:10.1371/journal.pone.0051507
- Liu X, Ramirez S, Pang PT, Puryear CB, Govindarajan A, Deisseroth K, Tonegawa S. 2012. Optogenetic stimulation of a hippocampal engram activates fear memory recall. *Nature* **484**:381–385. doi:10.1038/nature11028
- Liu Y, Jacques SL, Azimipour M, Rogers JD, Pashaei R, Eliceiri KW. 2015. OptogenSIM: a 3D Monte Carlo simulation platform for light delivery design in optogenetics. *Biomed Opt Express* **6**:4859. doi:10.1364/BOE.6.004859
- Lou Y, Luo W, Zhang G, Tao C, Chen P, Zhou Y, Xiong Y. 2014. Ventral tegmental area activation promotes firing precision and strength through circuit inhibition in the primary auditory cortex. *Front Neural Circuits* **8**:25. doi:10.3389/fncir.2014.00025
- Martins ARO, Froemke RC. 2015. Coordinated forms of noradrenergic plasticity in the locus coeruleus and primary auditory cortex. *Nat Neurosci* **18**:1483–1492. doi:10.1038/nn.4090
- Merker B. 2007. Consciousness without a cerebral cortex: A challenge for neuroscience and medicine. *Behav Brain Sci* **30**:63–81. doi:10.1017/S0140525X07000891
- Method of the Year 2010. 2011. . *Nat Methods* **8**:1–1. doi:10.1038/nmeth.f.321
- Mirenowicz J, Schultz W. 1996. Preferential activation of midbrain dopamine neurons by appetitive rather than aversive stimuli. *Nature* **379**:449–451. doi:10.1038/379449a0
- Mitani A, Shimokouchi M, Itoh K, Nomura S, Kudo M, Mizuno N. 1985. Morphology and laminar organization of electrophysiologically identified neurons in the primary auditory cortex in the cat. *J Comp Neurol* **235**:430–447.

doi:10.1002/cne.902350403

Mitlöhner J, Kaushik R, Niekisch H, Blondiaux A, Gee CE, Happel MFK, Gundelfinger E, Dityatev A, Frischknecht R, Seidenbecher C. 2020. Dopamine Receptor Activation Modulates the Integrity of the Perisynaptic Extracellular Matrix at Excitatory Synapses. *Cells* **9**:260. doi:10.3390/cells9020260

Mitzdorf U. 1985. Current source-density method and application in cat cerebral cortex: investigation of evoked potentials and EEG phenomena. *Physiol Rev* **65**:37–100. doi:10.1152/physrev.1985.65.1.37

Moczulska KE, Tinter-Thiede J, Peter M, Ushakova L, Wernle T, Bathellier B, Rumpel S. 2013. Dynamics of dendritic spines in the mouse auditory cortex during memory formation and memory recall. *Proc Natl Acad Sci* **110**:18315–18320. doi:10.1073/pnas.1312508110

Möller M, Denicola A. 2002. Protein tryptophan accessibility studied by fluorescence quenching. *Biochem Mol Biol Educ* **30**:175–178. doi:10.1002/bmb.2002.494030030035

Molnár Z, Kaas JH, de Carlos JA, Hevner RF, Lein E, Němec P. 2014. Evolution and development of the mammalian cerebral cortex. *Brain Behav Evol* **83**:126–39. doi:10.1159/000357753

Mountcastle PVB. 1998. Perceptual Neuroscience: The Cerebral Cortex. Harvard University Press.

Mowery TM, Kotak VC, Sanes DH. 2016. The onset of visual experience gates auditory cortex critical periods. *Nat Commun* **7**:10416. doi:10.1038/ncomms10416

Mylius J, Happel MFK, Gorkin AG, Huang Y, Scheich H, Brosch M. 2015. Fast transmission from the dopaminergic ventral midbrain to the sensory cortex of awake primates. *Brain Struct Funct*. doi:10.1007/s00429-014-0855-0

Nagel G, Ollig D, Fuhrmann M, Kateriya S, Musti AM, Bamberg E, Hegemann P. 2002. Channelrhodopsin-1: a light-gated proton channel in green algae. *Science* **296**:2395–8. doi:10.1126/science.1072068

Nagel G, Szellas T, Huhn W, Kateriya S, Adeishvili N, Berthold P, Ollig D, Hegemann P, Bamberg E. 2003. Channelrhodopsin-2, a directly light-gated cation-selective membrane channel. *Proc Natl Acad Sci U S A* **100**:13940–5.

doi:10.1073/pnas.1936192100

Niekisch H, Steinhardt J, Berghäuser J, Bertazzoni S, Kaschinski E, Kasper J, Kisse M, Mitlöhner J, Singh JB, Weber J, Frischknecht R, Happel MFK. 2019. Learning Induces Transient Upregulation of Brevican in the Auditory Cortex during Consolidation of Long-Term Memories. *J Neurosci* **39**:7049–7060. doi:10.1523/JNEUROSCI.2499-18.2019

Noback CR, Strominger NL, Demarest RJ, Ruggiero DA. 2005. The human nervous system: Structure and function: Sixth edition, The Human Nervous System: Structure and Function: Sixth Edition. doi:10.1007/978-1-59259-730-7

Ntamati NR, Lüscher C. 2016. VTA Projection Neurons Releasing GABA and Glutamate in the Dentate Gyrus. *eNeuro* **3**. doi:10.1523/ENEURO.0137-16.2016

O'Connell MN, Barczak A, Schroeder CE, Lakatos P. 2014. Layer specific sharpening of frequency tuning by selective attention in primary auditory cortex. *J Neurosci* **34**:16496–508. doi:10.1523/JNEUROSCI.2055-14.2014

Oberlaender M, de Kock CPJ, Bruno RM, Ramirez A, Meyer HS, Dercksen VJ, Helmstaedter M, Sakmann B. 2012. Cell Type-Specific Three-Dimensional Structure of Thalamocortical Circuits in a Column of Rat Vibrissal Cortex. *Cereb Cortex* **22**:2375–2391. doi:10.1093/cercor/bhr317

Olkowicz S, Kocourek M, Lučan RK, Porteš M, Fitch WT, Herculano-Houzel S, Němec P. 2016. Birds have primate-like numbers of neurons in the forebrain. *Proc Natl Acad Sci U S A* **113**:7255–60. doi:10.1073/pnas.1517131113

Ornstein K, Milon H, McRae-Degueurce A, Alvarez C, Berger B, Würzner HP. 1987. Biochemical and radioautographic evidence for dopaminergic afferents of the locus coeruleus originating in the ventral tegmental area. *J Neural Transm* **70**:183–191. doi:10.1007/BF01253597

Patton MH, Blundon JA, Zakharenko SS. 2019. Rejuvenation of plasticity in the brain: opening the critical period. *Curr Opin Neurobiol* **54**:83–89. doi:10.1016/j.conb.2018.09.003

Pisanello F, Mandelbaum G, Pisanello M, Oldenburg IA, Sileo L, Markowitz JE, Peterson RE, Della Patria A, Haynes TM, Emara MS, Spagnolo B, Datta SR, De Vittorio M, Sabatini BL. 2017. Dynamic illumination of spatially restricted or large brain volumes via a single tapered optical fiber. *Nat Neurosci* **20**:1180–1188.

doi:10.1038/nn.4591

Pisanello M, Pisano F, Sileo L, Maglie E, Bellistri E, Spagnolo B, Mandelbaum G, Sabatini BL, De Vittorio M, Pisanello F. 2018. Tailoring light delivery for optogenetics by modal demultiplexing in tapered optical fibers. *Sci Rep* **8**:4467. doi:10.1038/s41598-018-22790-z

Polter AM, Kauer JA. 2014. Stress and VTA synapses: implications for addiction and depression. *Eur J Neurosci* **39**:1179–88. doi:10.1111/ejn.12490

Prakash M, Medendorp WE, Hochgeschwender U. 2018. Defining parameters of specificity for bioluminescent optogenetic activation of neurons using in vitro multi electrode arrays (MEA). *J Neurosci Res*. doi:10.1002/jnr.24313

Radnikow G, Feldmeyer D. 2018. Layer- and Cell Type-Specific Modulation of Excitatory Neuronal Activity in the Neocortex. *Front Neuroanat* **12**:1. doi:10.3389/fnana.2018.00001

Radtke-Schuller S, Schuller G, Angenstein F, Grosser OS, Goldschmidt J, Budinger E. 2016. Brain atlas of the Mongolian gerbil (*Meriones unguiculatus*) in CT/MRI-aided stereotaxic coordinates. *Brain Struct Funct* **221**:1–272. doi:10.1007/s00429-016-1259-0

Reichenbach N, Herrmann U, Kähne T, Schicknick H, Pielot R, Naumann M, Dieterich DC, Gundelfinger ED, Smalla K-H, Tischmeyer W. 2015. Differential effects of dopamine signalling on long-term memory formation and consolidation in rodent brain. *Proteome Sci* **13**:13. doi:10.1186/s12953-015-0069-2

Roland PE, Hilgetag CC, Deco G. 2014. Cortico-cortical communication dynamics. *Front Syst Neurosci* **8**:1–11. doi:10.3389/fnsys.2014.00019

Rothschild G, Nelken I, Mizrahi A. 2010. Functional organization and population dynamics in the mouse primary auditory cortex. *Nat Neurosci* **13**:353–360. doi:10.1038/nn.2484

Russo SJ, Nestler EJ. 2013. The brain reward circuitry in mood disorders. *Nat Rev Neurosci* **14**:609–625. doi:10.1038/nrn3381

Saldeitis K, Happel MFK, Ohl FW, Scheich H, Budinger E. 2014. Anatomy of the auditory thalamocortical system in the mongolian gerbil: Nuclear origins and cortical field-, layer-, and frequency-specificities. *J Comp Neurol* **522**:2397–2430.

- Salinas-Hernández XI, Vogel P, Betz S, Kalisch R, Sigurdsson T, Duvarci S. 2018. Dopamine neurons drive fear extinction learning by signaling the omission of expected aversive outcomes. *eLife* **7**. doi:10.7554/eLife.38818
- Santana N, Artigas F. 2017. Laminar and Cellular Distribution of Monoamine Receptors in Rat Medial Prefrontal Cortex. *Front Neuroanat* **11**:87. doi:10.3389/FNANA.2017.00087
- Sara SJ. 2009. The locus coeruleus and noradrenergic modulation of cognition. *Nat Rev Neurosci* **10**:211–223. doi:10.1038/nrn2573
- Schaefer MK, Hechavarria JC, Kossi M. 2015. Quantification of mid and late evoked sinks in laminar current source density profiles of columns in the primary auditory cortex. *Front Neural Circuits* **9**:1–16. doi:10.3389/fncir.2015.00052
- Scheich H, Heil P, Langner G. 1993. Functional Organization of Auditory Cortex in the Mongolian Gerbil ( *Meriones unguiculatus* ) II. Tonotopic 2-Deoxyglucose. *Eur J Neurosci* **5**:898–914. doi:10.1111/j.1460-9568.1993.tb00941.x
- Scheich H, Stark H, Zuschratter W, Ohl FW, Simonis CE. 1997. Some functions of primary auditory cortex in learning and memory formation. *Adv Neurol* **73**:179–93.
- Schicknick H, Reichenbach N, Smalla K-H, Scheich H, Gundelfinger ED, Tischmeyer W. 2012. Dopamine modulates memory consolidation of discrimination learning in the auditory cortex. *Eur J Neurosci* **35**:763–774. doi:10.1111/j.1460-9568.2012.07994.x
- Schicknick H, Schott BH, Budinger E, Smalla KH, Riedel A, Seidenbecher CI, Scheich H, Gundelfinger ED, Tischmeyer W. 2008. Dopaminergic modulation of auditory cortex-dependent memory consolidation through mTOR. *Cereb Cortex* **18**:2646–2658. doi:10.1093/cercor/bhn026
- Schubert D, Kötter R, Luhmann HJ, Staiger JF. 2006. Morphology, Electrophysiology and Functional Input Connectivity of Pyramidal Neurons Characterizes a Genuine Layer Va in the Primary Somatosensory Cortex. *Cereb Cortex* **16**:223–236. doi:10.1093/cercor/bhi100
- Schubert D, Kötter R, Staiger JF. 2007. Mapping functional connectivity in barrel-related columns reveals layer- and cell type-specific microcircuits. *Brain Struct*

*Funct* **212**:107–119. doi:10.1007/s00429-007-0147-z

Schultz W. 2016. Dopamine reward prediction error coding. *Dialogues Clin Neurosci* **18**:23–32.

Schultz W. 2015. Neuronal Reward and Decision Signals: From Theories to Data. *Physiol Rev* **95**:853–951. doi:10.1152/physrev.00023.2014

Schultz W. 1998. Predictive reward signal of dopamine neurons. *J Neurophysiol* **80**:1–27. doi:10.1007/s00429-010-0262-0

Senova S, Scisniak I, Chiang C-C, Doignon I, Palfi S, Chaillet A, Martin C, Pain F. 2017. Experimental assessment of the safety and potential efficacy of high irradiance photostimulation of brain tissues OPEN. doi:10.1038/srep43997

Shen H. 2018. How to see a memory. *Nature* **553**:146–148. doi:10.1038/d41586-018-00107-4

Shohamy D, Adcock RA. 2010. Dopamine and adaptive memory. *Trends Cogn Sci* **14**:464–72. doi:10.1016/j.tics.2010.08.002

Sidor MM, Davidson TJ, Tye KM, Warden MR, Diesseroth K, Mcclung CA. 2015. In vivo Optogenetic Stimulation of the Rodent Central Nervous System. *J Vis Exp* 51483. doi:10.3791/51483

Slotnick SD, Moo LR, Segal JB, Hart J. 2003. Distinct prefrontal cortex activity associated with item memory and source memory for visual shapes. *Cogn Brain Res* **17**:75–82. doi:10.1016/S0926-6410(03)00082-X

Sponaugle AE, Badanich KA, Kirstein CL. 2008. Localization of stereotaxic coordinates for the ventral tegmental area in early adolescent, mid-adolescent and adult rats. *Brain Res* **1218**:215–223. doi:10.1016/j.brainres.2008.04.060

Stark H, Bischof A, Scheich H. 1999. Increase of extracellular dopamine in prefrontal cortex of gerbils during acquisition of the avoidance strategy in the shuttle-box. *Neurosci Lett* **264**:77–80. doi:10.1016/S0304-3940(99)00174-3

Stark H, Bischof A, Wagner T, Scheich H. 2001. Activation of the dopaminergic system of medial prefrontal cortex of gerbils during formation of relevant associations for the avoidance strategy in the shuttle-box. *Prog Neuro-Psychopharmacology Biol Psychiatry* **25**:409–426. doi:10.1016/S0278-5846(00)00171-8

- Stark H, Bischof A, Wagner T, Scheich H. 2000. Stages of avoidance strategy formation in gerbils are correlated with dopaminergic transmission activity. *Eur J Pharmacol* **405**:263–275. doi:10.1016/S0014-2999(00)00558-6
- Stark H, Rothe T, Wagner T, Scheich H. 2004. Learning a new behavioral strategy in the shuttle-box increases prefrontal dopamine. *Neuroscience* **126**:21–9. doi:10.1016/j.neuroscience.2004.02.026
- Stark H, Scheich H. 1997. Dopaminergic and serotonergic neurotransmission systems are differentially involved in auditory cortex learning: a long-term microdialysis study of metabolites. *J Neurochem* **68**:691–7.
- Stujenske JM, Spellman T, Gordon JA. 2015. Modeling the Spatiotemporal Dynamics of Light and Heat Propagation for In Vivo Optogenetics. *Cell Rep* **12**:525–534. doi:10.1016/j.celrep.2015.06.036
- Talwar SK, Xu S, Hawley ES, Weiss SA, Moxon KA, Chapin JK. 2002. Rat navigation guided by remote control. *Nature* **417**:37–38. doi:10.1038/417037a
- Thomas H, Tillein J, Heil P, Scheich H. 1993. Functional Organization of Auditory Cortex in the Mongolian Gerbil (*Meriones unguiculatus*). I. Electrophysiological Mapping of Frequency Representation and Distinction of Fields. *Eur J Neurosci* **5**:882–897. doi:10.1111/j.1460-9568.1993.tb00940.x
- Tischbirek CH, Noda T, Tohmi M, Birkner A, Nelken I, Konnerth A. 2019. In Vivo Functional Mapping of a Cortical Column at Single-Neuron Resolution. *Cell Rep* **27**:1319–1326.e5. doi:10.1016/J.CELREP.2019.04.007
- Tonegawa S, Liu X, Ramirez S, Redondo R. 2015. Memory Engram Cells Have Come of Age. *Neuron* **87**:918–931. doi:10.1016/j.neuron.2015.08.002
- Vasquez-Lopez SA, Weissenberger Y, Lohse M, Keating P, King AJ, Dahmen JC. 2017. Thalamic input to auditory cortex is locally heterogeneous but globally tonotopic. *eLife* **6**. doi:10.7554/eLife.25141
- Vogt N. 2017. Tailoring optogenetic illumination through tapered fibers. *Nat Methods* **14**:763–763. doi:10.1038/nmeth.4381
- Wang Y, Brzozowska-Prechtl A, Karten HJ. 2010. Laminar and columnar auditory cortex in avian brain. *Proc Natl Acad Sci U S A* **107**:12676–81. doi:10.1073/pnas.1006645107

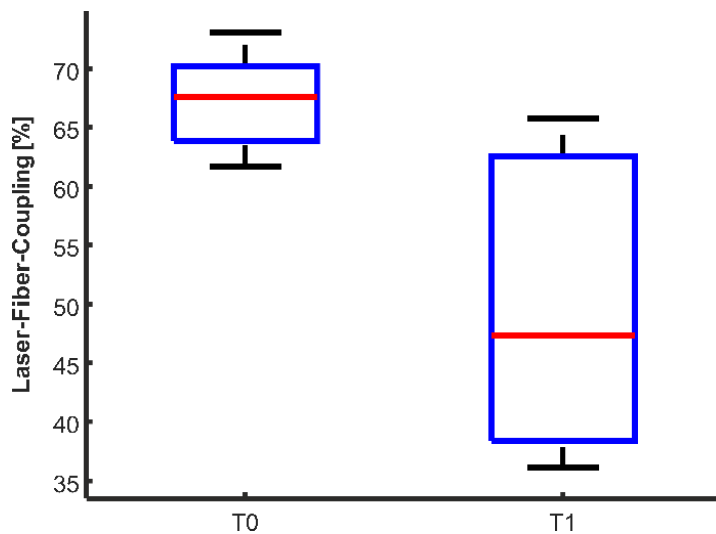
- Weidner TCS, Vincenz D, Brocka M, Tegtmeier J, Anja M, Ohl FW, Goldschmidt J, Lippert MT, Oelschlegel AM, Ohl FW, Goldschmidt J, Lippert MT. 2019. Matching stimulation paradigms resolve apparent differences between optogenetic and electrical VTA stimulation. *Brain Stimul.* doi:10.1016/j.brs.2019.11.005
- Weiler N, Wood L, Yu J, Solla SA, Shepherd GMG. 2008. Top-down laminar organization of the excitatory network in motor cortex. *Nat Neurosci* **11**:360–366. doi:10.1038/nn2049
- Weinberger NM. 2004. Specific long-term memory traces in primary auditory cortex. *Nat Rev Neurosci* **5**:279–290. doi:10.1038/nrn1366
- Wetzel W, Ohl FW, Scheich H. 2008. Global versus local processing of frequency-modulated tones in gerbils: an animal model of lateralized auditory cortex functions. *Proc Natl Acad Sci USA* **105**:6753–6758. doi:10.1073/pnas.0707844105
- Wetzel W, Ohl FW, Wagner T, Scheich H. 1998. Right auditory cortex lesion in Mongolian gerbils impairs discrimination of rising and falling frequency-modulated tones. *Neurosci Lett* **252**:115–8. doi:S0304394098005618 [pii]
- Wietek J, Prigge M. 2016. Optogenetics, Methods in Molecular Biology. New York, NY: Springer New York. doi:10.1007/978-1-4939-3512-3
- Witt K, Nuhsman A, Deuschl G. 2002. Dissociation of Habit-Learning in Parkinson's and Cerebellar Disease. *J Cogn Neurosci* **14**:493–499. doi:10.1162/089892902317362001
- Yizhar O, Fenno LE, Davidson TJ, Mogri M, Deisseroth K. 2011. Optogenetics in neural systems. *Neuron* **71**:9–34. doi:10.1016/j.neuron.2011.06.004
- Zempeltzi MM, Kisse M, Brunk MGK, Glemser C, Aksit S, Deane E, Maurya S, Schneider L, Ohl FW, Deliano M, Happel MFK. 2019. Task rule and choice are reflected by layer-specific processing in rodent auditory cortical microcircuits 1–21.

## Appendix

### Supplementary Figures

#### Laser-Fiber-Coupling Efficiencies of the used C1V1 animals

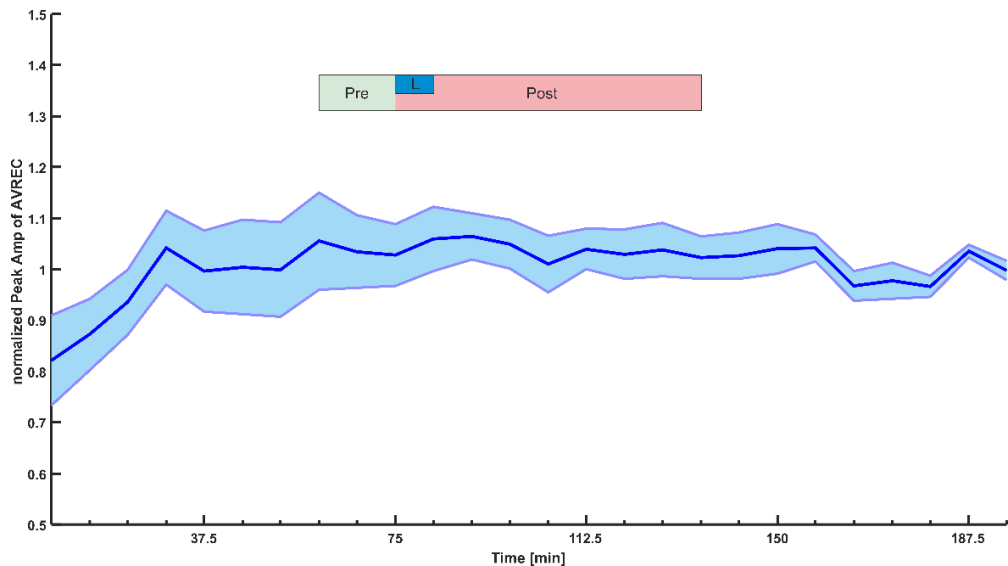
This graph displays the initial LFCs properties for T0, before implantation, and T1, after the experiment, for the animals of the C1V1 group used in the electrophysiological experiments.



SFig 1: LFCs of C1V1 group

This graph shows the LFCs for the implants of the C1V1 group used for the initial LFCs (T0, n=12) and the LFCs after the experiments (T1 n=10). T0 (min: 61.7%, mean: 67.14 %, median: 67.65 %, max: 73.0 %). T1 (min: 36.1 %, mean: 50.18 %, median: 47.4 %, max: 65.8 %). Note: The removal from the implanted fibers requires a certain amount of force, which might contribute to the percentage loss of the LFC of T1.

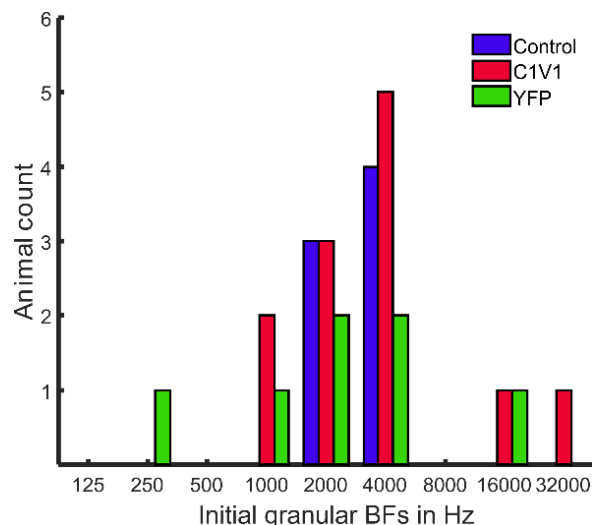
## Temporal stability of CSD signals



SFig 2: Temporal stability of normalized CSD signals

Peak amplitudes (mean  $\pm$  SEM) of the early AVREC BF have been normalized animal-wise (Control group, n=7) by the mean value of the entire time course (>3h). During the initial 30 min the signal stabilizes revealing an almost 20% weaker initial activity as during the later time points. Corresponding time points for the animal comparisons of the C1V1, YFP and Control groups are indicated for the initial three Pre- (pre, 60-75 min), the Laser- (L, 75-82.5 min) and the Post- measurements (75-135 min). Note: After normalization, the SEM varies roughly between  $\pm$  10%.

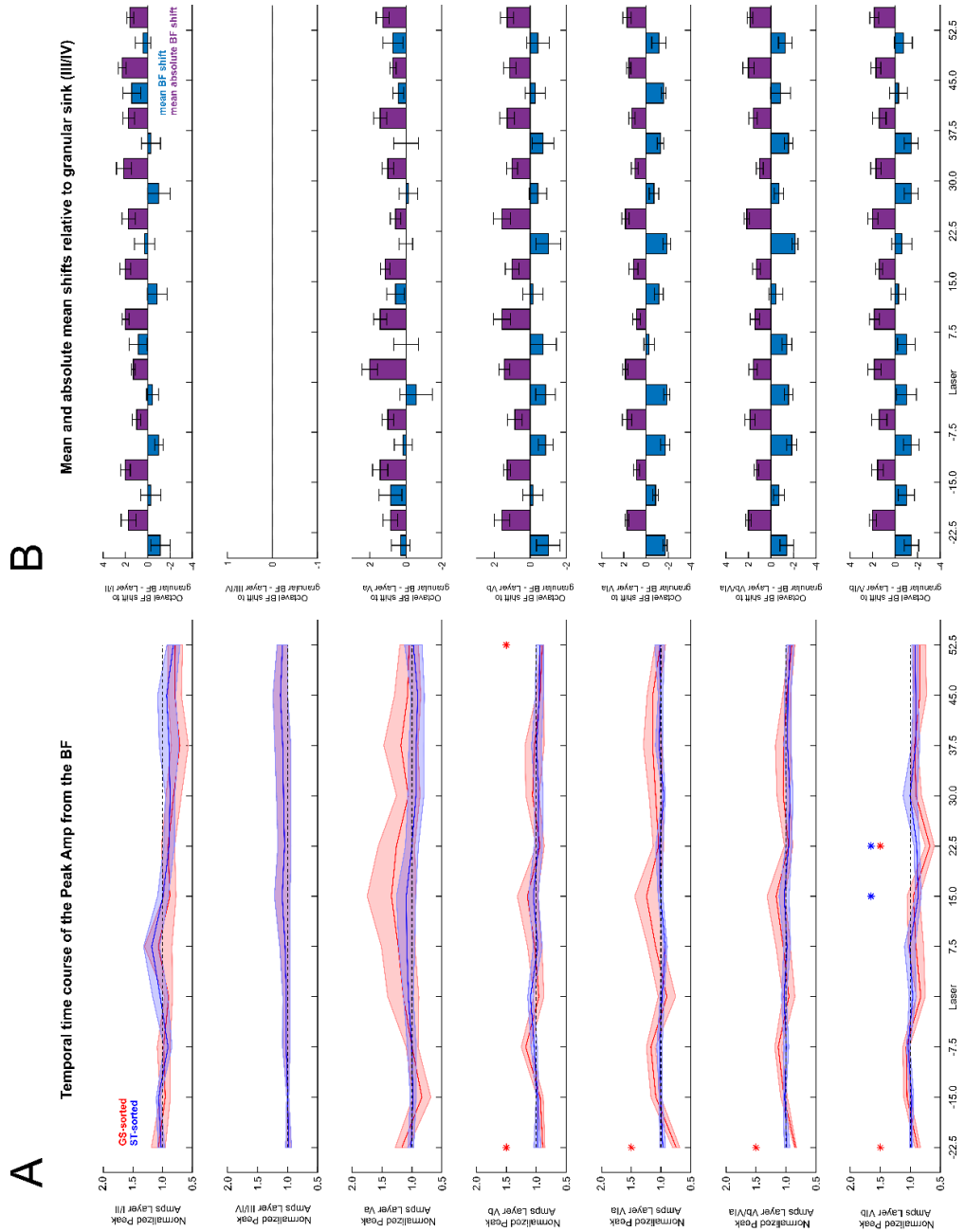
## Common initial granular BFs of the groups



SFig 3: Common initial BFs

The group wise initial BF distribution based on the early granular sink of layers III/IV shows Gaussian distribution for all animals. Mean and SEMs: Control ( $3.14 \pm 0.4$  Hz), C1V1 ( $6.33 \pm 2.6$  Hz) and YFP ( $4.18 \pm 2.04$  Hz). Kruskal-Wallis-Test p = 0.72, post-hoc Bonferroni-Test all p-values = 1.

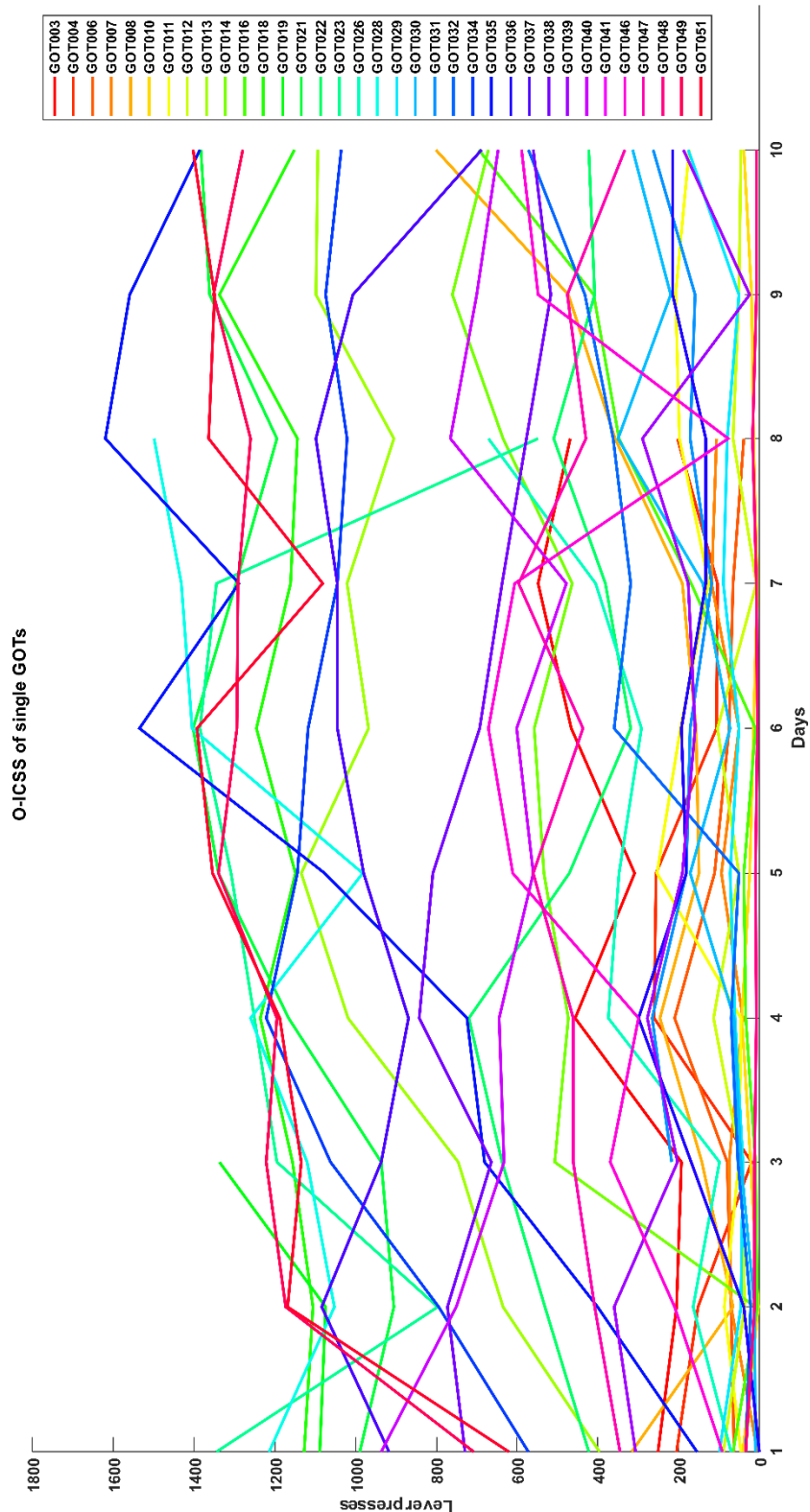
BF development and shift towards the granular sink (III/IV) for the Control group



SFig 4: Temporal BF time course and BF shifts for naïve Control group

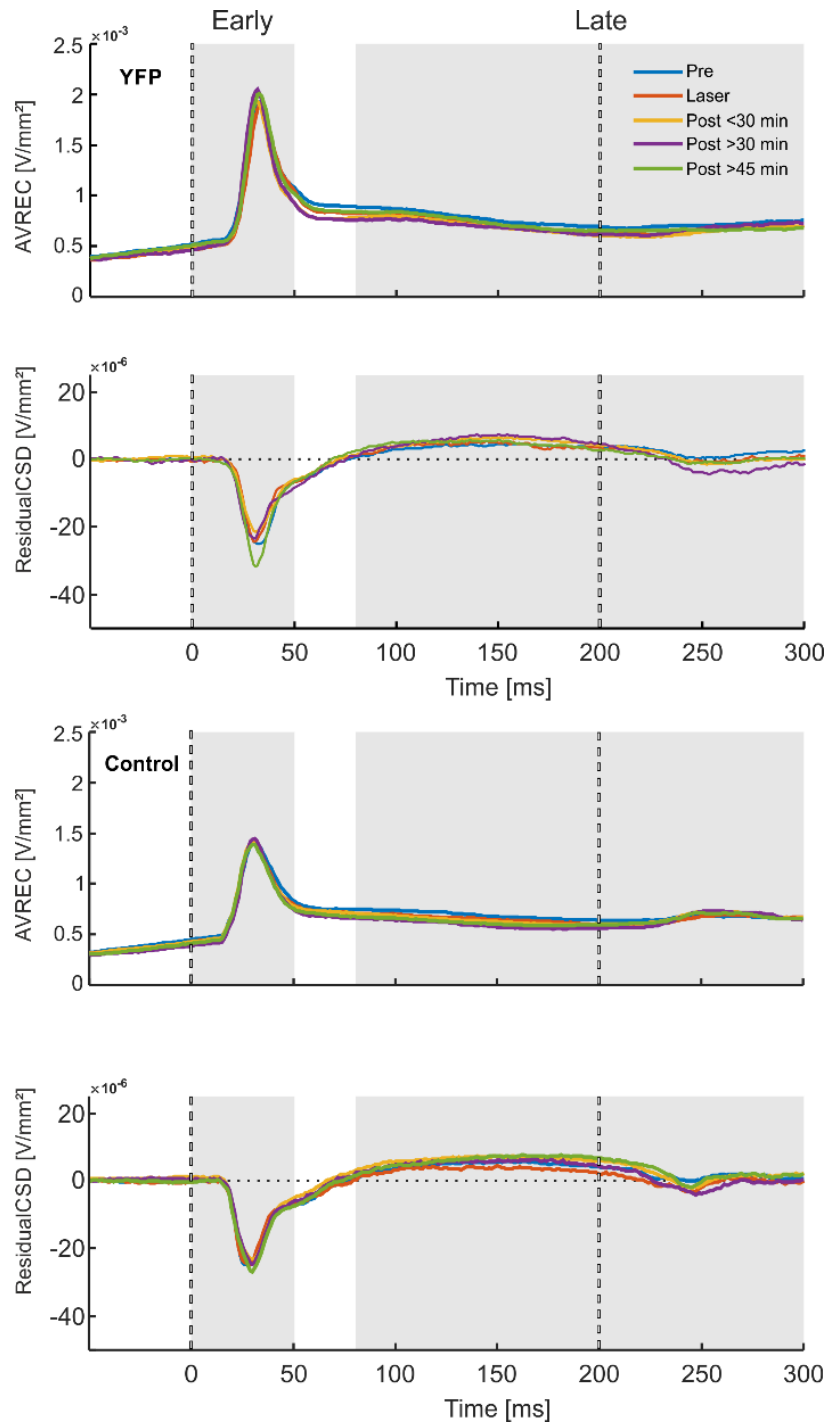
A) Temporal time course of the layer specific BFs of the Control group ( $n=7$ ). Red: GS-based sorted data, blue: ST-based sorted data. Significances ( $p \leq 0.05$ ) have been detected with a two-sample t-test against a normalization vector of 1, indicating positions at which the normalized PeakAmps differ towards 1. In general, ST-based sorted data display the most robust and stable signal (mean  $\pm$  SEM). B) Octaval BF shifts between different layers towards granular BFs (layer III/IV). Blue: mean shifts; violet: mean of the absolute shifts. Except for layer Va, most non-granular layers display a negative mean shift towards lower frequencies and mean absolute shifts vary between 1-2 octaves.

## Lever presses of single animals



SFig 5: Lever presses from all C1V1 animals for the 10 day training

## AVREC and ResidualCSD traces of the YFP and Control animals

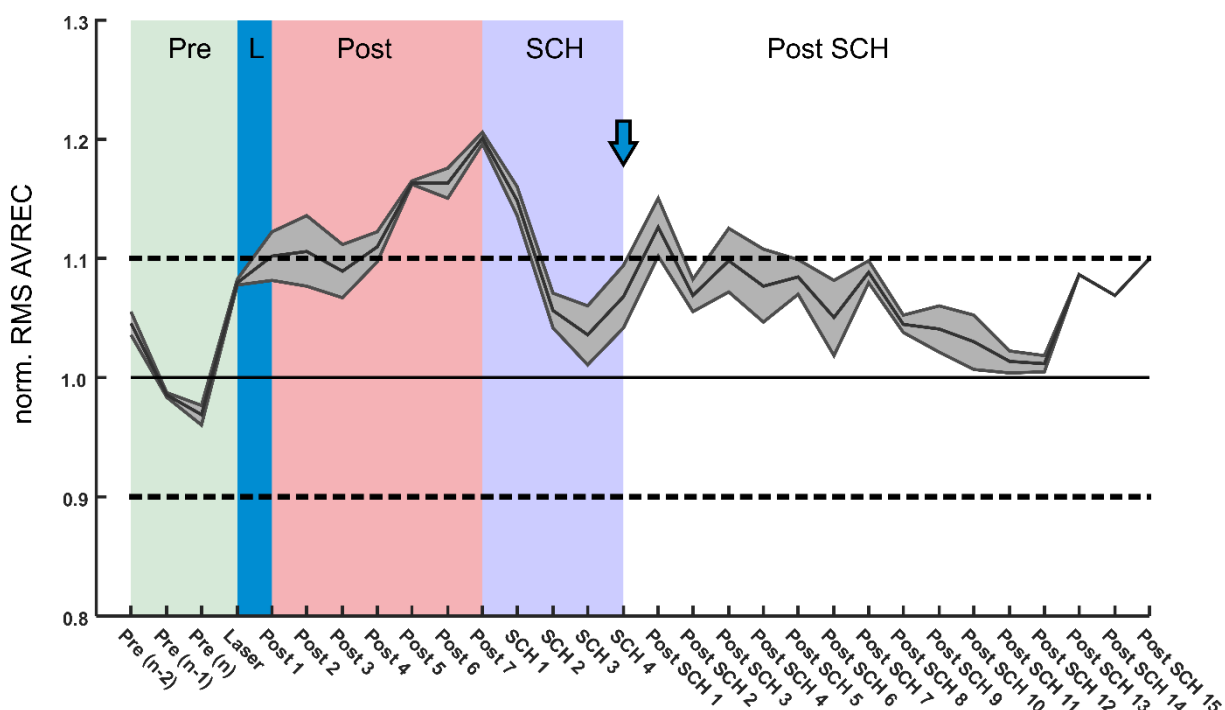


SFig 6: Grand average AVREC and ResidualCSD traces of the YFP and Control animals

Top: AVREC and ResidualCSD traces of the BF from the YFP group ( $n=7$ ) for the time bins Pre, Laser, Post <30 min, Post >30min and Post > 45 min. Bottom: AVREC and ResidualCSD traces of the BF from the Control group ( $n=7$ ) for the time bins Pre, Laser, Post <30 min, Post >30min and Post > 45 min. Corresponding areas for early and late activity are underlined in gray. Dashed lines at 0 and 200 ms indicate time window of tone presentation.

## Time course of C1V1 animals after SCH-23390 application

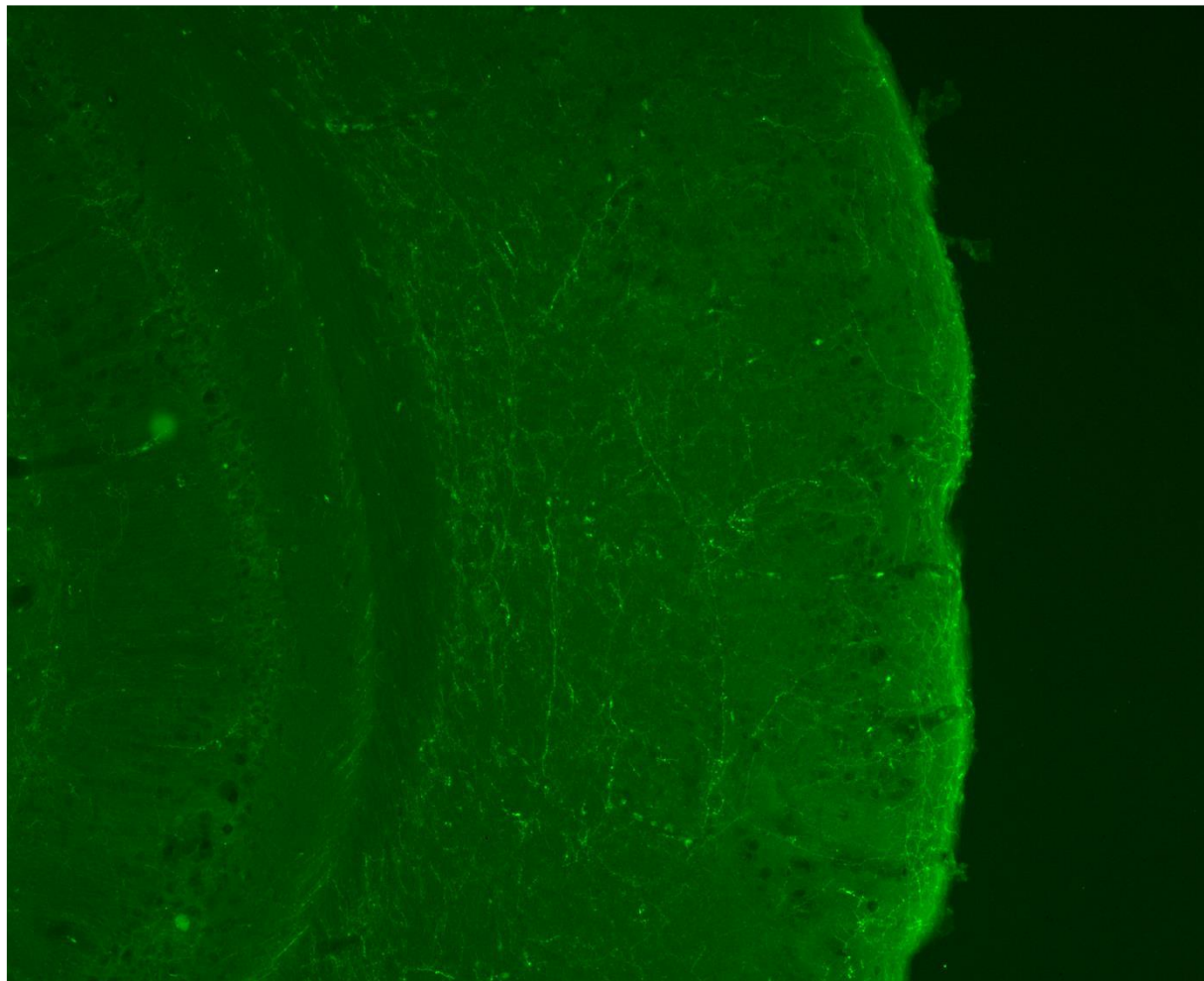
In order to verify the influence of DA on the increase of cortical processing, the potential effect of DA was aimed to be reversed and blocked by the application of SCH-23390, a D1-receptor antagonist. Two animals have been used for the standard paradigm for the effects of the VTA stimulation (1h of Pre-measurements, a laser-coupled VTA stimulation and a series of 7 Post-measurements). Since topical application of SCH-23390 crystalized on top of the cortical surface area, it was decided to apply it twice IP (after the Post- measurements and 30 min later). Before the start of the Post SCH set a second VTA stimulation was performed (measurements not included, indication by blue arrow).



SFig 7: Influence of SCH-23390 onto dopaminergic effects

Shown is the temporal course of the BF stimulation of two animals from the C1V1 group that were used for the investigation of the reversibility of VTA evoked dopamine in the ACx. Data have been normalized by the mean of the last three Pre-measurements. Two laser measurements were performed: the first before the set of Post-measurements and a second one (measurements not included) after the final SCH application and before the Post SCH phase (indicated by blue arrow).

Close up of cortical region after viral VTA transduction

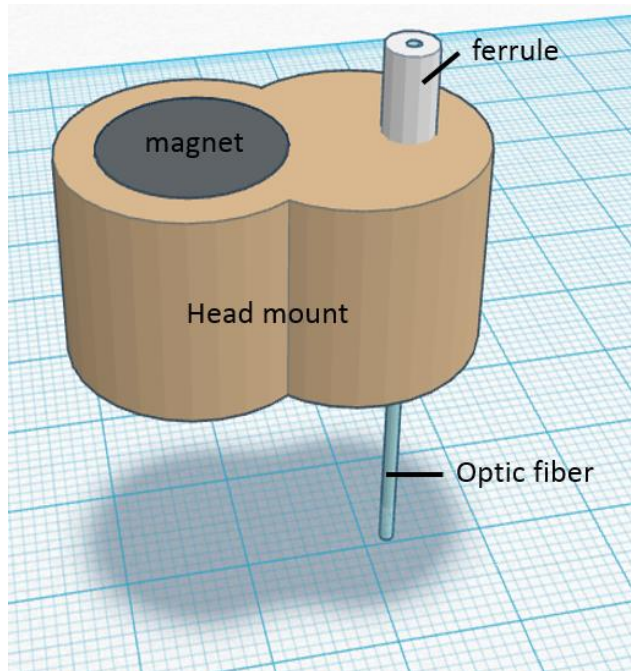


SFig 8 Corresponding cortical section of Figure 7B

High resolution image of the cortical section used in Figure 7B without layer indications. Note that recorded fluorescence is a result of expressed eYFP reporter protein used for the viral transduction of the VTA. Image from Brunk et al., 2019.

## Protocols

Preparation of a head mount for an optic fiber for VTA-Stimulation in Gerbils 1.1



SFig 9: Sketch for final head mount

**Required materials:** basic head mount template, ferrule<sup>6</sup>, ~ 5cm optic fiber<sup>7</sup>, Mirco Strip<sup>8</sup> (230/500 µm), UV glue<sup>9</sup>, cleaver<sup>10</sup>, fiber scope<sup>11</sup>, depth step 1 (metallic), depth step 2(purple platstic)

1. Remove any sharp edges from basic head mount by cutting. (Template will be broken off a master plate).
2. Place the ferrule within the head mount. Ensure that ferrule and head mount are plain on the bottom side. Use the depth step 1 to measure a plain bottom side.
3. De-isolate the optic fiber from one side with the Micro Strip and Push the free fiber back into the plastic cover to ensure it is fully detached from the isolation. Thread the fiber into the ferrule from the bottom side until it peers onto the upper side.

<sup>6</sup>THORLABS INC 1.25mm Ceramic ferrule 230µm

<sup>7</sup> FT200UMT - 0.39 NA, Ø200 µm Core Multimode Optical Fiber, High OH for 300 - 1200 nm, TECS Clad

<sup>8</sup> Micro-Strip Fiber Stripper

<sup>9</sup> LOCTITE 4305

<sup>10</sup> S90R - Ruby DualScribe™ Fiber Optic Scribe

<sup>11</sup> FS200 - Fiber Inspection Scope, FS200-FC and FS200-SMA Adapters Included

4. Apply some UV glue onto the fiber and push it even further into the ferrule to squeeze the glue in between the ferrule and the fiber. Harden the glue by UV-light. Also apply and harden some glue onto the upper and lower part of the ferrule as well.



SFig 10: Intermediate step of implant preparation

5. Use the cleaver to slit the outstanding fiber above the ferrule on the upper side to break the fiber.
6. Turn the head mount upside-down for polishing the upper side of the ferrule. Try to keep the ferrule straight while circling slightly onto a silicon oxide sandpaper. Polish freely until the feeling of edges has disappeared and it sounds like "sliding on ice". Check surface with the fiberscope for surface smoothness. Depending on Surface appearance further polishing might be required. Herby the drawing of 8s onto the sandpaper is recommended.



SFig 11: The three surface types: right: smooth with dust particles, middle: some minor scratches, left: shattered

A smooth surface with eventual dust particles is desirable. Surfaces with minor scratches should be polished with another sandpaper (diamond, alumina) until they look smooth. A shattered surface is the result of wrong handling and cannot be used.

Note: Before using another sandpaper, it is recommended to clean the fiber's surface with air and/or fiber cleaning spray to remove any rough particles from the previous sandpaper to avoid uneven results.

7. When the polishing is done, the remaining fiber on the bottom side will be trimmed to a length of 6 mm by usage of a depth step. First, slightly cut the fiber with the cleaver before breaking the fiber whilst still being inside the depth step.



SFig 12: Depth step

Note: The fiber should be cleaned with 3% H<sub>2</sub>O<sub>2</sub> and 0.9% NaCl to avoid future infections, before implantation.

## Nissl-staining protocol

### A. Counterstaining with Kresylviolett

0.05M Sodium-acetate buffer 5 min

0.5% Kresylviolett 5 min

### B. Differentiate and drain

0,05M Sodium-acetate buffer 3 min

50% Ethanol 2 min

70% Ethanol 2 min

95% Ethanol 2 min

### C. Clearing of the slices

Isopropanol: 96% Ethanol (2:1) 2 x 5min

Roticlear 3 x 5min

### D. Cover with Mowiol and coverslip

#### Used solutions:

0.05M Sodium-acetate buffer: Dissolve 6.8 g sodium-acetate in 1 l aqua dest and adjust pH with acetic acid to 4-4.2.

0.5% Kresylviolett: Dissolve 0.5 g Kresylviolett in 100 ml of 0.05 M sodium-acetate buffer.

## TH-staining protocol for gerbils

Established by Silvia Vieweg

### Immunostaining protocol with antibody diluent (Zytomed Systems, ZUC025-500)

#### Day 1:

- Warm up antibody diluent (used for antibody solution and as blocking buffer) up to RT.
- Dilute primary antibody (PAB, 1:1.000 rabbit anti-TH, Millipore) into the antibody diluent and stir for 5 min w/o foam formation
- Rinse brain slices three times with TBS (1:50 dilution from stock solution) covered for 10 min on a shaker
- Vacuum TBS from slices
- Apply 300 µl of PAB onto each brain slice
- Cover wells with aluminum foil and keep it over night (18h) on a shaker in a cool room.

#### Day 2:

- Dilute primary antibody (PAB, 1:400 anti-rabbit, Molecular probes) into the antibody diluent and stir for 5 min w/o foam formation at RT
- Warm up brain slices to RT and vacuum PAB solution
- Rinse brain slices three times with TBS (1:50 dilution from stock solution) covered for 10 min on a shaker
- Vacuum TBS from slices
- Apply 300 µl of SAB onto each brain slice and keep them covered for 2h at RT on a shaker
- Vacuum SAB from slices
- Rinse brain slices three times with TBS (1:50 dilution from stock solution) covered for 10 min on a shaker
- Transfer brain slices in tap water onto coverslides
- Cover up slices with Mowiol

## List of animals for the electrophysiological experiments

Table 5: Animal records

Lab-ID	THG	Construct	LFC (T0)	DoB	DoOP	DoM	WoOP	WoM	Group	Max. LPs
GOT_013	0274	C1V1	68,5%	01.03.2016	23.05.2016	29.06.2016	72,0	74,0	C1V1	1135
GOT_018	0298	C1V1	68,0%	08.03.2016	06.06.2016	14.07.2016	79,5	80,0	C1V1	1337
GOT_019	0297	C1V1	68,1%	12.01.2016	06.06.2016	30.06.2016	77,5	78,0	C1V1	1336
GOT_021	0285	C1V1	62,8%	07.03.2016	13.06.2016	23.08.2016	78,5	87,0	C1V1	1403
GOT_023	0370	C1V1	68,7%	20.04.2016	25.07.2016	30.08.2016	79,5	78,0	C1V1	1384
GOT_028	0383	C1V1	70,4%	26.04.2016	26.07.2016	25.08.2016	81,0	77,0	C1V1	1499
GOT_034	0479	C1V1	62,9%	15.06.2016	13.09.2016	24.10.2016	75,5	79,5	C1V1	1221
GOT_035	0450	C1V1	61,7%	07.06.2016	13.09.2016	26.10.2016	83,0	88,0	C1V1	1618
GOT_037	1271	C1V1	64,1%	08.02.2017	15.05.2017	29.06.2017	75,0	82,0	C1V1	1097
GOT_040	1281	C1V1	63,6%	08.02.2017	19.05.2017	27.06.2017	68,5	68,0	C1V1	936
GOT_049	1877	C1V1	73,0%	07.06.2017	22.08.2017	26.10.2017	67,0	76,0	C1V1	1351
GOT_051	1767	C1V1	65,1%	07.06.2017	24.08.2017	27.10.2017	74,0	82,0	C1V1	1403
GOT_042	1770	YFP	67,5%	18.05.2017	21.08.2017	04.10.2017	83,0	87,5	YFP	24
GOT_043	1772	YFP	61,0%	18.05.2017	21.08.2017	06.10.2017	78,0	84,0	YFP	330
GOT_044	1766	YFP	66,6%	22.05.2017	21.08.2017	10.10.2017	71,0	77,5	YFP	51
GOT_045 <sup>12</sup>	1776	YFP	62,4%	22.05.2017	21.08.2017	07.12.2017	66,0	92,0	YFP	289
GOT_052	3223	YFP	69,0%	23.05.2018	22.08.2018	26.09.2018	84,0	92,5	YFP	100
GOT_053	3224	YFP	68,0%	23.05.2018	21.08.2018	17.10.2018	98,0	98,0	YFP	51
GOT_054	3226	YFP	65,2%	22.05.2018	22.08.2018	18.10.2018	98,0	110,0	YFP	100
GOT_055	3227	YFP	64,5%	22.05.2018	21.08.2018	16.10.2018	96,0	108,0	YFP	34
GXL03	1871	-	-	05.06.2017	-	16.11.2017	-	82,4	Control	-
GXL04	0939	-	-	05.12.2016	-	23.11.2017	-	72,4	Control	-
GXL05	2309	-	-	10.09.2017	-	11.12.2017	-	71,5	Control	-
GXL06	2310	-	-	10.09.2017	-	14.12.2017	-	70,0	Control	-
GKD_02	2717	-	-	06.12.2017	-	07.03.2018	-	75,2	Control	-
GKD_06	2830	-	-	08.01.2018	-	12.04.2018	-	81,2	Control	-
GKD_08	2832	-	-	08.01.2018	-	19.04.2018	-	76,0	Control	-

A table of all animals used for this study. Lab-ID identifies the project ID for each animal. THG identifies the animals within the in house PyRat-System. Construct indicates whether a virus was transduced and if so, whether it was the AAV5-CaMKIIa-C1V1 (E162T)-p2A-eYFP (C1V1) or the AAV2-CaMKIIa-eYFP (YFP) construct. LFC (T0) indicates the initial laser light coupling efficiency of the used implants before the operation. DoB is the date of Birth. DoOP is the date of the optogenetical operation including the transduction of the virus and implantation of the optical fiber implant. DoM is the date of measurement. On this day the ACx was exposed and the animals have been used for acute experiments. WoOP is the weight the animals had on the day of the operation. WoM is the weight the animals had on the day of the measurement. Group indicates in which group the data of the animal have been assorted. Max LPs is the maximum lever presses the animal achieved during the 10-day training.

<sup>12</sup> Animal dismissed for E-phys data due to epileptic seizures

## List of abbreviations

A1/AI	Primary auditory cortex
AAF	Anterior auditory field
AAV	Adeno-associated virus
ACx	Auditory cortex
AP	Anterior-posterior
Att	Attenuation
AVREC	Averaged rectified current source density
BF	Best frequency
BW	Band width
C1V1	Chimeric Channel rhodopsin consisted of ChR-1 and VChR-1 and the optogenetic animal group
CAMKIIα	α-subunit of the $\text{Ca}^{2+}$ -calmodulin-dependent protein kinase II
CAP	Credit assignment problem
CF	Characteristic frequency
ChR	Channel rhodopsin
CNS	Central nervous system
Control	naïve non-transduced control group
CSD	Current source density
D	Dorsal field
DA	Dopamine
dB	Decibel
DV	Dorso-ventral
ECM	Extracellular matrix
ECoG	Electrocorticography
E-phys	Electrophysiology

eYFP	Enhanced yellow fluorescent protein
FD	Fluorescein-labelled dextran
GABA	γ-aminobutyric acid
GS-based	Granular sink based
HP	High-Performer
ICSS	Intracranial self-stimulation
IP	Intraperitoneal
ISI	Inter stimulus interval
KD	Ketamine dilution
kHz	kilo-Hertz
ML	Medio-lateral
Laser	VTA laser stimulation combined with pure tone presentation
LC	Locus coeruleus
LFC	Laser-fiber-coupling efficiency
LFP	Local field potentials
LP	Low-Performer
MGd/m/v	dorsal, medial, ventral division of the medial geniculate nucleus
MP	Medium-Performer
mW	milli-Watt
NAc	Nucleus Accumbens
NaCl	Sodium chloride
Near-BF	Near best frequency
Non-BF	Non best frequency
Oct	Octave
PeakAmp	Peak amplitude of AVREC trace

PFA	Paraformaldehyde
PFC	Prefrontal cortex
Post	time points after the laser stimulation
Pre	time points before the laser stimulation
ResidualCSD	Residual current source density
RMS	Root mean square
RPE	Reward prediction error
ROI	Region of interest
SEM	Standard error of mean
SPL	Sound pressure level
ST-based	Self-tuning based
STD	Standard deviation
T0	Time point before fiber implantation
T1	Time point after perfusion
TH	Tyrosine hydroxylase
TMRD	Tetramethylrhodamine-labelled dextran
V	Ventral field
VP	Ventroposterior field
VTA	Ventral tegmental area
WT	wild type
YFP	Yellow fluorescent protein and the YFP animal group

## List of Figures

Figure 1: Deep brain stimulation of the hypothalamus for memory retrieval .....	4
Figure 2: Column as the smallest unit of the auditory cortex .....	6
Figure 3: Summary of possible interlayer circuitry projections of the neocortex .....	12
Figure 4: Schematic representation of the reward prediction error within the neuronal population of the ventral tegmental area of monkeys .....	19
Figure 5: Verification of projections between the primary auditory cortex and the ventral tegmental area.....	21
Figure 6: Summary of the underlying question and previous studies .....	25
Figure 7: Anatomical locations and stereotactic verification .....	28
Figure 8: Intracranial self-stimulation and training performance .....	30
Figure 9: Conceptual visualization of anatomical estimations.....	31
Figure 10: Animal preparation for acute measurements.....	33
Figure 11: Schematic representation of AVREC and ResidualCSD signals .....	35
Figure 12: Cortical inputs and sink-layer association.....	37
Figure 13: Comparison example of an evoked BF stimulation with different kernel sizes .....	38
Figure 14: Layer depending sink detection.....	39
Figure 15: Anatomical validation based on initial C1V1 groups .....	45
Figure 16: Order of measurements and example measurement .....	50
Figure 17: Temporal changes of the early and late AVREC and ResidualCSD signals .....	52
Figure 18: Tuning curves for early/late AVREC and ResidualCSD time bins .....	53
Figure 19: Binned time courses for normalized single-trial early and late AVREC and ResidualCSD .....	54
Figure 20: Comparison of immediate laser induced effects .....	56
Figure 21: Temporal development of time bins for the single-trial sink peak amplitude data of layer-specific CSD-traces .....	58
Figure 22: Layer-specific changes of tuning sharpness.....	61
Figure 23: Slopes of layer tuning .....	62
Figure 24: Summary of VTA stimulation effects on cortical layers .....	77

## List of Supplementary Figures

SFig 1: LFCs of C1V1 group.....	97
---------------------------------	----

SFig 2: Temporal stability of normalized CSD signals .....	98
SFig 3: Common initial BFs .....	98
SFig 4: Temporal BF time course and BF shifts for naïve Control group.....	99
SFig 5: Lever presses from all C1V1 animals for the 10 day training .....	100
SFig 6: Grand average AVREC and ResidualCSD traces of the YFP and Control animals .....	101
SFig 7: Influence of SCH-23390 onto dopaminergic effects .....	102
SFig 8 Corresponding cortical section of Figure 7B.....	103
SFig 9: Sketch for final head mount.....	104
SFig 10: Intermediate step of implant preparation .....	105
SFig 11: The three surface types: right: smooth with dust particles, middle: some minor scratches, left: shattered.....	105
SFig 12: Depth step .....	106

## List of tables

Table 1: Layer associated BF-shift tendencies relative towards layer III/IV .....	41
Table 2: Group comparisons of LFCs .....	46
Table 3: Group comparison of fiber tip distance to area of co-fluorescence .....	47
Table 4: Group comparisons of anatomical VTA position .....	48
Table 5: Animal records.....	109